



UNIVERSITÀ CAMPUS BIO-MEDICO DI ROMA

PhD course in Biomedical Engineering
(XXIV - 2009/2011)

Non-invasive estimation of cardiac output in mechanically ventilated patients

Stefano Cecchini

A handwritten signature in black ink, appearing to read 'Stefano Cecchini', written in a cursive style.

Coordinator

Prof. Giulio Iannello

Supervisor

Prof. Sergio Silvestri

March 2012

Non-invasive estimation of cardiac output in mechanically ventilated patients

A thesis submitted by

Stefano Cecchini

in partial fulfillment of the requirements for the degree of

Doctor of Philosophy

in Biomedical Engineering

at Università Campus Bio-Medico di Roma

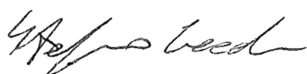
Coordinator

Prof. Giulio Iannello

Supervisor

Prof. Sergio Silvestri

March 2012



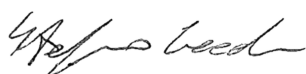
Abstract

Measurement of cardiac output provides an indication of ventricular function making the monitoring of this parameter an important component in the hemodynamic management of both critically ill patients and patients with suspected cardiovascular disease. The knowledge of cardiac output value also helps to guide therapy to maintain adequate tissue perfusion in the high-risk surgical patient.

The gold standard in the assessment of cardiac output consists in measuring the blood flow directly in the aorta requiring a very invasive procedure. Lots of methods have been implemented in order to indirectly estimate this parameter including: invasive methods, semi-invasive and non-invasive ones. Two invasive methods are considered “practical gold standards”: the thermodilution and the Fick method.

In this work of thesis a thorough analysis of the accuracy of these two methods have been performed, showing their strengths and weaknesses.

This thesis introduces and validates a new non-invasive method for the estimation of cardiac output in mechanically ventilated patients: a technological transfer to Cosmed s.r.l. is expected at the end of this study. The method is based on prolonged expiration, and relies on measurement of gas concentrations and flow rate. The sensors of a metabolic monitor (Quark RMR - Cosmed s.r.l., Italy) are employed with the purpose to integrate its functions and extend its use to the Intensive Care Unit.



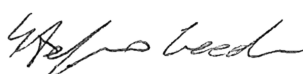
The monitor has been previously validated both *in-vitro* and *in-vivo* with the aim to test its functioning on mechanically ventilated patients and to identify the limits of accuracy of its measurements. The monitor's performance resulted unaltered by the presence of the mechanical ventilator into the breathing circuit, with or without bias flow.

A pneumatic system, with an *ad hoc* designed orifice resistance, has been realized and experimentally characterized to adapt the ventilatory patient circuit to the estimation of cardiac output by prolonging expiration. The use of this system results safe and risks of volutrauma, barotrauma, hypoxia and hypercapnia can be excluded.

Cardiac output is calculated by using two different elaboration algorithms employing data of gas concentration and flow rate, acquired during normal breathing and prolonged expiration.

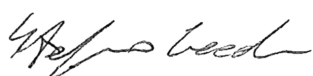
With the aim to quantify the agreement of the proposed method with the thermodilution, twenty mechanically ventilated patients, who have undergone cardiac surgery, have been enrolled.

Good correlation with thermodilution is found for both algorithms ($R > 0.8$). The application of the first algorithm gives mean cardiac output values slightly lower than those obtained by thermodilution (-6%), whilst the application of the second algorithm gives higher values (+30%). The standard deviations of the differences between paired measurements are: 0.72 L min^{-1} for the first algorithm and 1.07 L min^{-1} for the second one. Standard deviation obtained by the application of the



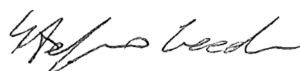
first algorithm is slightly lower than those relative to other minimally invasive techniques.

Prolonged expiration, standardization and automation of the procedure on mechanically ventilated patients all appear feasible with the proposed system, in order to obtain a non-invasive estimation of cardiac output.

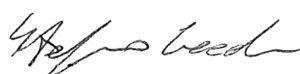


Contents

Nomenclature	9
Chapter 1	13
1.1 Research project	14
1.2 Cardiovascular system and CO	14
1.2.1 The two main control mechanism of CO.....	16
1.3 CO assessment	17
1.3.1 Futures and constraints of a CO assessment device in ICU.....	17
1.3.2 A brief overview of the methods	19
1.4 Indicator dilution technique	19
1.5 Thermodilution	22
1.6 Fick method	24
1.6.1 Oxygen-based Fick method	24
1.6.2 Carbon dioxide-based Fick method	25
1.7 Indirect Fick methods	27
1.7.1 Partial rebreathing method.....	27
1.7.2 Inert gas rebreathing	30
1.8 Doppler ultrasound	30
1.9 Thoracic bioimpedance	32
1.10 Pulse contour analysis	34
1.10.1 Arterial pressure waveform analysis with external calibration.....	35
1.10.2 Arterial pressure waveform analysis without external calibration	36
References	38
Chapter 2	43
2.1 Introduction	44
2.2 Thermodilution	44
2.2.1 Potential concerns with the method	44
2.2.3 Analysis of accuracy	46
2.3 Fick method	48
2.3.1 Measurement setup	48
2.3.2 Sensitivity analysis of the traditional Fick method: a theoretical approach ..	50



2.3.3 Sensitivity analysis of the traditional Fick technique: a numerical approach using the Monte Carlo method.....	53
References	56
Chapter 3.....	58
3.1 Introduction	59
3.2 Quark RMR	59
3.3 In-vitro validation of the Quark RMR for its application on mechanically ventilated patients	61
3.3.1 Overview.....	61
3.3.2 Theoretical background	62
3.3.3 Experimental set-up	63
3.3.4 Results.....	65
3.4 In-vivo validation of the Quark RMR	69
3.4.1 Preamble	69
3.4.2 Patients and protocol.....	70
3.4.3 Results.....	72
References	84
Chapter 4.....	86
4.1 The Kim method	87
4.1.1 Physiological background.....	87
4.1.2 The algorithm.....	89
4.2 Calculation of the slope of the CO₂ dissociation curve: the Godfrey method	91
4.3 Measurement setup	92
4.3.1 Orifice resistance characterization.....	95
4.3.2 Another solution for P-E realization	96
References	99
Chapter 5.....	100
5.1 Clinical experimentation.....	101
5.2 Patient population and therapy.....	101
5.3 Protocol and measurements.....	101



5.4 Statistical analysis.....	103
5.5 Results.....	104
5.6 Discussion	107
5.7 Limitations and assumptions.....	109
5.8 Risk assessment and precautions	110
5.9 Strengths.....	110
5.10 Conclusions	111
References	112
Appendix A	114
Appendix B	116
List of publications.....	123

Stefano Cecchini

Nomenclature

A, surface area of the chamber, [m²]

A_v, vessel cross-sectional area, cross-sectional area (A) of the vessel, [cm²]

BE, base excess, amount of acid or alkali needed to titrate 1 L of fully oxygenated blood to a pH of 7.40, [mEq L⁻¹]

C, concentration of indicator, concentration of the indicator in the chamber at any instant, [g L⁻¹]

CaCO₂, arterial concentration of carbon dioxide, carbon dioxide volume per volume unit of arterial blood, [mL L⁻¹]

CaO₂, arterial oxygen concentration, oxygen volume per volume unit of arterial blood, [mL L⁻¹]

CbCO₂, carbon dioxide concentration in blood, carbon dioxide volume per 100 mL of blood, [mL (100 mL)⁻¹]

c_f, coverage factor assuming a Student's reference distribution with a certain number of degrees of freedom and a certain confidence

CI, cardiac index, CO per square meter of body surface, [L min⁻¹ m⁻²]

CO, cardiac output, volume of blood pumped by one ventricle in unit of time, [L min⁻¹]

CO_G, cardiac output assessed by using the Godfrey method, [L min⁻¹]

CO_{NI}, cardiac output assessed by using a non-invasive method, [L min⁻¹]

CO_K, cardiac output assessed by using the Kim method, [L min⁻¹]

CO_T, cardiac output assessed by thermodilution, [L min⁻¹]

C_p, specific heat, [J kg⁻¹ K⁻¹]

CpCO₂, carbon dioxide concentration in plasma, carbon dioxide volume per 100 mL of plasma, [mL (100 mL)⁻¹]

CvCO₂, venous concentration of carbon dioxide, carbon dioxide volume per volume unit of venous blood, [mL L⁻¹]

CvO₂, venous concentration of oxygen, oxygen volume per volume unit of venous blood, [mL L⁻¹]

D, constant of diffusion, [m min⁻¹]

δq, uncertainty of the variable of interest, q

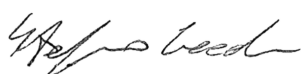
δx_i, uncertainty of the directly measured parameter, x_i.

dZ/dt_{max}, maximum value of the dZ/dt waveform, [Ω s⁻¹]

ΔCO, percentage difference between CO values estimated using non-invasive methods and thermodilution, [%]

E, thermal energy going in (E_{in}) or out (E_{out}) of the control volume, [J]

EF, ejection fraction, the fraction of blood pumped out the right or left ventricle respect on the ventricle's volume before the ejection



ϕ , bias flow, a minimum continuous flow useful for patient triggering conveyed through the patient circuit which does not participate to the pulmonary gas exchange, [L min⁻¹]

F, shunting fraction, ratio between shunted blood volume (V_s) and stroke volume (SV)

F_d , frequency shift in the Doppler ultrasound, [MHz]

$F_{E\text{CO}_2}$, mean expiratory fraction of carbon dioxide, mean fraction of carbon dioxide in the expiratory gas, [%]

$F_{E\text{N}_2}$, mean expiratory fraction of nitrogen, mean fraction of nitrogen in the expiratory gas, [%]

$F_{E\text{O}_2}$, mean expiratory fraction of oxygen, mean fraction of oxygen in the expiratory gas, [%]

$F_{I\text{CO}_2}$, mean inspiratory fraction of carbon dioxide, mean fraction of carbon dioxide in the inspiratory gas, [%]

$F_{I\text{N}_2}$, mean inspiratory fraction of nitrogen, mean fraction of nitrogen in the inspiratory gas, [%]

$F_{I\text{O}_2}$, mean inspiratory fraction of oxygen, mean fraction of oxygen in the inspiratory gas, [%]

f_0 , transmitted frequency in the Doppler ultrasound, [MHz]

h, thermal convection coefficient, [J K⁻¹ m⁻² min⁻¹]

HR, heart rate, number of cardiac cycles per minute [cycles min⁻¹] or [bpm] beats per minute

K, multiplicative coefficient for thermodilution, which takes into account heat loss through the walls and into the catheter by the injectate

k_1 , k_2 and k_3 , empirical parameters, parameters defined by empirical relationships in the Godfrey method

Hb, hemoglobin concentration, mass of hemoglobin per 100 mL of blood, [g (100 mL)⁻¹]

m_{in} , injected mass, mass of indicator injected into the mixing chamber, [g]

m_{out} , ejected mass, mass of indicator, which flows out of the mixing chamber, [g]

m_L , diffused mass, mass of indicator, which leaves the chamber due to diffusion, [g]

P, aortic pressure waveform, [mmHg]

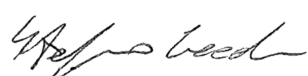
$P_{a\text{CO}_2}$, arterial partial pressure of carbon dioxide, partial pressure of carbon dioxide in the arterial blood, [mmHg]

$P_{A\text{CO}_2}$, alveolar partial pressure of carbon dioxide, partial pressure of carbon dioxide in the alveolar gas, [mmHg]

$P_{a\text{O}_2}$, arterial partial pressure of oxygen, partial pressure of oxygen in the arterial blood, [mmHg]

$P_{A\text{O}_2}$, alveolar partial pressure of oxygen, partial pressure of oxygen in the alveolar gas, [mmHg]

PBF, pulmonary blood flow, volume of blood that actively participates to the gas exchange in unit of time, [L min⁻¹]



PEEP, positive end expiratory pressure, set value of pressure generated by the ventilator into the breathing circuit at the end of the expiration, [cmH₂O]

P_{et}CO₂, end-tidal CO₂, partial pressure of CO₂ at the end of the expiration, [mmHg]

pH, measure of the acidity or basicity of a solution defined as the negative logarithm (base 10) of the molar concentration of hydronium ions

pK, negative logarithm (base 10) of the bicarbonate dissociation constant

P_vCO₂, venous partial pressure of carbon dioxide, partial pressure of carbon dioxide in the venous blood, [mmHg]

Q, blood flow-rate, the rate of displacement of a volume of blood per unit time into a vessel, [L min⁻¹]

q, general dependent variable, $q=f(x_1, x_2, \dots, x_n)$

ρ, general fluid density, [kg m⁻³]

R, instantaneous exchange ratio, instantaneous ratio between carbon dioxide production and oxygen consumption

REE, resting energy expenditure, [kcal die⁻¹]

R_f, breathing frequency, number of respiratory act per minute, [breaths min⁻¹]

RQ, exchange ratio, ratio between carbon dioxide production (V_{CO_2}) and oxygen uptake (V_{O_2}) during the whole respiratory act

S, solubility of carbon dioxide in blood, slope of the carbon dioxide dissociation curve in the blood, [mL L⁻¹ mmHg⁻¹]

S*, solubility of carbon dioxide in blood, calculated from measured physiological parameters

s, slope, slope of the parabolic curve derived from the quadratic regression of P_ACO₂ as a function of P_AO₂ registered during a prolonged expiration

SaO₂, oxygen saturation of the arterial blood, percentage of hemoglobin saturated with oxygen into the arterial blood, [%]

S_T, speed of the target in the Doppler ultrasound, [m s⁻¹]

SV, stroke volume, amount of blood pumped by the left ventricle during heart contraction, [L]

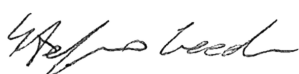
SvO₂, oxygen saturation of the venous blood, percentage of hemoglobin saturated with oxygen into the venous blood, [%]

T, general fluid temperature, [K]

ϑ, angle between the direction of the moving blood and the transmitted ultrasound beam in the Doppler ultrasound

v, blood velocity, distance that a particle of blood travels into one second, [cm s⁻¹]

V_C, burnt amount of ethanol, difference between the volume of ethanol before the burning test and after, [mL]



V_{DALV} , alveolar dead space, amount of pulmonary gas, which does not participate to the alveolar exchanges. [L]

V_E , expiratory volume, amount of gas expired by the subject, [L]

V_E , minute ventilation, amount of gas delivered by the ventilator in one minute, [$L \text{ min}^{-1}$]

VET, ventricular ejection time, [s]

V_i , injectate volume, volume of fluid injected during thermodilution, [m^3]

V_I , inspiratory volume, amount of gas inspired by the subject, [L]

V_P , volume of electrically participating thoracic tissue during the thoracic bioimpedance, [mL]

V_s , shunted blood volume, amount of blood, which does not participate to the alveolar gas exchange, [L]

V_T , tidal volume, amount of gas ventilated during each act, [L]

VTI, stroke distance, the integral of blood velocity curve respect on time, [m]

\dot{V}_{CO_2} , carbon dioxide production, amount of carbon dioxide produced by the subject in unit of time, [$mL \text{ min}^{-1}$]. V_{CO_2} is the volume of CO_2 produced in a certain time interval, [mL]

\dot{V}_{O_2} , oxygen uptake, amount of oxygen consumed by the subject in unit of time, [$mL \text{ min}^{-1}$].

V_{O_2} is the volume of O_2 consumed in a certain time interval, [mL]

x_i , general parameter of interest, $i=1:n$

z_0 , thoracic base impedance, [Ω]

Z_{tot} , equivalent impedance of the arterial tree, [$mmHg \text{ min L}^{-1}$]

Chapter 1

1.1 Research project

The focus of this research is the design and validation of a method for the non-invasive assessment of cardiac output (CO) on mechanically-ventilated patients.

This work derives from an industrial project, involving the Laboratory of Measurements and Biomedical Instrumentation at Università Campus Bio-Medico di Roma and Cosmed s.r.l., which aims to a technological transfer to the company: the focus is improving the functions and potentialities of a metabolic monitor (Quark RMR, Cosmed s.r.l.) by adding new tools for non-invasive CO assessment. Being the metabolic monitor based on indirect calorimetry, i.e., it is able to analyze respiratory gases and measure metabolic expenditure, the investigated method uses the gas-analysis to estimate the value of CO.

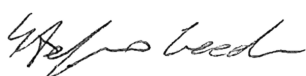
1.2 Cardiovascular system and CO

The human circulatory system transports oxygen (O₂) and nutrient-rich blood to all tissues in the body and removes waste products, which accumulate as a result of metabolic processes. The system is composed of three main components: heart, blood vessels, and blood.

The function of the heart is to provide the pumping force necessary to move blood throughout the body. Blood returning from the body enters the right atrium via the superior and inferior vena cava. It then flows into the right ventricle, which pumps it through the pulmonary artery to the lungs for oxygenation. The left atrium receives oxygenated blood from the lungs, and the left ventricle pumps it, via the aorta, into the arteries. Arteries carry blood away from the heart toward the capillaries where nutrients, wastes and gases are exchanged with tissue cells. The capillary blood empties into veins, which carry blood back to the heart. Blood is the carrier, which transports O₂ and nutrients to the cells and waste products away from the cells [1].

The overall efficiency of the heart and circulatory system is usually characterized by a few important parameters. They are Heart Rate (HR, number of cardiac cycles per minute [cycles min⁻¹] or [bpm] beats per minute), Cardiac Output (the amount of blood pumped into the aorta each minute by the ventricle of the heart [L min⁻¹]), and Ejection Fraction (EF, the fraction of blood pumped out of the right or left ventricle respect on the ventricle's volume before the ejection). Whereas the HR is measured with good accuracy by pressure variations or electrical cardiac activity per unit of time, an accurate assessment of CO and EF is more complicated.

As reported above, in this work we focus on CO measurement. CO is directly related, as it will be described in the following, to stroke volume (SV), which is the volume of blood expelled by the left ventricle within each heart contraction [L], and HR.



The physics of fluid flowing through rigid tubes provides a basis for understanding the flow of blood through the blood vessels, even though the blood vessels are not rigid tubes and blood is not a simple homogeneous and inviscid fluid.

Considering the velocity (v) as the distance that a particle of blood travels into one second [cm s^{-1}], the blood flow-rate (Q) as the rate of displacement of a volume of blood per unit time [L min^{-1}] into a vessel, v and Q are related one to another by the cross-sectional area (A_v) of the vessel [cm^2]:

$$Q = \frac{60}{1000} v \cdot A_v \quad (1.1)$$

Law of conservation of mass requires that the amount of fluid, flowing through a completely isolated rigid tube, is constant: this implies that the average velocity of the fluid will vary inversely with the cross-sectional area. Thus, fluid flow velocity is higher in the section of the tube with the smaller cross-sectional area and slower in the section of the tube with the greater cross-sectional area.

SV represents the integral of the blood flow-rate waveform (Q) ejected by the left ventricle into the aorta during one heart contraction, i.e., in a time interval lasting $60/\text{HR}$ seconds (Fig. 1).

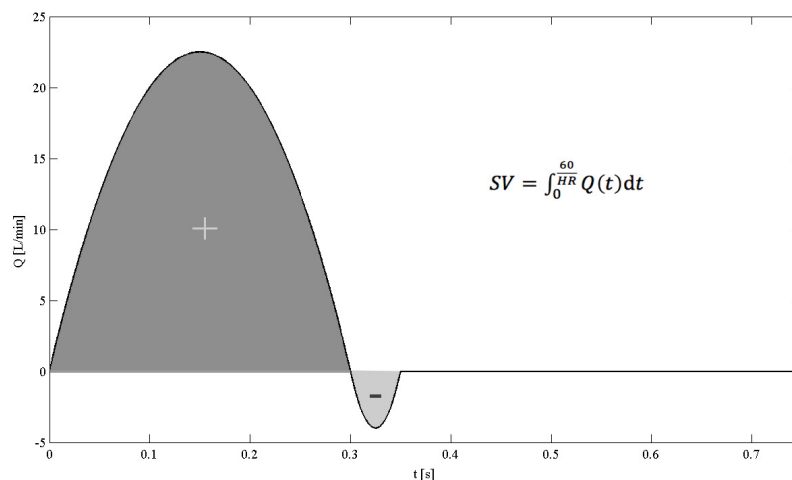


Figure 1 Flow-rate waveform [2] and SV calculation.

In Fig. 1 a typical blood flow waveform is reported: beyond the expected forward flow, a back flow is the result of the heart valve snapping shut, which produces a slight, temporary negative pressure. This phenomenon cannot be neglected in the SV calculation. Considering that typical resting HR in adult is 60-90 bpm, in this example 80 bpm is considered and a typical value of SV is obtained: about 80 mL (with a back flow of about 3 mL).

Stefano Cecchini

CO is obtained by adding the SV values of all the acts within one minute. Considering, for simplicity, that SV does not vary within a minute, in the common practice CO [L min⁻¹] is calculated as the product of SV and HR [3]:

$$CO = SV \cdot HR \quad (1.2)$$

CO varies widely with the level of activity. Therefore, such factors as the level of body metabolism, whether the person is exercising, age and size of the body as well as a number of other factors can influence CO value.

For a normal young healthy adult man the resting CO averages about 5-6 L min⁻¹. For women, this value is 10 % to 20 % lower. For an Olympic athlete at maximum workout, CO exceeds 30 L min⁻¹. For a patient in circulatory shock CO can be less than 2 L min⁻¹. The wide range suggests that CO is a key indicator of one's hemodynamic state. Thus, it would be an interesting goal to accurately, reliably, and continuously determine CO using minimally invasive methods.

Since CO varies markedly with body size, it has been important to find some means by which the CO values of different-sized patients can be compared with each other. At this purpose the cardiac index (CI) has been defined as the CO per square meter of body surface [L min⁻¹ m⁻²].

Another parameter, which is highly correlated with CO value, is pulmonary blood flow (PBF), which is the volume of blood that actively participates to the gas exchange in the lungs per unit of time [L min⁻¹]; the remaining part is shunted. The shunting fraction, F, is the ratio between the shunted blood volume (V_S) and stroke volume (SV), and is involved into a direct relation between CO and PBF:

$$F = \frac{V_S}{SV} = 1 - \frac{PBF}{CO} \quad (1.3)$$

and consequently

$$CO = \frac{PBF}{1-F} \quad (1.4)$$

1.2.1 The two main control mechanism of CO

The primary controller of CO is venous return, which represents the quantity of blood flowing from the veins into the right atrium each minute. The main reason why peripheral factors are normally more important in controlling CO is that the heart has a built-in mechanism that allows it to pump automatically whatever amount of blood flows into the right atrium from the veins. According to this mechanism, called the *Frank-Starling law of the heart*, when the venous blood into the heart increases, it stretches the wall of the heart chambers. As a result of the stretch, the cardiac muscle contracts with increased force and empties the chambers almost as much as ever. Therefore, all the extra blood flowing into the heart is automatically pumped, without delay, into the aorta and flows again through the systemic circulation.

Another important factor caused by stretching the heart is the effect on HR. Stretch of the sinus node in the wall of the right atrium has a direct effect on the rhythmicity of the node itself to increase HR as much as 10 % to 15 %; this increase in rate helps to pump the extra blood. Therefore CO is controlled mainly by peripheral factors that determine venous return [4].

1.3 CO assessment

Knowledge of cardiac function is an important tool for determining the hemodynamic status of an individual, whether he/she is a trained athlete or a patient in a critical care setting.

The decision to measure CO must be a balance between perceived risk and benefit to the patient. Thompson [5] has identified several areas where the CO measurement may be helpful and, therefore, indicated: (1) congenital and acquired heart disease, (2) shock states, (3) multiple organ failure, (4) cardiopulmonary interactions during mechanical ventilation, (5) clinical research that leads to a better understanding of a disease process, and (6) assessment of selected new therapies.

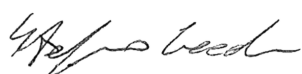
In this work we will mainly consider the ICU setting and, in particular, mechanically ventilated patients. In this context, it is important that CO is not treated as an isolated variable or primary endpoint but rather is used in conjunction with qualitative indicators of the adequacy of flow (e.g. blood lactate, central venous oxygen saturation, artero-venous saturation difference, capillary refill, and urine output), thus allowing adjustment to match the metabolic need of the individual patient.

As a principal determinant of oxygen delivery and blood pressure, CO represents an important variable. Its measurement, therefore, should offer potentially useful information to the anesthesiologist caring for the complex perioperative patient [6], critically ill patient and patients with suspected cardiovascular disease (i.e. valvular stenosis, myocarditis, cardiomyopathy, and arteriosclerosis) [1,7], and results crucial to improve patient outcomes during major surgery and open-heart surgery [8]. This concept has been reinforced in the literature wherein the use of CO and related parameters (i.e., SV, EF, left and right ventricular stroke indices, pulmonary vascular resistance and systemic vascular resistance) as part of goal-directed therapy appears to offer benefits to perioperative and other patient populations [9,10,11].

1.3.1 Futures and constraints of a CO assessment device in ICU

There are certain features, which could provide the clinician with an ideal CO measurement system. At the same time clinical and physiological constraints make it difficult to obtain the ideal conditions.

Automated and continuous measurement



An automatic and continuous assessment of the CO value is highly desirable in a clinical environment, like ICU, where the physician is distracted from many tasks and sudden variations in the patient's state may happen. Automating the system would also improve the accuracy by eliminating the influence of the operator on the measurement.

Reduced invasiveness

The majority of the techniques in use today are invasive, since they require entrance into the body at some locations, either to insert a catheter or to withdraw blood. This increases the risk of infection, thrombosis, vessel perforation and air embolization, and interferes with the cardiovascular system.

The ideal device should be non-invasive, present minimal risk to the patient and not interfere with the desired hemodynamic measurement. For practical reasons, some compromises in terms of invasiveness may be necessary. However, by combining functions into as few probes as possible and through careful design, risk and measurement interference can be minimized [1].

Clinical adaptability

The device should be more easy-to-use than current methods.

Time response and accuracy

Since, as written above, the cardiovascular system's parameters are continuously changing, it is important to detect any variation promptly. Moreover the system should be as more accurate as possible: the challenge of a CO measurement system is to maintain tolerable limit on accuracy, perhaps $\pm 10\%$ or better, and provide the clinician with a measure that is timely and reliable [1].

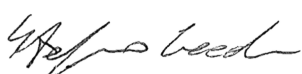
Cost and size

The measurement system should be cost effective and the number of disposable components should be minimized. The system should be preferably small and easily integrated into the ICU, an area already congested with equipment and cables.

Accuracy

One of the considered aspects is particularly critical: obtaining an accurate measurement of CO. It is a rather difficult and invasive task to obtain an accurate measurement of CO, since it would require collecting and measuring all of the blood pumped from the heart into the aortic outflow tract.

In fact, the most direct and accurate way of measuring CO is to use highly invasive techniques. One could conceivably place an ultrasonic flow probe around a major vessel protruding from the heart such as the aorta, locate a temperature sensing element, such as thermistor or hot-film anemometer, in the blood stream, or use electromagnetic flow probe based on Faraday's law of electromagnetic induction (i.e., the movement of a conductor through a magnetic field induces a voltage proportional to the velocity of the conductor) [1]. In these ways, instantaneous pulsatile



flow would be obtained with a millisecond time resolution. SV would be calculated by integrating the flow curve over a cardiac cycle. CO would then be obtained by multiplying SV by HR. Unfortunately, these direct flow measurements require thoracotomy (surgical incision of the chest wall), which will never be performed in humans for routinely diagnostic or monitoring purposes.

It is necessary, therefore, to develop indirect methods for the measurement of CO with an equivalent accuracy.

1.3.2 A brief overview of the methods

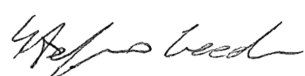
The first technique for measuring CO was described by Adolph Fick in 1870 [12]. This had become the unique accepted standard for the measurement of CO until the development of usable dye dilution techniques. The dye dilution technique for CO determination was based on the work of Stewart in the late 19th century and later modified by Hamilton in the 1940s. In 1953 thermodilution was firstly described by Fegler [13] as an adaptation of the dye dilution technique to the use of heat as indicator; thanks to Swan *et al.* [14] this technique became a widespread clinical measurement of CO. As these two last techniques were found to be as reliable as the Fick technique over a wide range of clinical conditions [15], they have been defined “accepted method of reference” in the measurement of CO [16]: this is mainly due to their direct assessment of the parameter, which, on the other hand, makes the methods quite invasive.

More recently non-invasive or minimally invasive techniques have been gaining in popularity, but none of these has achieved higher reliability than the three above-reported methods. The debate about the best method for the measurement of CO is still open probably due to the impossibility to assess the “true value” of the CO on humans. Anyway Fick, dye dilution and thermodilution still remain the “practical Gold Standards” against which all other methods are compared [6]. However, these methods are cumbersome to perform and have the potential for adverse events [17].

In the following a thorough picture of the state of the art in CO assessment is reported: the methods, which have had acceptance and spread will be described below.

1.4 Indicator dilution technique

The use of exogenous indicators to determine circulation time was first reported as early as 1761, when Haller described the measurement of pulmonary circulation time in an animal model using colored dye. During the 1890s, George Stewart further developed the concept of indicator dilution in a series of papers on circulation time [18,19,20].



The indicator dilution method became widely accepted when Hamilton, in 1948, demonstrated that this technique agreed with the Fick method.

The technique involves the introduction of a predetermined amount of substance at a single point in the bloodstream, preferably where uniform mixing occurs, and then analyzing the flowing blood at a point downstream to obtain a time dilution curve; the CO is obtained by analyzing the time-dependent concentration curve and it is inversely proportional to the integrated area under the curve.

To give an example let us consider a mixing chamber, where Q is the constant volumetric flow rate into and out of the chamber, m_{in} is the mass of indicator injected into the inflow stream and m_{out} the quantity which flows out, $C(t)$ is the concentration of the indicator in the chamber at any instant, and m_L is the mass of indicator that leaves the chamber due to diffusion through the wall, considering the reasonable hypothesis of absence of indicator out of the wall.

The differential mass of indicator that flows out of the chamber is:

$$dm_{out} = C(t)Qdt \quad (1.5)$$

where $C(t)$ at the outlet is the same as the concentration of the indicator in the mixing chamber, assuming complete mixing in the chamber. Thus, the total mass that leaves the chamber is:

$$m_{out} = \int_0^{\infty} C(t)dt \quad (1.6)$$

In case of absence of indicator out of the wall, the mass of indicator, which leaves the chamber due to diffusion through the chamber wall, is proportional to the concentration of indicator, $C(t)$, and the surface area of the chamber, A :

$$dm_L = C(t)ADdt \quad (1.7)$$

where D is a constant for diffusion.

The total mass of indicator leaving the chamber due to diffusion is:

$$m_L = AD \int_0^{\infty} C(t)dt \quad (1.8)$$

Considering a mass-balance into the chamber, the total mass of indicator leaving the chamber is equal to the mass of indicator entering the chamber minus the mass loss of indicator due to diffusion:

$$m_{out} = m_{in} - m_L \quad (1.9)$$

which leads to the following equations:

$$Q \int_0^{\infty} C(t)dt = m_{in} - AD \int_0^{\infty} C(t)dt \quad (1.10)$$

$$Q = \frac{m_{in}}{\int_0^{\infty} C(t)dt} - AD \quad (1.11)$$

The integral is calculated from the area under the indicator dilution curve (Fig. 2), and the effect of diffusion is taken into account by a multiplying calibration factor.

As the system behaves as a first order, the effects of indicator recirculation are minimized by cutting the curve using an exponential decay (Fig. 2).

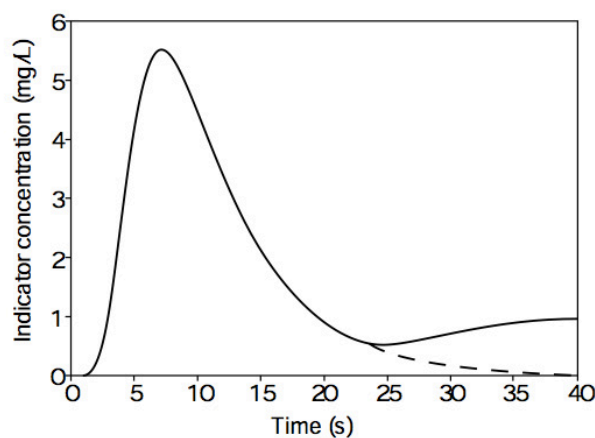


Figure 2 Indicator concentration curve during Indicator Dilution Technique.

A schematic representation of the method is reported in Fig. 3. It can be seen that the value of the integral (AUC) has an inverse proportionality respect on the blood flow.

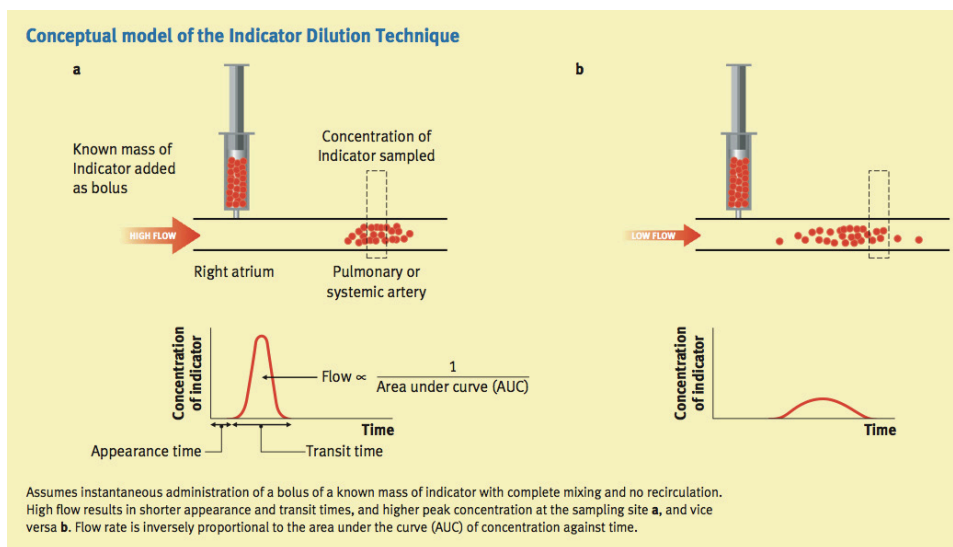


Figure 3 Schematic representation of the Indicator Dilution Technique [21].

The advantage of this technique is that CO measurement can be made in less than one minute. Beyond the invasivity of the method, the main disadvantage is that only 50 % of indicator is removed by the kidneys within 10 min after injection. This limits the rapidity with which repeated measurements can be performed. The greatest source of error is using the exponential decay to extrapolate the downslope of the curve of the indicator concentration [22].

Stefano Cecchini

1.5 Thermodilution

The most common difficulties with indicator dilution techniques have been lack of indicator stability, poor accuracy in concentration measurement and indicator accumulation. The use of thermal indicators (thermodilution) may help to solve some of these issues. This approach was described by Fegler in 1954 for the first time [23]: a warm or cold bolus is injected into the right atrium and the temperature of blood is measured by a thermistor downstream the injection point. Initially, this method resulted in significant indicator loss during transit because of the distance between the injection point and the measurement point.

In 1967, Branthwaite and Bradley [24] used a thermistor-tipped pulmonary artery catheter (Fig. 4). Indicator loss was minimized because of the short path between indicator injection in the right atrium and measurement in the pulmonary artery. In 1970, when Swan and Ganz [14] developed a multilumen, flow directed, thermal sensitive measurement catheter the method gained popular acceptance.

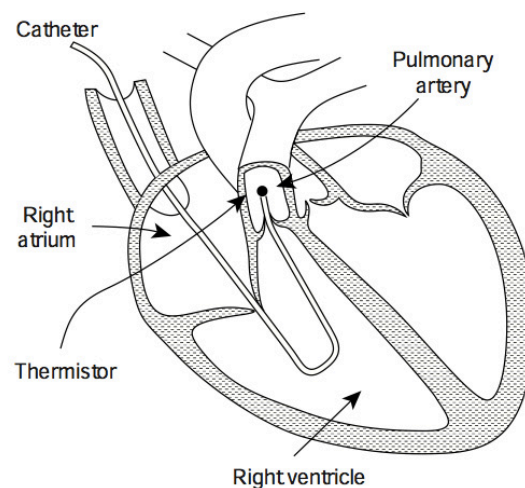


Figure 4 Catheter in place for thermal dilution measurement [3].

Cold injectate is the only practical thermal indicator [14,25] because a warm injectate would need to be considerably warmer than the blood with the risk to be hot enough to denature proteins (60°C).

A bolus of cold solution is injected into the right atrium, via the jugular or subclavian vein, and the blood temperature is recorded in the pulmonary artery, through a thermistor. Considering the principle of conservation of energy for a system that does not produce/consume energy, the total amount of thermal energy entering must equal the total thermal energy that leaves the system.

Considering the thermal energy carried by a differential volume of fluid, it equals:

$$dE = \rho C_p T(t) Q dt \quad (1.12)$$

Stefano Cecchini

being ρ the density of the fluid, C_p the specific heat of the fluid, $T(t)$ the temperature of the fluid at any instant, Q the volumetric flow rate, and dt the differential time.

Considering constant the volumetric flow rate and the thermal properties of the fluid, the total energy is:

$$E = \rho C_p Q \int_0^{\infty} T(t) dt \quad (1.13)$$

Back to our system, the total thermal energy that enters (E_{in}) is the sum of energy carried by the blood flow and the injectate. The subscript b refers to blood and subscript i refers to injectate.

$$E_{in} = \rho_b C_{p_b} Q \int_0^{\infty} T_b(t) dt + \rho_i C_{p_i} V_i T_i \quad (1.14)$$

The total thermal energy that leaves the system (E_{out}) is the sum of the energy carried out of the system by blood flow and thermal energy loss through the walls of the atrium and ventricle. The different thermal capacity between blood and injectate makes the first return to T_b much more slowly than the second; thus, it can be considered that the injectate reaches instantly T_b :

$$E_{out} = \rho_b C_{p_b} Q \int_0^{\infty} T(t) dt + \rho_i C_{p_i} V_i T_b + hA \int_0^{\infty} (T(t) - T_b) dt \quad (1.15)$$

where $T(t)$ is the temperature recorded by the thermistor at any instant, h is the thermal convection coefficient, and A is the internal surface area of the right atrium and right ventricle.

In the thermal energy conservation:

$$E_{in} = E_{out} \quad (1.16)$$

Using Eq. (1.14), (1.15) and (1.16) it is obtained:

$$\rho_b C_{p_b} Q \int_0^{\infty} (T(t) - T_b) dt = \rho_i C_{p_i} V_i (T_i - T_b) - hA \int_0^{\infty} (T(t) - T_b) dt \quad (1.17)$$

and solving for Q :

$$Q = \frac{\rho_i C_{p_i} V_i (T_i - T_b)}{\rho_b C_{p_b} \int_0^{\infty} (T(t) - T_b) dt} - \frac{hA}{\rho_b C_{p_b}} \quad (1.18)$$

The heat loss through the walls could be accounted together with the heat loss into the catheter, using a multiplicative coefficient (K) that is function of the catheter type being used:

$$Q = \frac{\rho_i C_{p_i} V_i (T_i - T_b)}{\rho_b C_{p_b} \int_0^{\infty} (T(t) - T_b) dt} K \quad (1.19)$$

The thermal dilution method has the advantage that recirculation does not represent an issue due to the large surface available in the circulation to bring the injectate temperature to body temperature. A disadvantage is that the injection site and the sensing site must be close to avoid large heat losses, and the absence of total mixing in the ventricle can cause poor accuracy [3]. Moreover the most common approximation is based on the assumption that the indicator solution has no effect on the thermal properties of the blood.

Over the past decade, intermittent bolus thermodilution has been realized in a semi-continuous mode using a thermal filament which provides random thermal pulses of 4-7 °C at 30 s intervals: the blood temperature rises by direct energy transfer and the temperature change is detected by a

thermistor at the distal end [26]. In this case, the volume factor in the numerator of Eq. (1.19) is not relevant and must be replaced by a measurement of the heat introduced: this is the operating principle of the Vigilance (Edwards Lifesciences, Inc.). This method avoids the need for fluid to be injected and provides time-averaged estimates of Q at 5-10 min intervals, but may be poorly accurate at high Q ($> 10 \text{ L min}^{-1}$) or if sudden changes in Q occur [21].

Even in the absence of physiologic noise, the measurement by thermodilution can only be expected to be within 2–7 % of the true value. This accuracy is, however, well within a clinically acceptable range and is no inferior than that of other methods. In addition, with the aim to support the overall accuracy of thermal dilution, Ganz and colleagues [27] determined that the sensitivity of the result to mechanical and technique-dependent factors, such as catheter insertion length and speed of injection, was within 3 %. They considered this to be biologically insignificant [28].

The advantages of thermodilution technique are: 1) the technique does not require the withdrawal of blood for measurement and allows a CO estimation in less than one minute, 2) measurements are minimally affected by recirculation, 3) the measurement catheter is multipurpose, as it allows pressure and saturation measurements, blood sampling and injections. The disadvantages are: 1) the correct positioning of the catheter in the pulmonary artery requires a passage through the central venous system and the heart, with risks of damage to tissues, embolus formation, and electrical hazards, because of the conductive path the catheter forms with the heart, 2) the injection of fluid poses some risks of infection and air embolization, 3) the method is less accurate at low CO values ($< 2 \text{ L min}^{-1}$), as, compared to the Fick method, the accuracy approaches 20 % [16].

1.6 Fick method

1.6.1 Oxygen-based Fick method

Fick principle states that the total uptake or release of any substance by an organ is the product of blood flow rate to the organ and the artero-venous concentration difference of the substance [12]. This theory is applied to estimate the PBF and provides a mass balance at pulmonary level, which describes the diffusion of gas through the alveolar membrane between blood and air:

$$PBF = \frac{\dot{V}_{O_2}}{CaO_2 - CvO_2} \quad (1.20)$$

$$CaO_2 = 10[(1.38 \cdot Hb \cdot SaO_2) + 0.003 \cdot PaO_2] \quad (1.21)$$

$$CvO_2 = 10[(1.38 \cdot Hb \cdot SvO_2) + 0.003 \cdot PvO_2] \quad (1.22)$$

where \dot{V}_{O_2} [mL min^{-1}] is the oxygen uptake, Hb is the hemoglobin concentration [g dL^{-1}], CaO_2 [mL L^{-1}] and CvO_2 [mL L^{-1}] are the oxygen volume per volume unit of arterial and venous

blood respectively, SaO_2 [%] and SvO_2 [%] are the hemoglobin saturation of arterial and venous blood respectively, and PaO_2 [mmHg] and PvO_2 [mmHg] are the oxygen partial pressure in arterial and venous blood respectively. Hemoglobin is able to carry 1.38 mL of oxygen per gram. Therefore, by multiplying the hemoglobin concentration by 1.38 mL g^{-1} it is possible to calculate the oxygen carrying capacity of the individual. Since the biggest part of hemoglobin is saturated, it is possible to calculate the oxygen content of a sample by measuring the arterial (SaO_2) and venous (SvO_2) oxygen saturation. The formula can be simplified by considering negligible the amount of oxygen present in plasma.

Hb is often set to the value obtained from the arterial blood sampled immediately before the onset of the measurement period, i.e. it is not continuously measured. SaO_2 is continuously measured using a pulse oximeter and SvO_2 using a fiber-optic based probe, which is placed into the pulmonary artery and provides instant readings.

\dot{V}_{O_2} is the product of minute ventilation (VE) measured by spirometry, and the difference between inspired and expired oxygen concentrations (F_{IO_2} and F_{EO_2}), measured with a gas analyzer by sampling air at the mouth.

As reported in Eq. (1.4) CO can be calculated using the PBF value and the shunt fraction.

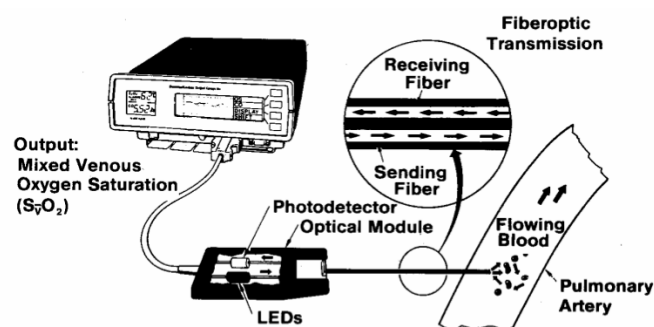


Figure 5 Reflection spectrophotometry.

The technology for measuring SvO_2 is based on reflection spectrophotometry (Fig. 5). This involves transmitting light of selected wavelengths down a fiber-optic in the catheter body to the blood flowing past the catheter tip. The reflected light is then transmitted back through a second fiber-optic to a photodetector located in the optical module. Since hemoglobin and oxyhemoglobin absorb light differently at selected wavelengths, the reflected light can be analyzed to determine the SvO_2 percentage.

1.6.2 Carbon dioxide-based Fick method

Eq. (1.20) can also be applied to CO_2 mass conservation in the following form:

Stefano Cecchini

$$PBF = \frac{\dot{V}_{CO_2}}{CvCO_2 - CaCO_2} \quad (1.23)$$

being \dot{V}_{CO_2} [mL min⁻¹] the carbon dioxide production, $CvCO_2$ [mL L⁻¹] and $CaCO_2$ [mL L⁻¹] the carbon dioxide volume per volume unit of venous and arterial blood respectively.

By supposing a linear CO₂ dissociation curve, Eq. (1.23) becomes:

$$PBF = \frac{\dot{V}_{CO_2}}{S(PvCO_2 - PaCO_2)} \quad (1.24)$$

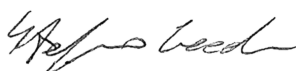
being $PvCO_2$ [mmHg] and $PaCO_2$ [mmHg] the partial pressure of CO₂ in venous and arterial blood respectively, and S [mL L⁻¹ mmHg⁻¹] the slope of the CO₂ dissociation curve in the blood. The arterial and mixed venous partial pressure of CO₂ can be determined by analyzing arterial and mixed venous blood using gas-blood analyzers. As arterial and mixed venous blood samples are required, the method results quite invasive.

An underlying assumption common to Fick method, and to all those methods not allowing beat-to-beat estimates, including thermodilution, is that the obtained value constitutes an average value of CO during the whole measurement period.

However, choosing CO₂ as the reference gas introduces some advantages respect on considering O₂ [3]: 1) when a patient receives high concentrations of supplemental O₂, e.g. during mechanical ventilation, even a small error in the measurement of O₂ concentration yields to poor accuracy on \dot{V}_{O_2} estimation, thus \dot{V}_{CO_2} measurement is, generally speaking, more accurate; 2) some oxygen analyzers show poor accuracy at high O₂ concentrations; 3) CO₂ is virtually absent in the inspired air, it is more soluble than O₂ in blood and its dissociation curve is more linear than the oxygen's one.

A further simplification of the method is allowed if two other assumptions are made: 1) a CO₂ equilibration happens, at the end of the breath, between alveoli and arterial blood, and 2) the gas exchange between alveoli and pulmonary capillaries is equal to the one taking place between alveoli and external environment. This implies that all CO₂ participating to the alveolar exchange is released, without any retention in the lungs, while expiration proceeds. This would allow the estimation of an invasive parameter, such as $PaCO_2$, using measurement on the expiratory gas flow: in particular the end-tidal CO₂ can be assumed equal to $PaCO_2$ corrected for alveolar deadspace.

Considering this, $PvCO_2$ remains the only parameter, which would require an invasive assessment.



1.7 Indirect Fick methods

With the aim to eliminate all the sources of invasivity and estimating both arterial and venous concentration from measurements made by gas analysis at the subject's mouth, some techniques have been developed on the basis of the differential application of the Fick method to the CO₂ (Eq. 1.23) in two different phases: the first phase is the steady state and the second phase starts when a sudden perturbation is introduced into the CO₂ elimination process.

Several techniques have been proposed to induce such a perturbation, including a breath-holding [29] and adding pure CO₂ to the inspiratory gas [8]. Other solutions are more suitable for mechanically ventilated patients, such as changing the minute ventilation [30] or, more recently, changing the respiratory rate delivered by a ventilator [31]. However, only one of these methods has fostered a commercial solution, which is described in the following paragraph.

1.7.1 Partial rebreathing method

One of the indirect Fick methods, based on the partial CO₂ rebreathing, has led to the development of a commercial device (NICO, Novametrix Medical Systems, Inc.) [32]. The partial rebreathing method combines measurements obtained during a non-rebreathing period with the ones obtained during a subsequent rebreathing period: this involves a transitory interruption of CO₂ elimination by addition of a dead space to the ventilatory circuit, which leads to a progressive increase in end-tidal CO₂.

Eq. (1.23) can be applied to both non-rebreathing (superscript *N*) and rebreathing (superscript *R*) phases:

$$PBF = \frac{\dot{V}_{CO_2}^N}{c_{vCO_2}^N - c_{aCO_2}^N} \quad (1.25)$$

$$PBF = \frac{\dot{V}_{CO_2}^R}{c_{vCO_2}^R - c_{aCO_2}^R} \quad (1.26)$$

Using the following algebraic expression:

$$X = \frac{A}{B} = \frac{C}{D} = \frac{A-C}{B-D} \quad (1.27)$$

and considering unchanged the PBF during the manoeuvre:

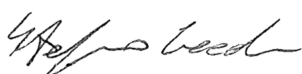
$$PBF = \frac{\dot{V}_{CO_2}^N - \dot{V}_{CO_2}^R}{(c_{vCO_2}^N - c_{aCO_2}^N) - (c_{vCO_2}^R - c_{aCO_2}^R)} \quad (1.28)$$

Assuming also that CvCO₂ varies slowly thanks to the small time constant of body CO₂ storage in comparison to the time of rebreathing [32]:

$$PBF = \frac{\dot{V}_{CO_2}^N - \dot{V}_{CO_2}^R}{(c_{aCO_2}^R - c_{aCO_2}^N)} \quad (1.29)$$

To calculate arterial content of carbon dioxide the NICO uses the following formula:

$$CaCO_2 = (6.957 \cdot Hb + 94.864) \cdot \log(1.0 + 0.1933PaCO_2) \quad (1.30)$$



As written above, $PaCO_2$ is assumed equal to the end-tidal alveolar CO_2 ($PetCO_2$) corrected for alveolar dead space, thanks to the high diffusivity of CO_2 through the alveolar membrane [33]:

$$PaCO_2 = PetCO_2 \frac{V_T}{V_T - V_{DALV}} \quad (1.31)$$

being V_T the tidal volume and V_{DALV} the alveolar dead space.

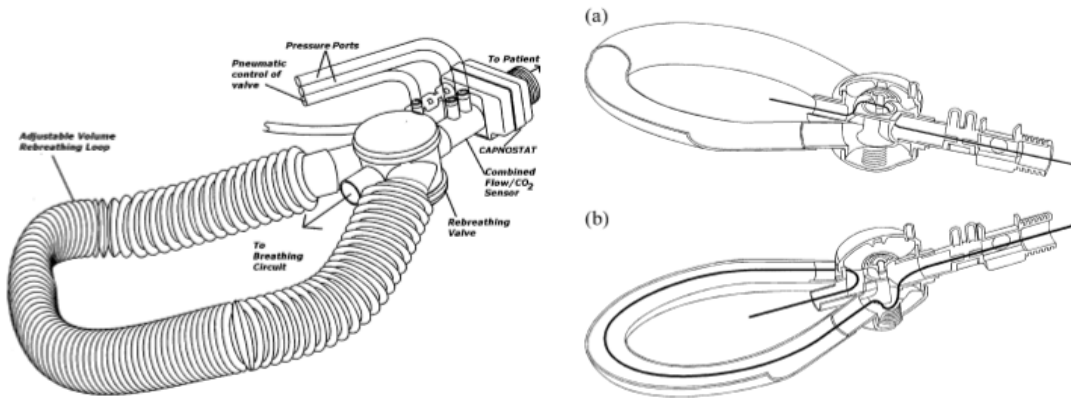


Figure 6 The partial rebreathing circuit and its functioning [32].

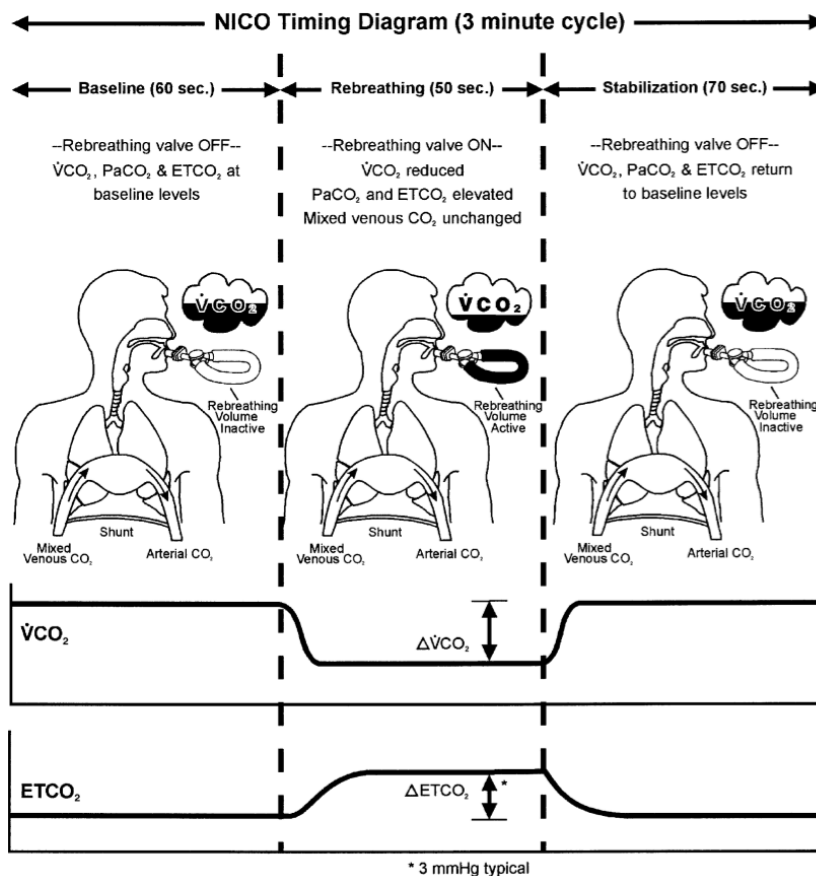


Figure 7 The functioning cycle of the NICO [32].

In Fig. 6 the partial rebreathing circuit is reported: through a valve an additional dead space (35 mL) is introduced into the patient circuit for a period of 30-50 s intermittently every 3 min. The rebreathing valve has the function to exclude the volume rebreathing loop (a) or not (b). In the first case the subject ventilates normally at baseline level, whilst in the second one an amount less than the total CO₂ volume, from the previous expired tidal volume, is rebreathed by the subject (Fig. 7). The values collected during the non-rebreathing period are averaged, whilst those relative to the rebreathing period are plateau values, as reported in Fig. 7. Having a cycle of 3 min this method does not provide a continuous estimation of the CO.

As the previous methods based on the Fick technique, this one measures non-shunted blood rather than total CO and a correction factor for intrapulmonary shunt must be applied (Eq. 1.3 and 1.4).

The method for estimating F employs SaO₂ and F_IO₂ [34,35]. The noninvasive method of shunt estimation is an adaptation of Nunn's iso-shunt plots [36]. These plots (Fig. 8) are a series of continuous curves that describe the relationship between arterial PaO₂ and F_IO₂ for different levels of intrapulmonary shunt [%].

SaO₂ is determined non-invasively with pulse oximetry. Using SaO₂, PaO₂ value is estimated and then employed, together with F_IO₂, in the shunt equations to make a non-invasive estimation of the patient's intra-pulmonary shunt [32].

The most relevant clinical study, which compared the CO₂ rebreathing method to thermodilution on 40 postoperative cardiac patients, reports a mean error of -0.14 L min⁻¹ and a precision of 0.77 L min⁻¹ [37].

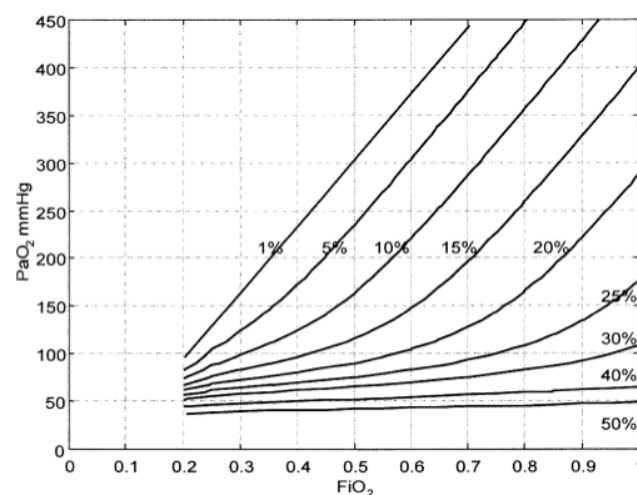


Figure 8 Iso-shunt plots. Shunt fraction percentage is shown in each isocline [32].

1.7.2 Inert gas rebreathing

The rebreathing device (Innocor, Innovision A/S, Odense, Denmark) measures gas concentrations in a gas mixture of enriched concentrations of oxygen (O₂), soluble (N₂O) and insoluble (NF₆) gases from a closed rebreathing assembly [38]: the subject is due to breathe into this assembly. During the rebreathing procedure, blood-soluble N₂O diffuses from the alveoli to the systemic circulation, and blood-insoluble NF₆ remains in the pulmonary fields. The disappearance rate of N₂O in the bag volume is proportional to the pulmonary blood flow, which is assumed to be equal to the CO of the left ventricle [39]. Changes in the composition of the mixture are measured and analyzed with a photoacoustic sensor, and five breaths are used by the Innocor device to calculate CO. This method results valid particularly during exercise when the pulmonary blood flow increases and pulmonary volume expands. The accuracy and precision of the inert gas rebreathing technique has been established by comparisons to the thermodilution and the Fick methods.

The rebreathing method significantly affects CO at rest, as it makes HR increase even maintaining SV constant [17].

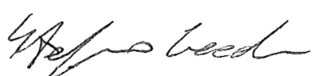
1.8 Doppler ultrasound

Because of high-frequency sound waves (typically 4-10 MHz), ultrasound easily penetrates skin and other body soft tissues. As it encounters tissues of different acoustic density, a fraction of emitted ultrasound signal is reflected. If the ultrasound beam is directed to a moving target, the reflected sound wave changes its frequency: this phenomenon is called *Doppler shift*. The value of this frequency shift (F_d) is directly proportional to the speed of the target (S_T):

$$S_T = \frac{F_d C}{2f_0 \cos\theta} \quad (1.32)$$

where C is the velocity of sound in blood, f₀ is the transmitted frequency, and θ is the angle between the direction of the moving blood and the transmitted ultrasound beam. In this technique, the Doppler frequency shift is combined with the ultrasonic two-dimensional imaging to measure vessel cross-sectional area: the amount of reflected signal is dependent upon the density and acoustical impedance of the tissue within the region scanned. By using the amplitudes of the reflected waves, a two-dimensional image can be constructed and the cross-sectional area (A) of the blood vessel measured [1].

SV can be calculated by multiplying the integral of blood velocity curve respect on time (i.e. the so called 'stroke distance', VTI) by A. Eq. (1.2) allows obtaining CO value.



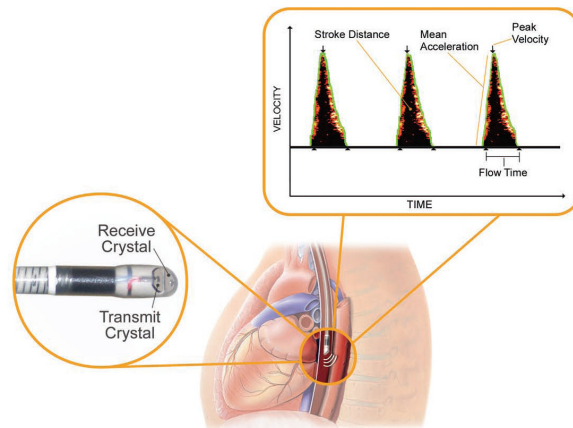


Figure 9 Representation of the esophageal Doppler and the velocity waveform.

Doppler signals can be obtained with an ultrasound probe placed externally, at the suprasternal notch and directed at the ascending aorta (transthoracic Doppler), at the tip of an endotracheal tube, or at the tip of a trans-esophageal probe (Fig. 9) and directed at the descending thoracic aorta (trans-esophageal Doppler).

In the transthoracic Doppler, with the aim to measure ascending aortic blood flow with surface ultrasound, the suprasternal transducer is positioned to receive an audible signal from the aortic root. The ultrasound beam needs to be transmitted parallel to the direction of blood flow through the aortic valve: in practice this alignment is affected by operator skill as well as anatomy and position of the subject. Generally speaking, angles higher than 20° yield clinically unacceptable underestimated measurements of velocity and consequently of CO.

The cross-sectional area of the aorta has been determined in many instances by two-dimensional or M-mode echocardiography but most commonly is derived from a nomogram based on age, sex, height, and weight. This last solution is subject to further potential sources of poor accuracy. As reported in Fig. 9, in the trans-esophageal Doppler the probe is positioned in the esophagus at the midthoracic level, placed in the direction of flow in a blind fashion, and subsequently adjusted to obtain the optimal Doppler signal. As esophageal Doppler involves measurements on descending aorta, a correction factor is necessary to account for blood distributed to the head and upper extremities. This correction is not needed in the transthoracic Doppler: as measurements are taken from the aortic root, the technique is not affected by changes in distribution of CO between the upper and lower part of the body.

Inconsistent results have been obtained by comparing trans-thoracic Doppler ultrasound and thermodilution: an unacceptable variability for clinical monitoring has been reported. The authors of these researches concluded also that Doppler techniques were too much operator-dependent [40,41,42] and that frequent manipulation of the probe was necessary to obtain

accurate data. Moreover, trans-thoracic Doppler estimation of CO in the intensive care unit has other limitations, such as difficulty to identify the aortic root in some subjects, size of the device, and cost. This technique gives, by definition, a non-continuous measurement of cardiac function and it is not useful as trend monitoring system over hours and days [43].

Trans-esophageal Doppler is ideal for intra-operative use and offers some advantages over the trans-thoracic approach: 1) thanks to the close proximity of the descending aorta, it provides an optimal positioning to obtain Doppler signals, 2) provides stability of the transducer and continuous monitoring. On the other hand, the probe is not well tolerated by conscious patients: thus, the use is generally limited to anesthetized or sedated patients, and the method is unsuitable on patients with severe esophageal pathology.

A small amount of literature has considered trans-esophageal Doppler: whether this noninvasive technique can be considered equivalent or superior to invasive monitoring techniques, it still requires further investigation, but encouragement can be drawn from initial investigations.

1.9 Thoracic bioimpedance

This technique measures electrical resistance changes through the thorax as aortic blood volume increases and decreases during systole and diastole.

Bioimpedance is a non-invasive technique, which involves the application of a small alternating current across the chest via skin electrodes. This current is thought to distribute primarily to blood because of its high electrical conductivity compared with muscle, fat and air. Pulsatile changes in thoracic blood volume result in changes of electrical impedance. The rate of change of impedance during systole is measured allowing a value of CO to be derived.

This technique requires four pairs of disposable surface electrodes, two pairs are applied to the base of the neck on directly opposite sides and two pairs are placed at the level of the sternal-xiphoid process junction, again directly opposite from each other (Fig. 10). The device emits a sinusoidal low current (2 mA) at high frequency (50 kHz) through the transmitting electrodes and the sensing electrodes measure the thoracic electrical bioimpedance variation in the form of a voltage signal [44].

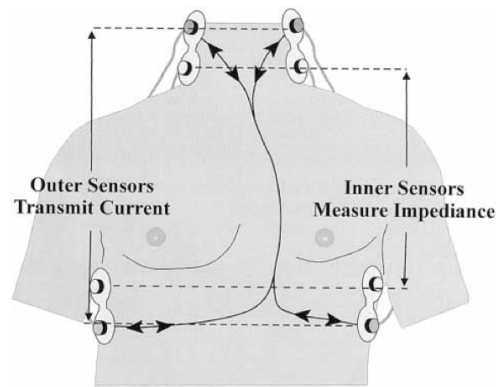


Figure 10 Placement of electrodes for the measurement of thoracic electrical bioimpedance [45].

The signal, caused by the arterial volume variation, the velocity of aortic blood, and the alignment of red blood cells, is similar in shape to the arterial blood pressure waveform: a reduction of impedance is registered during systole. Usually ten cardiac cycles are averaged. The first derivative of the impedance waveform, dZ/dt , provides information about dynamic variations in CO.

By measuring the maximum value of the dZ/dt waveform, dZ/dt_{max} , CO can be calculated using the following equation:

$$CO = \frac{V_P}{z_0} \cdot VET \cdot \left(\frac{dZ}{dt}\right)_{max} \cdot HR \quad (1.33)$$

where V_P is the volume of electrically participating thoracic tissue [mL], z_0 the thoracic base impedance [Ω], VET is the ventricular ejection time [s], and dZ/dt_{max} the maximum value of the dZ/dt waveform [$\Omega \text{ s}^{-1}$].

Although the thoracic impedance method is potentially attractive, being noninvasive, continuous, easily applicable and well tolerated, at this stage it cannot be used in clinical practice for reliable measurement of absolute CO values [43].

In clinical trials, bioimpedance CO measurements have shown inconsistent results. The technique appears to be reliable in healthy volunteers but performs unpredictably in critically ill patients, in high-risk surgical patients, and in the operating room [46,47,48]. Despite recent advances, the technique remains subject to the influence of positive end-expiratory pressure (PEEP), chest wall edema, obesity, pleural fluid, and severe pulmonary edema [49]. Furthermore patient movement can cause motion artifact from the electrode site and electrode location may have substantial effects on the impedance cardiogram [1].

From a meta-analysis of 154 studies on thoracic bioimpedance, Raaijmakers *et al.* [50] concluded that thoracic bioimpedance might be useful for trend analysis but, especially in

certain subgroups of patients, there was limited correlation with established methods of CO determination.

A second technique, bioreactance, is the analysis of the variation in the frequency spectra of a delivered oscillating current that occurs when the current flows through the thoracic cavity and the blood is ejected. This is different from the traditional bioimpedance technique that analyses only the changes in signal amplitude [43].

1.10 Pulse contour analysis

This continuous CO measurement method converts the arterial pressure wave into the CO wave: it is based upon the principle that the stroke volume of one heartbeat generates a corresponding arterial pressure wave. This method was suggested for the first time by Otto Frank in 1899 [51]: he had the intuition that the aortic pressure waveform comes from the interaction between stroke volume and the mechanical characteristics of the arterial tree.

Several algorithms describing the physical properties of the arterial tree have been proposed. These algorithms aim to the reproduction of the mechanical behaviour of the aortic system in order to obtain the aortic pressure waveform, $P(t)$, from the measured instantaneous blood flow, $Q(t)$, and vice-versa. This happens through the estimation of an equivalent impedance of the arterial tree, Z_{tot} : the inverse procedure is obviously allowed. Then, SV can be calculated by integration of the systolic portion of arterial pressure curve (Fig. 11), as follows [52]:

$$SV = \frac{\int_0^T P(t) dt}{Z_{tot}} \quad (1.34)$$

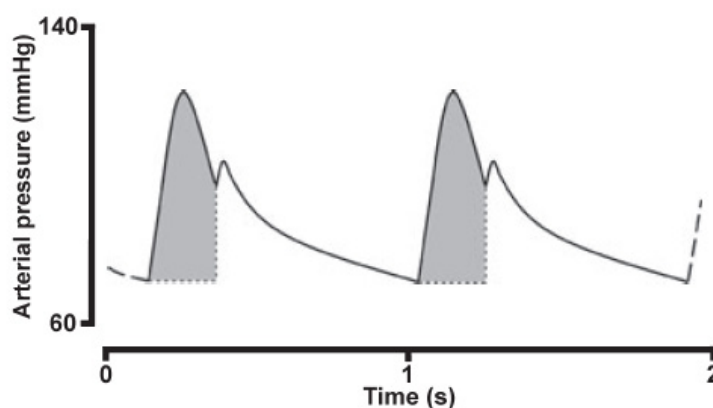


Figure 11 Portion of the arterial pressure, which is involved into the calculation of SV.

The simplest model of arterial tree consists of a single resistance (peripheral resistance), which represents the arterial tone (i.e. the degree of vasoconstriction of the small arteries) [53] (Fig. 12, Model 1). As the peripheral resistance alone cannot account for the shape of the arterial pulse

curve (Fig. 12), other elements must be added to the model. By adding a capacitance element, to represent the blood vessel compliance, a more physiological pulse wave can be obtained (Fig. 12, Model 2). Furthermore, an additional resistance to represent the characteristic aortic impedance would allow the generation of a predicted pressure waveform very similar to the measured (Fig. 12, Model 3): this constitutes the three elements Windkessel model. More complicated models may account for wave reflection phenomena.

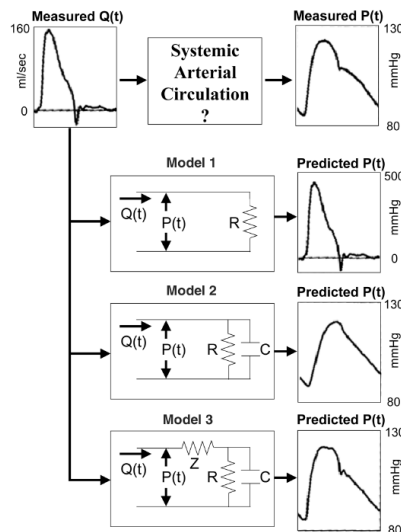


Figure 12 Example of electrical equivalent for the aortic tree.

The pressure waveform is not measured from the aorta but from a peripheral artery (radial or femoral); this requires the assumption of unchanged pulse shape between these different locations.

Several studies have compared CO as measured using thermodilution and pulse contour [54,55], and found fair agreement between values obtained using the two techniques (i.e., error close to $\pm 1.5 \text{ L min}^{-1}$ [53]). However, patients who had poorly defined arterial waveforms or who presented arrhythmia have always been excluded because pulse contour methods cannot provide reliable results in such conditions.

1.10.1 Arterial pressure waveform analysis with external calibration

The values attributed to the model parameters are initially estimated according to the patient's sex and age, and from the pressure waveform. They are then refined following a calibration using an indicator dilution technique: transpulmonary thermodilution for the PiCCO (Pulsion Medical Systems, Munich, Germany) or lithium chloride dilution for the PULSECO (LiDCO Ltd, Cambridge, UK). Recalibrating every 4 hours (or at least before any important data

acquisition) may augment the accuracy of pulse contour estimated CO in critically ill patients, who are likely to exhibit frequent changes in degree of arteriolar vasoconstriction [56].

More recent versions of data elaboration algorithms take also into account the shape of the pressure waveform, the decrease and the slope of the aortic pressure at different times after the dicrotic notch, as well as the position of the dicrotic notch itself: i.e., a steep decrease after the dicrotic notch of the pressure wave indicates a more flexible aorta with a high compliance, whereas a slow decrease after the dicrotic notch indicates a rather stiff aorta with lower compliance [57].

1.10.2 Arterial pressure waveform analysis without external calibration

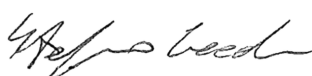
The recently marketed FloTrac/Vigileo system (Edwards Lifesciences, Irvine, CA) uses the arterial pressure waveform in connection with patient demographic data to calculate CO without external calibration. The algorithm is based on the principle that pulse pressure is proportional to stroke volume and inversely proportional to aortic compliance.

The device is connected to any existing peripheral arterial line using the FloTrac pressure transducer, and no intravenous access is required. CO is displayed on a continuous basis on the Vigileo monitor after entering patient height, weight, and age.

Another algorithm is implemented in the non-invasive finger blood pressure systems Finometer, Portapres (Finapres Medical Systems, Amsterdam, The Netherlands), and more recently, Nexfin monitoring system (BMEYE B. V., Amsterdam, The Netherlands). The Finapres methodology uses the volume-clamp technique of Penáz [58] and the Physiocal calibration of Wesseling *et al.* [59].

About Nexfin, arterial volume is clamped by applying variable pressures in an inflatable cuff around the finger, which counters the pulsatile arterial pressure. An optical plethysmograph in the cuff measures arterial volume continuously. The automatic calibration system in the Nexfin determines the volume at which the artery is unloaded, i.e. when transmural pressure equals zero, assuming that the arterial wall does not interfere with the measurement. Because finger arterial pressure is different from brachial pressure in wave shape and absolute levels, waveform transformation and level corrections are applied in the Nexfin system to reconstruct brachial pressure [60]. The brachial pressure is subsequently used to determine the pulse contour derived beat-to-beat CO as showed in the Section 1.10.

The Finapres and its portable variant Portapres were shown to be inaccurate in healthy subjects [61] and critical care patients [62], respectively.



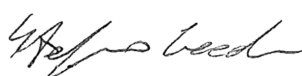
Several studies performed in critically ill or perioperative patients have shown that although the methods, which do not require external calibration, might be able to track relative CO changes, uncalibrated use does not yield reliable absolute CO values.

Although all described methods are commercially available, the majority of these have not achieved widespread use in clinical practice mainly for: high cost of both devices and disposable components, outcome dependence on the operator experience, non-continuous assessment of CO, and concerns about accuracy, precision, and reproducibility [63].

After this overview, aiming to depict the CO assessment scenario and evidence the critical aspects, in the following chapters we will concentrate on CO measurement through gas analysis and we will introduce a new non-invasive method.

References

- ¹ Ehlers, K. C., K. C. Mylrea, C. K. Waterson, and J. M. Calkins. Cardiac output measurement. A review of current techniques and research. *Ann. Biomed. Eng.* 14(3):219-239, 1986.
- ² Ganong, W. F. *Review of Medical Physiology*. Stamford, CT: Appleton and Lange, 1999.
- ³ Faddy, S. C. Cardiac output, Fick technique for. In: *Encyclopedia for medical devices and instrumentation*, J. G. Webster. New York: Wiley-Interscience, pp. 12-21, 1988.
- ⁴ Guyton, A. C., C. E. Jones, and T. G. Coleman. *Circulatory Physiology: Cardiac Output and Its Regulation*, 2nd ed. Philadelphia, PA, Saunders, p. 6, 1973.
- ⁵ Thompson, A. E. Pulmonary artery catheterization in children. *New Horiz.* 5:244–250, 1997.
- ⁶ Pugsley J. and A. B. Lerner. Cardiac output monitoring: is there a gold standard and how do the newer technologies compare? *Seminars in Cardiothoracic and Vascular Anesthesia* 14(4):274-282, 2010.
- ⁷ Christensen, P. and J. Grønlund. Repeatability of the single-breath method for estimation of pulmonary blood-flow: comparison among four data-reduction procedures. *Clinical Physiology* 6:221-234, 1986.
- ⁸ Mohammed, M. M. J. and R. Hainsworth. Evaluation using dogs of a method for estimating cardiac output from a single breath. *J. Appl. Physiol.* 50(1):200-202, 1981.
- ⁹ Kehlet, H. and M. Bundgaard-Nielsen. Goal-directed perioperative fluid management: why, when, and how? *Anesthesiology* 110:453-455, 2009.
- ¹⁰ Rhodes, A., M. Cecconi, M. Hamilton, J. Poloniecki, J. Woods, O. Boyd, D. Bennett, R. M. Grounds. Goal-directed therapy in high-risk surgical patients: a 15-year follow-up study. *Intensive Care Med.* 36:1327-1332, 2010.
- ¹¹ Rivers, E., B. Nguyen, S. Havstad, J. Ressler, A. Muzzin, B. Knoblich, E. Paterson, and M. Tomlanovich. Early goal-directed therapy in the treatment of severe sepsis and septic shock. *N. Engl. J. Med.* 345:1368-1377, 2001.
- ¹² Fick, A. Ueber die messung des blutquantums in den hertzventrikeln. *Sitzungsberichte der Physiologisch-Medizinosche Gesellschaft zu Wuerzburg* 2:16, 1870.
- ¹³ Fegler, G. The reliability of the thermodilution method for determination of the CO and the blood flow in central veins. *Quart. J. Exp. Physiol.* 42:254-266, 1957.
- ¹⁴ Swan, H. J. C., W. Ganz, J. Forrester, H. Marcus, G. Diamond, and D. Chonette. Catheterization of the heart in man with use of flow-directed balloon-tipped catheter. *N. Engl. J. Med.* 283: 447–451, 1970.
- ¹⁵ Taylor, S.H. Measurement of the cardiac output in man. *Proc. R. Soc. Med.* 59 (Suppl. 1):35-53, 1966.



- ¹⁶ Sorensen, M. B., N. E. Bille-Brahe, and H. C. Engell. Cardiac output measurement by thermal dilution: reproducibility and comparison with the dye-dilution technique. *Ann. Surg.* 183:67-72, 1976.
- ¹⁷ Bartels, S. A., W. J. Stok, R. Bezemer, R. J. Bocksem, J. van Goudoever, T. G. V. Cherpanath, J. J. van Lieshout, B. E. Westerhof, J. M. Karemaker, and C. Ince. Noninvasive cardiac output monitoring during exercise testing: Nexfin pulse contour analysis compared to an inert gas rebreathing method and respired gas analysis. *J. Clin. Monit. Comput.* 25:315-321, 2011.
- ¹⁸ Stewart, G. N. Researches on the circulation time in organs and on the influences which affect it. *Journal of Physiology* 15:1-89, 1893.
- ¹⁹ Stewart, G. N. Researches on the circulation time and on the influences which affect it. IV. The output of the heart. *Journal of Physiology* 22:159-83, 1897.
- ²⁰ Stewart, G. N. The measurement of the output of the heart. *Science* 5:137, 1897.
- ²¹ Holmes, T. W. L. and D. J. Williams. Cardiac output measurement. *Anaesthesia & Intensive Care Medicine* 11(2):58-61, 2009.
- ²² Daily, E. and J. Shroeder. *Techniques in bedside hemo-dynamic monitoring*. St. Louis: Mosby pp. 110-131, 1981
- ²³ Fegler, G. Measurement of cardiac output in anaesthetized animals by a thermodilution method. *Quarterly Journal of Experimental Physiology and Cognate Medical Science* 39: 153-64, 1954.
- ²⁴ Branthwaite, M.A. and Bradley R. D. Measurement of cardiac output by thermal dilution in man. *Journal of Applied Physiology* 24: 434-8, 1968.
- ²⁵ Ganz, W. and H. J. C. Swan. Measurement of blood flow by thermodilution. *Am. J. Cardiol.* 29:241-246, 1972.
- ²⁶ Philip, J. H., M. C. Long, M. D. Quinn, and R. S. Newbower. Continuous thermal measurement of cardiac output. *IEEE Trans. Biomed. Eng.* BME-31(5):393-400, 1984.
- ²⁷ Ganz, W., R. Donoso, H. S. Marcus, J. S. Forrester, H. J. C. Swan. A new technique for measurement of cardiac output by thermodilution in man. *Am. J. Cardiol.* 27:392-396, 1971.
- ²⁸ Forrester, J. S., W. Ganz, G. Diamond, T. McHugh, D. W. Chonette, H. J. C. Swan. Thermodilution cardiac output determination with a single flow-directed catheter. *Am. Heart. J.* 83:306-311, 1972.
- ²⁹ Gedeon, A., P. Krill and B. Österlund. Pulmonary blood flow (cardiac output) and the effective lung volume determined from a short breath hold using the differential Fick method. *J. Clin. Monit. Comput.* 17(5):313-321, 2002.
- ³⁰ Gedeon, A., L. Forslund, G. Hedenstierna, and E. Romano. A new method for noninvasive bedside determination of pulmonary blood flow. *Med. Biol. Eng. Comput.* 18:411-418, 1980.

- ³¹ Peyton, P. J., D. Thompson, and P. Junor. Non-invasive automated measurement of cardiac output during stable cardiac surgery using a fully integrated differential CO₂ Fick method. *J. Clin. Monit. Comput.* 22(4):285-292, 2008.
- ³² Jaffe, M. B. Partial CO₂ rebreathing cardiac output—operating principles of the NICO™ system. *J. Clin. Monit. Comput.* 15(6):387-401, 1999.
- ³³ Capek, J. M. and R. J. Roy. Noninvasive measurement of cardiac output using partial CO₂ rebreathing. *IEEE Trans. Biomed. Eng.* 35(9):653-661, 1988.
- ³⁴ Kück, K., D. G. Haryadi, J. A. Orr, M. B. Jaffe. Arterial blood gas measurements improve noninvasive cardiac output estimates from partial CO₂ rebreathing Fick technique. *Crit. Care Med.* 27(Suppl. 1):A109, 1999.
- ³⁵ Sapsford, D. J. and J. G. Jones. The P_iO₂ vs. SpO₂ diagram: A non-invasive measure of pulmonary oxygen exchange. *Eur. J. Anaesth.* 12: 375-386, 1995.
- ³⁶ Nunn, J.F. *Applied Respiratory Physiology*. 4th Ed. Oxford, England: Butterworth Ltd, 1993.
- ³⁷ Österlund B., A. Gedeon, P. Krill, G. Johansson, S. Reiz. A new method of using gas exchange measurements for the noninvasive determination of cardiac output: Clinical experiences in adults following cardiac surgery. *Acta Anaesthesiol. Scand.* 39:727-732, 1995.
- ³⁸ Christensen, P., P. Clemensen, P. K. Andersen, S. W. Henneberg. Thermodilution versus inert gas rebreathing for estimation of effective pulmonary blood flow. *Crit. Care Med.* 28(1):51–56, 2000.
- ³⁹ Triebwasser, J. H , R. I. Johnson, R. P. Burpo, J. C. Campbell, W. C. Reardon, C. G. Blomqvist. Noninvasive determination of cardiac output by a modified acetylene rebreathing procedure utilizing mass spectrometer measurements. *Aviat. Space Environ. Med.* 48(3):203–209, 1977
- ⁴⁰ Freund, P. R. Transesophageal Doppler scanning versus thermodilution during general anesthesia. *Am. J. Surg.* 153:490-503, 1987.
- ⁴¹ Spahn, D. R., E. R. Schmid, M. Tornic, R. Jenni, L. von Segesser, M. Turina, and A. Baetscher. Noninvasive versus invasive assessment of cardiac output after cardiac surgery: clinical validation. *J. Cardiothorac. Anesth.* 4:46-59, 1990.
- ⁴² Cariou A., M. Monchi, L. M. Joly, F. Bellenfani, Y. E. Claessens, D. Thébert, F. Brunet, and J. F. Dhainaut. Noninvasive cardiac output monitoring by aortic blood flow determination: evaluation of the Sometec Dynemo-3000 system. *Crit. Care Med.* 26:2066-2072, 1998.
- ⁴³ Nusmeier, A., J. G. van der Hoeven, and J. Lemson. Cardiac output monitoring in pediatric patients. *Expert Review of Medical Devices* 7(4):503-517, 2010.
- ⁴⁴ Mathews, L. and R. K. Singh. Cardiac output monitoring. *Annals of Cardiac Anaesthesia* 11(1):56-68, 2008.

- ⁴⁵ Botero, M. and E. B. Lobato. Advances in noninvasive cardiac output monitoring: an update. *Journal of Cardiothoracic and Vascular Anesthesia* 15(5):631-640, 2001.
- ⁴⁶ Perrino, A. C., A. Lippman, C. Ariyan, T. Z. O'Connor, and M. Luther. Intraoperative cardiac output monitoring: comparison of impedance cardiography and thermodilution. *J. Cardiothorac. Vasc. Anesth.* 8:24-29, 1994.
- ⁴⁷ Barin, E., D. G. Haryadi, S. I. Schookin, D. R. Westenskow, V. G. Zubenko, K. R. Bellaev, and A. A. Morozov. Evaluation of a thoracic bioimpedance cardiac output monitor during cardiac catheterization. *Crit. Care Med.* 28:698-702, 2000.
- ⁴⁸ Imhoff, M., J. H. Lehner, and D. Lohlein. Noninvasive whole-body electrical bioimpedance cardiac output and invasive thermodilution cardiac output in high-risk surgical patients. *Crit. Care Med.* 28:2812- 2818, 2000.
- ⁴⁹ Sageman, W. S. and D. E. Amundson. Thoracic electrical bioimpedance measurement of cardiac output in post-aortocoronary bypass patients. *Crit. Care Med.* 21(8):1139-42, 1993.
- ⁵⁰ Raaijmakers, E., T. J. Faes, R. J. Scholten, H. G. Goovaerts, and R. M. Heethaar. A meta-analysis of published studies concerning the validity of thoracic impedance cardiography. *Ann. N. Y. Acad. Sci.* 873:121-127, 1999.
- ⁵¹ Frank, O. Die Grundform des arteriellen Pulses. Erste Abhandlung. *Mathematische Analyse. Zeitschrift für Biologie* 37: 485-526, 1899.
- ⁵² Wesseling, K. H., B. Dewitt, and A. P. Weber. A simple device for the continuous measurement of cardiac output. *Adv. Cardiovasc. Phys.* 5:1-52, 1983.
- ⁵³ Berton, C. and B. Cholley. Equipment review: new techniques for cardiac output measurement - oesophageal Doppler, Fick principle using carbon dioxide, and pulse contour analysis. *Critical Care* 6(3):216-221, 2002.
- ⁵⁴ Sakka, S. G., K. Reinhart, and A. Meier-Hellmann. Comparison of pulmonary artery and arterial thermodilution cardiac output in critically ill patients. *Intensive Care Med.* 25:843-846, 1999.
- ⁵⁵ Goedje, O., K. Hoeke, M. Lichtwarck-Aschoff, A. Faltchauser, P. Lamm, and B. Reichart. Continuous cardiac output by femoral arterial thermodilution calibrated pulse contour analysis: comparison with pulmonary arterial thermodilution. *Crit. Care Med.* 27:2407-2412, 1999.
- ⁵⁶ Linton, N. W. and Linton R. A. Estimation of changes in cardiac output from the arterial blood pressure waveform in the upper limb. *Br. J. Anaesth.* 86:486-496, 2001.
- ⁵⁷ Felbinger, T. and D. Reuter. Comparison of pulmonary arterial thermodilution and arterial pulse contour analysis: evaluation of a new algorithm. *Journal of Clinical Anaesthesia* 14:296-301, 2002.

- ⁵⁸ Penàz, J. Criteria for set point estimation in the volume clamp method of blood pressure measurement. *Physiol. Res.* 41(1):5–10, 1992.
- ⁵⁹ Wesseling, K. H., B. De Wit, G. M. A. van der Hoeven, J. Van Goudoever, and J. J. Settels. Physiocal, calibrating finger vascular physiology for Finapres. *Homeostasis* 36:67–82, 1995.
- ⁶⁰ Guelen, I., B. E. Westerhof, G. L. van der Sar, G. A. van Montfrans, F. Kiemeneij, K. H. Wesseling, W. J. Bos. Validation of brachial artery pressure reconstruction from finger arterial pressure. *J Hypertens* 26(7):1321–1327, 2008.
- ⁶¹ Remmen, J. J., W. R. Aengevaeren, F. W. Verheugt, T. van der Werf, H. E. Luijten, A. Bos, and R. W. Jansen. Finapres arterial pulse wave analysis with Modelflow is not a reliable non-invasive method for assessment of cardiac output. *Clin. Sci. (Lond)* 103(2):143-149, 2002.
- ⁶² Gerhart U. M., C. Schöeller, D. Böcker, and H. Hohage. Non-invasive estimation of cardiac output in critical care patients. *J. Clin. Monit. Comput.* 16(4):263-268, 2000.
- ⁶³ Peyton, P. J. and S. W. Chong. Minimally invasive measurement of cardiac output during surgery and critical care: a meta-analysis of accuracy and precision. *Anesthesiology* 113(5):1220-1235, 2010.

Chapter 2

2.1 Introduction

As mentioned in the previous chapter, thermodilution and Fick methods are the “practical Gold Standards” and have been widely used as reference methods for evaluating the performance of innovative techniques.

The accuracy assessment of a method requires the use of a completely reliable CO measurement technique, something that cannot be accomplished in humans [1]. Thus, the definition of “Gold Standard”, in this case, is more related to the suitability of the method’s theoretical model in describing the physiological mechanism rather than to the proved reliability of the method through comparison with the “true value” of CO.

In the following the two practical Gold Standards will be taken into consideration with particular interest to their accuracy in the CO assessment. Accuracy will be considered, as it has widely been done in literature, as the closeness of agreement between one method and the reference. A theoretical approach, based on the measurement models, will be used.

2.2 Thermodilution

2.2.1 Potential concerns with the method

A number of studies in both experimental animals and humans have compared the thermodilution technique with other CO measurements, such as indicator dilution techniques, direct Fick method, and electromagnetic flowmetry [2,3,4]. Many of them raised concerns for important sources of error in thermodilution technique.

Accurate measurements of both blood (T_b) and injectate (T_i) temperatures, immediately preceding injection, result particularly critical. In the thermodilution formula, Eq. (2.1) [5], the difference between these two temperatures (typically 16 °C when using room temperature injectate) is in direct proportion to CO, and consequently also potential errors in determining this differences reflects on CO values:

$$CO = \frac{\rho_i C_{P_i}}{\rho_b C_{P_b}} \frac{V_i (T_i - T_b)}{\int_0^{\infty} (T(t) - T_b) dt} K \quad (2.1)$$

T_b is invasively measured by the thermistor (Fig. 1) placed at the tip of the Swan-Ganz catheter before the bolus injection.

On the other hand, the Swan-Ganz catheter is not equipped with a thermistor at the bolus injection point, into the right atrium, for the measurement of T_i : this aspect seems to be crucial in determining the accuracy and precision of the method.

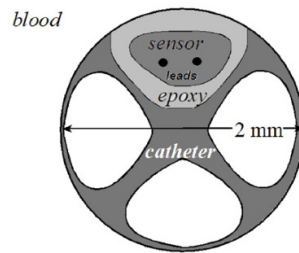


Figure 1 Cross-section of the Swan-Ganz catheter: only one thermistor is mounted on the tip of the catheter [6].

The use of two thermistors (the classical distal thermistor and an injectate thermistor) improves the precision for both ambient temperature (0.41 L min^{-1} vs. 0.55 L min^{-1}) and cooled (0.35 L min^{-1} vs. 0.43 L min^{-1}) injections [1], and enhances the accuracy respect on the Fick method: i.e., in the study by Lehman *et al.*, conventional thermodilution measurements significantly overestimated Fick measurements by 0.32 L min^{-1} and 0.50 L min^{-1} ($p < 0.001$), using ambient temperature and cooled injectate, respectively, in contrast to the dual thermistor measurements, which resulted statistically similar (-0.08 L min^{-1} and -0.08 L min^{-1} , $p = 0.34$) to Fick measurements.

Using a set-up including two thermistors, one positioned externally to the catheter and one in the right atrium, Lehman *et al.* measured the change of temperature experienced by the injectate during the travel into tubing and thermodilution catheter, before the injection into the blood stream (Fig. 2): it averaged $2.8 \text{ }^\circ\text{C}$.

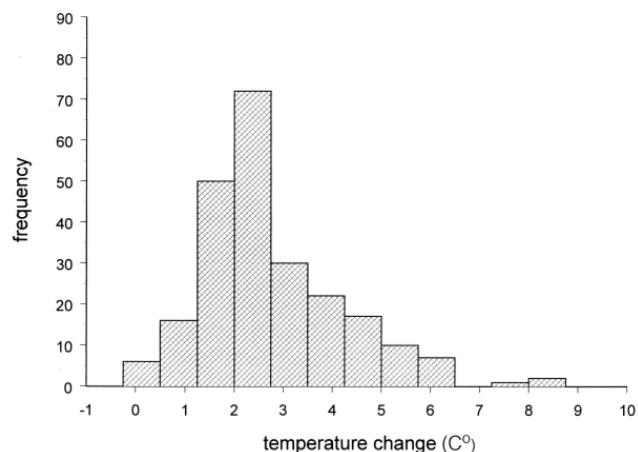


Figure 2 Frequency histogram of the injectate warming as it travels down the length of tubing and thermodilution catheter towards the injection port positioned in the right atrium [1].

Manufacturers attempt to compensate for this error in T_i assessment, by automatic or manual entry of an empirically derived “correction factor” [7], but this is sometimes inadequate in predicting temperature changes during clinical use in humans: Lehman *et al.* also demonstrated

Stefano Cecchini

that, using the correction factor, the injectate temperature remained underestimated, causing an incorrectly high CO (Eq. 2.1).

In fact, overestimation of CO by thermodilution respect on other techniques has been widely reported in literature [8,9]: e.g., $+2.2 \% \pm 8.3 \%$ respect on the CO₂-based Fick method, and $+10.8 \% \pm 16.0 \%$ respect on O₂-based Fick method ($p=0.0001$) [10].

Anyway, the effect of errors in the assessment of T_i can be minimized by using injectate at room temperature [11] to reduce the unmeasured bolus temperature variation; on the other hand, reducing the temperature differential between blood and injectate increases the effect of “noise” in the baseline temperature measurement on the calculation of the area under the temperature-time curve.

Other concerns about the use of thermodilution were mentioned and discussed by testing commercial systems on an artificial circulation [12]: the use of ice cold injectate reduces the variability of CO measurements but leads to a further substantial overestimation of flow-rate, and the volume of injectate used in thermodilution must be chosen according to a compromise. At one extreme a small volume leads to a temperature change that is lost in the fluctuation of baseline temperature, at the other extreme, a large injectate volume will alter the flow rate (measurement of which is being attempted), will be incompletely mixed with blood flow, and will take an appreciable time to be injected in relation to the mean transit time of blood from injection site to sensor. In [12] a net effect of increasing the injectate volume on the accuracy and variability of thermodilution measurement was unpredictable and in the experiments it resulted different for each thermodilution product tested.

In conclusion it happens that the injectate volume and temperature for optimum accuracy are different from those for optimum reproducibility, they differ from manufacturer to manufacturer, and may change in different experimental or clinical situations.

In the best *in-vitro* conditions, Mackenzie *et al.* [12] found that the standard error of the thermodilution value at a flow rate of 5 L min^{-1} is seldom less than 0.5 L min^{-1} or 10 %. Under clinical conditions and with the influence of respiration, the error of this method is likely to increase.

After this analysis of concerns and influence factors relative to the thermodilution technique, in the following a theoretical approach will be used to estimate the thermodilution accuracy from the accuracy of each directly measured parameter.

2.2.3 Analysis of accuracy

With reference to Eq. (2.1), T_i [°C] is the bolus temperature, measured externally to the catheter, T_b [°C] and $T(t)$ [°C] are measured by the thermistor placed at the tip of the catheter before and

after the bolus injection, respectively. Considering the above-reported concerns, in this analysis an index (K) is introduced to take into account the bolus warming.

Table I resumes the accuracy of the sensors involved into the CO assessment.

Table I Accuracy of the thermistors used for CO assessment by thermodilution.

Parameter	Device	Range [°C]	Accuracy [°C] at 95 % of confidence ¹
T _i	Thermistor-Edwards Lifesciences	-1 ÷ +45	± 0.1
T _b and T(t)	Thermistor embedded into catheter-Edwards Lifesciences	-1 ÷ +45	± 0.1

The law of propagation of uncertainty is here applied: this analysis uses the first partial derivative of the dependent variable $q=f(x_1, x_2, \dots, x_n)$ with respect to the directly measured variables of interest ($x_i, i=1:n$) [13]:

$$\delta q = \sqrt{\left(\frac{\partial q}{\partial x_1} \delta x_1\right)^2 + \left(\frac{\partial q}{\partial x_2} \delta x_2\right)^2 + \dots + \left(\frac{\partial q}{\partial x_n} \delta x_n\right)^2} \quad (2.2)$$

where δq is the uncertainty of the variable of interest, q , and δx_i represents the uncertainty of the directly measured parameter x_i .

Eq. (2.1) can be rewritten in the following form:

$$CO = \frac{\rho_i C_{P_i}}{\rho_b C_{P_b}} \frac{V_i (T_i - T_b)}{\int_0^\infty (T(t) - T_b) dt} K = \alpha \frac{N}{D} \quad (2.3)$$

where $\alpha = K \frac{\rho_i C_{P_i} V_i}{\rho_b C_{P_b}}$, $N = T_b - T_i$, and $D = \int_0^\infty (T(t) - T_b) dt$. α depends on the physical properties of bolus and blood, on the quantity of injectate, and on the value of K. At this stage, α is considered not being source of uncertainty.

To make an example of the whole uncertainty of CO in typical conditions, the following mean values of temperature are considered [14]: $T_i=0$ °C, considering cold injectate, $T_b=37$ °C, and T(t) comprised within 1 °C from T_b . Here, as an example, the didactic values, reported by Geddes in [14], are considered: $N = -37$ °C, $D = -1.59$ °C · s, $V_i = 5$ mL, $K = 0.82$, $\frac{\rho_i C_{P_i}}{\rho_b C_{P_b}} = 1.08$. α results equal to 4.46 mL and CO equal to 6220 L min⁻¹. The time-interval, on which the integral is calculated (thermodilution curve not null), is considered equal to 2 s.

In order to evaluate the uncertainty of the integral in D, it is discretized with $\Delta t = 0.1$ s and $N = 20$:

$$D = \int_0^\infty (T(t) - T_b) dt = \Delta t \sum_{j=1}^N T_j - T_b \quad (2.4)$$

¹ Data extracted from the datasheet of MP20/30, MP40/50, MP60/70/80/90 Patient Monitor Intellivue, Philips, Inc.

where T_j is the value of $T(t)$ at the j -th time instant.

Applying the Eq. (2.2) to N , D and, then, to Q it is obtained:

$$\delta N = \sqrt{\left(\frac{\partial N}{\partial T_i} \delta T_i\right)^2 + \left(\frac{\partial N}{\partial T_b} \delta T_b\right)^2} = \sqrt{(-0.1)^2 + (0.1)^2} = 0.14 \text{ } ^\circ\text{C} \quad (2.5)$$

$$\delta D = \sqrt{\left(\frac{\partial D}{\partial T} \delta T\right)^2 + \left(\frac{\partial D}{\partial T_b} \delta T_b\right)^2} = \Delta t \cdot N \sqrt{(0.1)^2 + (-0.1)^2} = 0.28 \text{ } ^\circ\text{C} \cdot \text{s} \quad (2.6)$$

$$\begin{aligned} \delta CO &= \sqrt{\left(\frac{\partial CO}{\partial N} \delta N\right)^2 + \left(\frac{\partial CO}{\partial D} \delta D\right)^2} = \alpha \sqrt{\left(\frac{1}{D} \delta N\right)^2 + \left(-\frac{N}{D^2} \delta D\right)^2} = \\ &4.46 \sqrt{\left(\frac{1}{-1.59} 0.14\right)^2 + \left(\frac{-37}{-1.59^2} 0.28\right)^2} \cong 18.3 \frac{\text{mL}}{\text{s}} = 1096 \frac{\text{mL}}{\text{min}} \end{aligned} \quad (2.7)$$

δCO is about 17 % of the CO value.

It must be underlined that this theoretical approach takes into account only the accuracy of the two temperature sensors. Other sources of error, regarding the assumptions at the base of the method, the discrepancy between the model and the physiological behaviour, and all the concerns reported in the previous section, are not considered.

In the next section, the other “practical Gold Standard” will be analyzed.

2.3 Fick method

2.3.1 Measurement setup

As reported in Chapter 1, the aim of this work is introducing a method for the non-invasive assessment of CO on mechanically ventilated patients. The aim of the industrial project is integrating the features of the metabolic monitor Quark RMR, which bases its functioning principle on the indirect calorimetry: as it provides continuous measurements of the whole body oxygen uptake and carbon dioxide production, attention has been focused on studying a method based on gas-analysis.

The Fick method, describing the direct relation between pulmonary blood flow and respiratory gases concentrations, results the reference for all methods involving the analysis of gas for CO assessment. Moreover, as reported in the Section 2.1, it is one of the two “practical Gold Standards” together with thermodilution.

In the following an analysis of the accuracy of the Fick method will be reported with the aim to identify its limits and weaknesses.

As reported in the Chapter 1, the Fick equation has the following form:

$$PBF = \frac{\dot{V}_{O_2}}{CaO_2 - CvO_2} \quad (2.8)$$

$$CaO_2 = 10[(1.38 \cdot Hb \cdot SaO_2) + 0.003 \cdot PaO_2] \quad (2.9)$$

$$CvO_2 = 10[(1.38 \cdot Hb \cdot SvO_2) + 0.003 \cdot PvO_2] \quad (2.10)$$



In Eq.s (2.9) and (2.10) the two terms related to O_2 partial pressure into the plasma are often neglected [10]:

$$PBF = \frac{\dot{V}_{O_2}}{13.8 \cdot Hb \cdot (SaO_2 - SvO_2)} \quad (2.11)$$

$$CO = F \cdot PBF \quad (2.12)$$

Considering a mechanically ventilated patient, the measurement setup, which implements the direct Fick method, consists of:

- gas flowmeter placed at the ventilator outlet and oxygen sensor at the “Y” of the breathing circuit: \dot{V}_{O_2} [$mL \min^{-1}$];
- pulse oxymeter: SaO_2 [%];
- blood analyzer: Hb [$g \text{ dL}^{-1}$];
- fiber-optic catheter: SvO_2 [%].
- microprocessor and interface for the acquisition and elaboration of signals, and visualization of results.

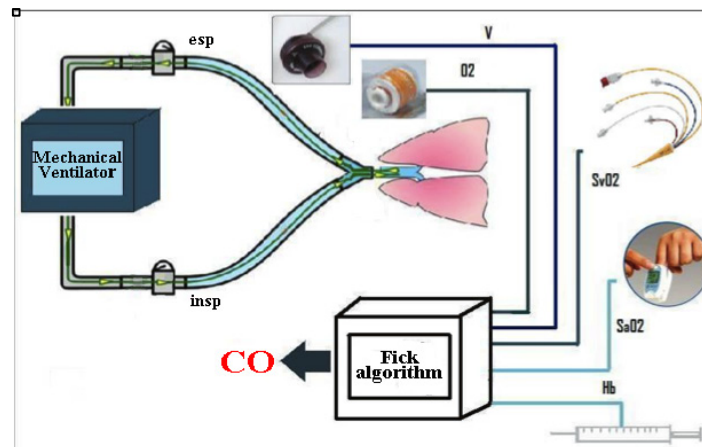


Figure 3 Schematic representation of the measurement setup for the implementation of the traditional Fick method on mechanically ventilated patients.

The gas flowmeter, the oxygen sensor and the pulse oxymeter are integrated in the Quark RMR (Cosmed s.r.l.): in fact, the system calculates \dot{V}_{O_2} and measures SaO_2 .

Hb is not measured continuously, but the values resulting from the blood sample analysis can be used as constant within the measuring period. Thus, performing the blood sample analysis with the same frequency adopted during the normal procedure in ICU and inserting the updated Hb value into the system whenever a new analysis will be performed result adequate: this is acceptable because it has been proved that the percentage of variance of Hb during the day is 1.7 % [15] and a mean variation of 0.08 g dL^{-1} is calculated when a blood sample is analyzed

every 3 hours. In the following this variation will be combined to the analyzer's accuracy in order to obtain the whole accuracy on Hb assessment every 3 hours.

The fiber-optic catheter is the unique invasive element, which allows a continuous measurement of the oxygen venous saturation.

In the following it will be described the influence on PBF estimation of the measurement accuracies of each parameter.

2.3.2 Sensitivity analysis of the traditional Fick method: a theoretical approach

Considering the PBF equation (Eq. 2.8), the Eq. (2.2) becomes:

$$\delta PBF = \sqrt{\left(\frac{\partial PBF}{\partial \dot{V}_{O_2}} \delta \dot{V}_{O_2}\right)^2 + \left(\frac{\partial PBF}{\partial Hb} \delta Hb\right)^2 + \left(\frac{\partial PBF}{\partial SaO_2} \delta SaO_2\right)^2 + \left(\frac{\partial PBF}{\partial SvO_2} \delta SvO_2\right)^2} \quad (2.13)$$

The degree to which erroneous measures of \dot{V}_{O_2} , Hb, SaO₂, and SvO₂ can influence PBF will be quantified as follows.

An error sensitivity can be introduced for each parameter (x_i) [16]:

$$I_{x_i} = \frac{\partial q}{\partial x_i} \cdot \frac{x_i}{q} \quad (2.14)$$

where q is the target variable.

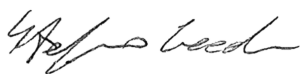
In the following table the I_x values and the partial derivatives are reported:

Table II Values of the sensitivity index for each parameter.

x_i	$\frac{\partial PBF}{\partial x_i}$	I_x
\dot{V}_{O_2}	$\frac{1}{13.8 \cdot Hb \cdot (SaO_2 - SvO_2)}$	1
Hb	$-\frac{\dot{V}_{O_2}}{13.8 \cdot Hb^2 \cdot (SaO_2 - SvO_2)}$	-1
SaO ₂	$-\frac{\dot{V}_{O_2}}{13.8 \cdot Hb \cdot (SaO_2 - SvO_2)^2}$	$-\frac{SaO_2}{SaO_2 - SvO_2}$
SvO ₂	$\frac{\dot{V}_{O_2}}{13.8 \cdot Hb \cdot (SaO_2 - SvO_2)^2}$	$\frac{SvO_2}{SaO_2 - SvO_2}$

The $I_{\dot{V}_{O_2}}$ and I_{Hb} , equal to 1 and -1 respectively, indicate that the percentage relative accuracy in the measurement of \dot{V}_{O_2} and Hb result into a percentage relative accuracy in the PBF assessment of the same entity: errors in \dot{V}_{O_2} measurement causes errors in PBF having same sign, whilst errors in Hb causes errors in PBF having opposite sign.

On the other hand, I_{SaO_2} and I_{SvO_2} depend on the parameters values.



With the aim to analyze variations of these indexes according to SaO_2 and SvO_2 values a simulation is provided. Typical ranges of SaO_2 and SvO_2 in physiological and pathological conditions are 90 % - 100 % and 60 % - 80 %, respectively.

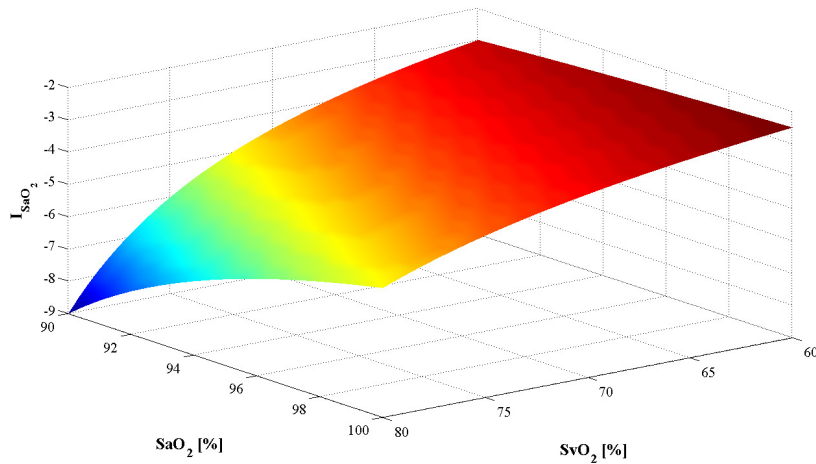


Figure 4 Trend of I_{SaO_2} in dependence of SaO_2 and SvO_2 values.

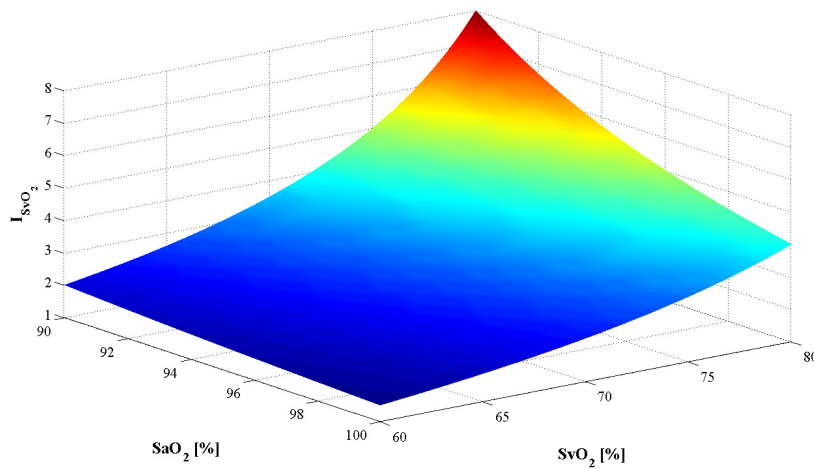


Figure 5 Trend of I_{SvO_2} in dependence of SaO_2 and SvO_2 values.

The values of the indexes reported in Fig. 4 and 5 have module always higher than 1, but present different signs: in particular errors in SvO_2 cause errors in PBF having the same sign, whilst errors in SaO_2 cause errors in PBF having the opposite sign.

Considering Eq. (2.13), the relative error in PBF measurement has the following expression:

$$\frac{\delta PBF}{PBF} = \sqrt{\left(\frac{\delta \dot{V}_{O_2}}{\dot{V}_{O_2}}\right)^2 + \left(-\frac{\delta Hb}{Hb}\right)^2 + \left(-\frac{SaO_2}{SaO_2 - SvO_2} \frac{\delta SaO_2}{SaO_2}\right)^2 + \left(\frac{SvO_2}{SaO_2 - SvO_2} \frac{\delta SvO_2}{SvO_2}\right)^2} \quad (2.15)$$

To make an example we can consider accuracy values of commercial devices, which could be potentially involved into the measurement. Taking into account the above-reported considerations about Hb assessment, at this stage, the calculation of the overall accuracy is performed when Hb is measured every 3 hours using, for example, the STKS (Beckman Coulter).

In [15] the hemoglobin was measured every hour on 7686 subjects during the diurnal period. If the four Hb values obtained within three consecutive hours are grouped, the calculated mean standard deviation takes into account the physiological variations during that period: $SD_{Hb}=0.08$ g dL⁻¹. Thus, the 3-hours physiological variability of Hb at a level of confidence of 95 %, assuming a Student's reference distribution with three degrees of freedom, has the following value [17]:

$$\delta_{Hb_{physiol}} [g dL^{-1}] = c_f \frac{SD_{Hb}}{\sqrt{4}} = 0.13 g dL^{-1} \quad (2.16)$$

$\delta_{Hb_{physiol}}$ is about 0.9 % of the mean value of Hb reported in [15] and the STKS accuracy in Hb measurement is ± 2 %; the whole accuracy $\frac{\delta Hb}{Hb}$ results the combination of sensor accuracy and physiological variability. In this case the two variables are independent:

$$\frac{\delta Hb}{Hb} = \sqrt{\left(\frac{\delta Hb}{Hb_{sens}}\right)^2 + \left(\frac{\delta Hb}{Hb_{physiol}}\right)^2} = \sqrt{4 + 0.8} = 2.2 \% \quad (2.17)$$

Table III Accuracy values of commercial devices.

<i>Parameter</i>	<i>Device</i>	<i>Range</i>	<i>Accuracy [%] at 95 % of confidence²</i>
\dot{V}_{O_2}	Deltatrac Metabolic Monitor-Datex Ohmeda	5-2000 mL min ⁻¹	± 5
SaO ₂	Satlite-Datex Instrumentarium	100-80 % 80-50 %	± 2 ± 3
SvO ₂	Vigilance-Edwards Lifesciences	30 -99 %	± 2
Hb	STKS-Beckman Coulter + physiological variability	0-30 g dL ⁻¹	± 2.2

Introducing the values reported in Table III into Eq. (2.15), the PBF relative uncertainty is:

$$\frac{\delta PBF}{PBF} [\%] = \sqrt{29.8 + 4 \frac{SaO_2^2 + SvO_2^2}{(SaO_2 - SvO_2)^2}} \quad (2.18)$$

With the aim to represent the trend of the relative uncertainty $\frac{\delta PBF}{PBF}$ a numerical simulation of Eq. (2.18) has been performed and its results are reported in Fig. 6.

² Data extracted from the datasheets of the devices.

The surface in Fig. 6 is obtained by plotting Eq. (2.18) on the identified range of SaO_2 and SvO_2 .

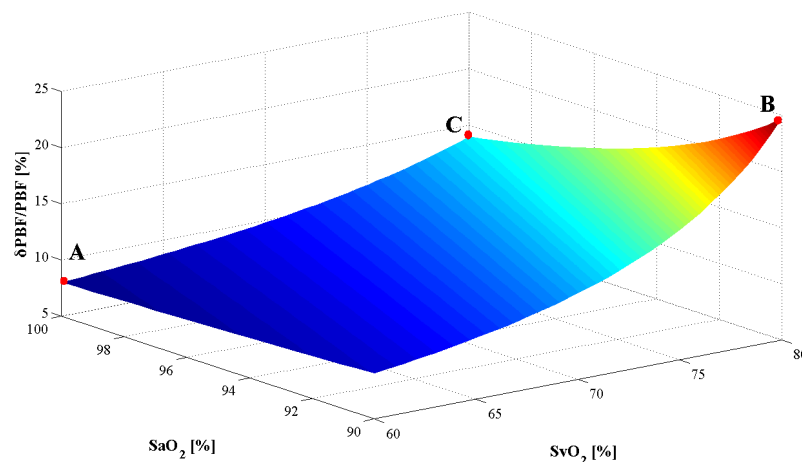


Figure 6 PBF relative error as a function of SaO_2 and SvO_2 . A and B represent the minimum and the maximum of the relative error, respectively.

From Fig. 6 it is clear that the lower artero-venous difference of O_2 saturation the higher the relative accuracy of PBF measurement: PBF, calculated by the Fick method, becomes increasingly unreliable as oxygen extraction falls. Points A ($\frac{\delta PBF}{PBF} \cong 8\%$) and B ($\frac{\delta PBF}{PBF} \cong 25\%$) represent the maximum and minimum relative accuracy in PBF assessment using the traditional Fick method.

As in ICU $F_{I O_2}$ values higher than environmental ones are often used (i.e., higher than 40%), SaO_2 value is frequently around 100%. This would guarantee accuracy values lower than 15% (point C) for each value of SvO_2 .

2.3.3 Sensitivity analysis of the traditional Fick technique: a numerical approach using the Monte Carlo method

A further analysis is performed by applying the Monte Carlo method [17], MCM, (see Appendix A) to the PBF equation: MCM allows the evaluation of PBF uncertainty as resulting from uncertainties in the assessment of each parameter of Eq. (2.11). Differently from the previous analysis, which estimates the uncertainty of the PBF from the uncertainty of the input quantities, MCM simulates the probability density function (PDF) of the output as a function of the PDFs of the input variables: these functions describe the distribution of N measurements around the mean value.

Considering that a certain number of measurements is performed for each parameter to estimate PBF, gaussian distributions are taken into consideration: mean values (\bar{x}_i) equal to physiological values for \dot{V}_{O_2} and Hb [16], and to the limits of range for SaO_2 and SvO_2 are chosen (Table IV). The standard deviations of the PDFs (Table IV) are obtained from the values of accuracy (Table III), which are considered as limits of accuracy corresponding to a level of confidence of 95 %. Considering that gaussian PDFs are used and that the number of samples, recommended by GUM, is $N=10^5$, the normalized standard deviations for the parameter x_i (S_{x_i}) are obtained as follows [13]:

$$S_{x_i} = \frac{Accuracy(x_i) \cdot \bar{x}_i}{1.96} \quad (2.19)$$

Table IV Values of the parameters used for the Monte Carlo simulation.

Configuration	$\bar{V}_{O_2}, S_{\dot{V}_{O_2}}$ [mL min ⁻¹]	\bar{Hb}, S_{Hb} [g dL ⁻¹]	$\bar{SaO_2}, S_{SaO_2}$ [%]	$\bar{SvO_2}, S_{SvO_2}$ [%]
A	200, 5	15.0, 0.2	100.0, 1.0	60.0, 0.6
B	200, 5	15.0, 0.2	90.0, 0.9	80.0, 0.8

The results of the application of MCM to the PBF estimation are reported in Fig. 7 for both configurations (A and B).

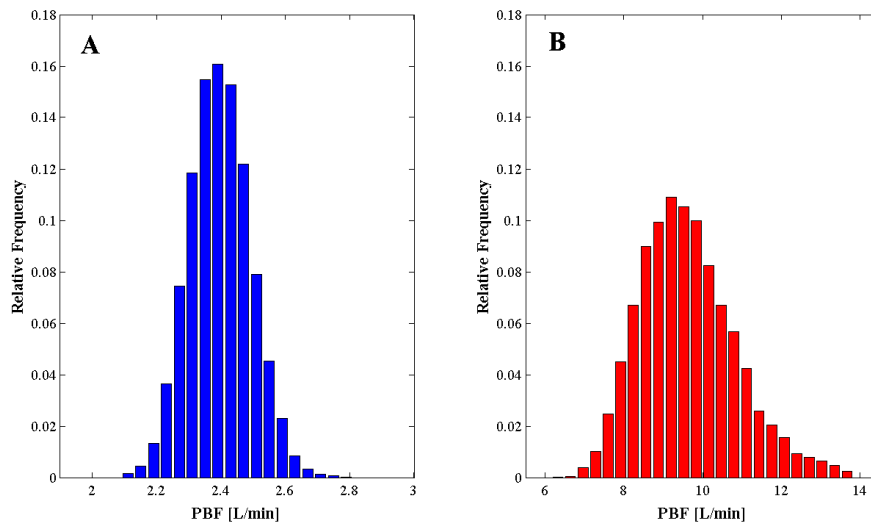


Figure 7 Probability density functions of PBF for the two parameter's configurations considered: A and B.

The PDFs reported in Fig. 7 are in agreement with the relative accuracy surface reported in Fig. 6. This can be demonstrated by calculating the relative accuracy in PBF assessment from the PDFs obtained using MCM:

$$\frac{\delta PBF}{PBF}_{MCM} [\%] = \frac{1.96 \cdot S_{PBF}}{PBF} \cdot 100 \quad (2.20)$$

The results are resumed in the following table:

Table V Comparison between relative errors obtained from the analytical approach and MCM.

Configuration	$\frac{\delta PBF}{PBF}$ [%]	$\frac{\delta PBF}{PBF_{MCM}}$ [%]
A	7.9	7.8
B	24.7	25.1

As results from the sensitivity analysis, the accuracy of the Fick method can be highly influenced by accuracy in the assessment of the artero-venous saturation difference, mostly if the two values of saturation (SaO_2 and SvO_2) are close one another. However, it should be taken into consideration that this difference is often higher than 20 % in mechanically ventilated patients, because $F_{I O_2}$ values are much higher (e.g., 50 %) than environmental one (about 21 %). Unfortunately SvO_2 measurement is the only one to be invasive, as \dot{V}_{O_2} can be measured at the mouth of the patient circuit of the ventilator, SaO_2 using a pulse-oxymeter placed at the patient's finger, and Hb can be considered constant and results from the blood analysis routinely performed to monitor the patient's state.

Considering that aim of this work is studying and implementing a non-invasive method for the CO estimation on mechanically ventilated patients, the measurement of SvO_2 using a fiber-optic catheter is not acceptable. To eliminate this element of invasivity, one of the indirect Fick methods, founded on a physiological model introduced by Kim *et al.* in 1966 [18], is chosen: it considers CO_2 as reference gas and involves a prolonged expiration.

In the following chapter the Quark RMR and its validation will be presented.

References

- ¹ Lehmann, K. G. and M. S. Platt. Improved accuracy and precision of thermodilution cardiac output measurement using a dual thermistor catheter system. *Journal of American College of Cardiology* 33(3):884-91, 1999.
- ² Sorensen, M. B., N. E. Bille-Brahe, and H. C. Engell. Cardiac output measurement by thermal dilution: reproducibility and comparison with the dye-dilution technique. *Ann. Surg.* 183:67-72, 1976.
- ³ Dhingra, V. K., J. C. Fenwick, K. R. Walley, D. R. Chittock, and J. R. Ronco. Lack of agreement between thermodilution and Fick cardiac output in critically ill patients. *Chest* 122:990-7, 2002.
- ⁴ Merjavy, J. P., J. W. Hahn, and H. B. Barner. Comparison of thermodilution cardiac output and electromagnetic flowmeter. *Surg. Forum* 25:145-7, 1974.
- ⁵ Wessel, H. U., M. H. Paul, G. W. James, and A. R. Grahn. Limitations of thermal dilution curves for cardiac output determinations. *J. Appl. Physiol.* 5:643-52, 1971.
- ⁶ Rocha, A. F., I. dos Santos, F. A. O. Nascimento, M. D. B. Melo, D. Haemmerich, and J. W. Valvano. Effects of the time response of the temperature sensor on thermodilution measurements. *Physiol. Meas.* 26(6):885-901, 2005.
- ⁷ Forrester, J. S., W. Ganz, G. Diamond, T. McHugh, D. W. Chonette, H. J. C. Swan. Thermodilution cardiac output determination with a single flow-directed catheter. *Am. Heart. J.* 83:306-311, 1972.
- ⁸ Botero, M., D. Kirby, E. B. Lobato, E. D. Staples, and N. Gravenstein. Measurement of cardiac output before and after cardio-pulmonary bypass: comparison among aortic transit-time ultrasound, thermodilution, and non-invasive partial CO₂ rebreathing. *J. Cardiothorac. Vasc. Anesth.* 18:563-572, 2004.
- ⁹ Bajorat, J., R. Hofmockel, D. A. Vagts, M. Janda, B. Pohl, C. Beck, and G. Noeldge-Schomburg. Comparison of invasive and less-invasive techniques of cardiac output measurement under different haemodynamic conditions in a pig model. *Eur. J. Anaesthesiol.* 23:23-30, 2006.
- ¹⁰ Brandi, L. S., R. Bertolini, M. Pieri, F. Giunta, and M. Calafà. Comparison between cardiac output measured by thermodilution technique and calculated by O₂ and modified CO₂ Fick methods using a new metabolic monitor. *Intensive Care Med.* 23:908-15, 1997.
- ¹¹ Ganz, W. and H. J. C. Swan. Measurement of blood flow by thermodilution. *Am. J. Cardiol.* 29:241-246, 1972.

- ¹² Mackenzie, J. D., N. E. Haites, and J. M. Rawles. Method of assessing the reproducibility of blood flow measurement: factors influencing the performance of thermodilution cardiac output computers. *Br. Heart J.* 55:14-24, 1986.
- ¹³ Joint Committee for Guides in Metrology (JCGM/WG1). Evaluation of measurement data—guide to the expression of uncertainty in measurement. *JCGM 2008;100*.
- ¹⁴ Geddes, L. A. Cardiac Output Measurement. *The Biomedical Engineering Handbook: Second Edition*. Ed. Joseph D. Bronzino Boca Raton: CRC Press LLC, 2000.
- ¹⁵ Pocock, S. J., D. Ashby, A. G. Shaper, M. Walker, and P. M. G. Broughton. Diurnal variations in serum biochemical and haematological measurements. *J. Clin. Pathol.* 42:172-179, 1989.
- ¹⁶ Feustel, P. J., R. J. Perkins, J. E. Oppenlander, H. H. Stratton, and I. L. Cohen. Feasibility of continuous oxygen delivery and cardiac output measurement by application of the Fick principle. *Am. J. Respir. Crit. Care Med.* 149:751-8, 1994.
- ¹⁷ Evaluation of measurement data-Supplement 1 to the “Guide to the Expression of uncertainty in Measurement”-Propagation of Distribution using Monte Carlo Method. *JCGM101:2008*.
- ¹⁸ Kim, T. S., H. Rahn, and L. E. Fahri. Estimation of true venous and arterial P_{CO_2} by gas analysis of a single breath. *J. Appl. Physiol.* 21(4):1338-1344, 1966.

Chapter 3

3.1 Introduction

The investigated method for the cardiac output estimation will be thoroughly described in the next chapter: it involves a prolonged expiration and it is completely based on the measurement of gas fractions and flow rate. The metabolic monitor Quark RMR (Cosmed s.r.l., Italy) is going to be used at this purpose. An *in-vitro* and *in-vivo* validation of the system are needed to assess its suitability to measurements on mechanically ventilated patients, at $F_{I}O_2$ different from the environmental one, and connected directly to the patient's circuit.

3.2 Quark RMR

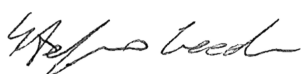
The introduction of advanced technology into the area of patient monitoring in Intensive Care Unit has made available many important measurements [1]. Among these, REE (Resting Energy Expenditure) is the preferred assessment of energy balance to provide appropriate nourishment to patients [2-5]. Indirect calorimetry allows the estimation of REE and RQ (Respiratory Quotient), in a non-invasive way, through the measurement of V_{O_2} (O_2 uptake) and V_{CO_2} (CO_2 production) [6]. This will be extensively explained in the following sections, as it is the working principle of the Quark RMR.

Since 1919, the Harris-Benedict Equation [7] has been used to predict a normal, nourished individual's REE, but this has been demonstrated to be unreliable in the malnourished and critically ill patients [8]. Being this equation based on anthropometric variables, correction factors were proposed for various clinical conditions in order to compensate for the poorly accurate estimation of REE [9]. However, these values are approximations and are not capable of determining the true REE in each critically ill patient.

The Quark RMR is a metabolic monitor for measurement of patient's energy requirement (by indirect calorimetry), which can be utilized for the evaluation of the clinical response to artificial feeding during long-term care or the admission into the ICU ward. It is important to quantify the energy requirements of critically ill patients because both overfeeding and underfeeding may be detrimental for the patient's clinical course and recovery. By directly measuring the REE it is possible to obtain the correct nutritional balance in critically ill patients, improving their response to medical therapies and thus, reducing the duration of stay in hospital with a significant impact on healthcare costs.

Considering that, the Quark RMR is essential for:

- clinical nutrition and research;
- Intensive Care Units;
- bariatric surgery;



- clinical assessment of neoplastic patients, burn patients, patients in neurovegetative coma or with transplants.

The main features of the system are:

- indirect calorimetry with continuous measurement of V_{O_2} , V_{CO_2} , REE, RQ, and metabolic substrates, i.e., fat, proteins, and carbohydrates;
- automatic quality control during the test by checking the gas concentrations;
- kit for ICU for the measurement on patients undergoing mechanically assisted ventilation;
- measurement kit with oxygen-enriched gas mixtures.

The Quark RMR utilizes a rapid infrared sensor for the CO_2 fraction assessment, and a paramagnetic one for the O_2 fraction (Table I). Both analyzers are reliable and do not need maintenance for long periods. The gas flow rate is measured by a turbine flowmeter (Table I).

In order to eliminate humidity, a special Nafion tubing, equalizing the humidity of sample gas to the level of ambient air, is used for the gas sampling line. All gas values are corrected to standard temperature and pressure, dry conditions (STPD).

Table I Sensor equipment of the Quark RMR.

Sensor	Functioning principle	Range	Accuracy	Response time
O_2	paramagnetic	0 % - 60 %	± 0.02 %	120 ms
CO_2	infrared	0 % - 10 %	± 0.02 %	100 ms
Gas flow	turbine flowmeter	0.08 L s^{-1} - 8 L s^{-1}	± 2 %	N/A

All data are elaborated by a software program, based on Cosmed proprietary algorithms, for the calculation of non-directly measured parameters, detection of the respiratory act and recognition of the inspiration and the expiration phase on the base of flow measurement and gas concentration trends. An auto-learning procedure is included to detect the ventilation bias flow (ϕ).

Three modalities of test execution are implemented:

Canopy Helmet: the Quark RMR is supplied with a dilution helmet of the expiratory flow for patient with spontaneous breathing. This method does not require a mouthpiece or facemask and is more comfortable for obese patients. Gas is sampled at the expiratory port through a sampling line, while the ventilation is measured by a turbine. The ventilation output of the helmet is regulated in order to maintain the $F_{E}CO_2$ within a prefixed range of values.

ICU: in the ICU setting, the Quark RMR can be integrated with the ventilator for the measurement of REE in patients undergoing mechanically assisted ventilation. During the test, it

is possible to measure the gas concentrations (O_2 and CO_2) and the ventilatory parameters, to detect ϕ , and to identify the inspiratory and expiratory phases with the use of an algorithm based on flow and expiratory CO_2 analysis.

Facial mask: simplified “breath-by-breath” analysis by using the Quark RMR with disposable facial masks on patients who are spontaneously breathing. The system performs real time measurement of patient’s inspiratory and expiratory flows (flowmeter at the mouth), and inspired and expired gas fractions ($F_{I}O_2$, $F_{E}O_2$, $F_{I}CO_2$, and $F_{E}CO_2$) through a sampling line applied to the flowmeter. This application is not frequently used in clinical and research settings, but it represents a valid alternative in commercial applications of weight management.

Before each test, the metabolic monitor needs to be calibrated: for the gas analyzers a certified mixture composed by 5 % of CO_2 and 15 % of O_2 is sampled, whilst the turbine flowmeter is calibrated through a syringe of 3 L.

3.3 In-vitro validation of the Quark RMR for its application on mechanically ventilated patients [10]

3.3.1 Overview

The calibration of an indirect calorimetry monitoring device requires an *in-vitro* test system allowing the realization of a known and fixed RQ, V_{O_2} , and V_{CO_2} . As the Quark RMR should work with artificially ventilated patients in intensive care environment, the calibration system includes a patient circuit coupling with a mechanical ventilator.

From a detailed analysis of the literature, two families of metabolism calibrators have been identified: the first is based on the delivery of known gas blending mixtures and the second on the realization of a chemical reaction for a single point calibration. In this study the interest is focused on the last method, being easier to perform and calibration not being the main focus of the research.

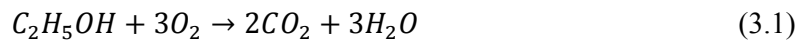
Damask *et al.* [11] showed that burning methanol inside a lung model provides a fixed value of RQ equal to 0.667. Takala *et al.* [12] burned ethanol in a lamp within a glass jar, which was connected to the inspiratory line of the ventilator. Miodownik *et al.* [13] designed and realized a quantitative methanol-burning lung model. Gas exchange measurements were validated over a wide range of $F_{I}O_2$, underlining the main issues related to the characterization of a metabolism simulator. More recently, Rosenbaum *et al.* [14] presented the development of a practical bench setup of a metabolic lung simulator to generate a wide range of reference values of V_{O_2} and V_{CO_2} . From the study of the literature, it emerges that a deep analysis of the uncertainty of RQ measurement has not been performed yet.

In this phase of the work an ethanol burning system is used to calibrate the Quark RMR metabolic monitor for the measurement of RQ, V_{O_2} , and V_{CO_2} , which are crucial in the proposed method for the assessment of CO. The calibration is carried out with regard to the mechanical ventilation mode (ICU mode) and involves the combustion of ethanol.

The implementation of the measurement model allows for the estimation of the overall accuracy of the metabolic monitor in calculating RQ by means of Monte Carlo method.

3.3.2 Theoretical background

The ethanol combustion reaction is



By considering the molar coefficients of the reaction (3.1) the ratio RQ is:

$$RQ = \frac{2}{3} = 0.667 \quad (3.2)$$

According to an algorithm, implemented into the Quark RMR and also in the majority of commercially available metabolic monitors, V_{O_2} is calculated by the following equation [15]:

$$V_{O_2} = V_I \cdot F_I O_2 - V_E \cdot F_E O_2 \quad (3.3)$$

and V_{CO_2} by a similar equation:

$$V_{CO_2} = V_E \cdot F_E CO_2 - V_I \cdot F_I CO_2 \quad (3.4)$$

where V_I and V_E are the inspiratory and expiratory volume, respectively, and $F_I X$ and $F_E X$ are the mean inspiratory and expiratory fractions of the gas X (with X=O₂, CO₂ or N₂).

The relation between V_I and V_E is given by the Haldane transformation, which assumes that the quantity of nitrogen (N₂) is constant in both inspired and expired gas. If there is no net nitrogen uptake, then V_I can be calculated by the following equation [15]:

$$V_I = \frac{F_E N_2}{F_I N_2} V_E \quad (3.5)$$

being $F_I N_2$ and $F_E N_2$ the mean inspired and expired nitrogen concentrations, respectively. Since the gases flowing into the ventilatory circuit are usually only O₂, CO₂ and N₂, then $F_I N_2$ and $F_E N_2$ can be calculated as follows:

$$F_I N_2 = 1 - F_I O_2 - F_I CO_2 \quad (3.6)$$

and


$$F_E N_2 = 1 - F_E O_2 - F_E CO_2 \quad (3.7)$$

By defining k as:

$$k = \frac{F_E N_2}{F_I N_2} \quad (3.8)$$

the formula for V_{O_2} becomes:

$$V_{O_2} = (k \cdot F_I O_2 - F_E O_2) V_E \quad (3.9)$$



and for V_{CO_2} is:

$$V_{CO_2} = (F_E CO_2 - k \cdot F_I CO_2) V_E \quad (3.10)$$

Then, the Quark RMR calculates RQ through the following expression:

$$RQ = \frac{V_{CO_2}}{V_{O_2}} = \frac{F_E CO_2 - k \cdot F_I CO_2}{k \cdot F_I O_2 - F_E O_2} \quad (3.11)$$

By substituting Eq.s (3.6), (3.7) and (3.8) in Eq. (3.11), RQ becomes:

$$RQ = \frac{F_E CO_2 (1 - F_I O_2 - F_I CO_2) - F_I CO_2 (1 - F_E O_2 - F_E CO_2)}{F_I O_2 (1 - F_E O_2 - F_E CO_2) - F_E O_2 (1 - F_I O_2 - F_I CO_2)} \quad (3.12)$$

Equation (3.12) shows that RQ depends only on the inspired and expired O_2 and CO_2 fractions.

Another definition, which will be useful in the next sections, is represented by the Wier equation [15]. This equation derives from the knowledge of the amount of O_2 and CO_2 consumed and produced, respectively, by the metabolism of the energetic substrates, i.e., fats, carbohydrates, and proteins [6].

$$REE [kcal \cdot die^{-1}] = (3.94V_{O_2} + 1.11V_{CO_2}) \cdot 1.44 \quad (3.13)$$

The percentage discrepancy between the theoretical (P^T) and measured (P^M) values of a generic parameter (P) is defined as follows:

$$E_P [\%] = \frac{P^M - P^T}{P^T} 100 \quad (3.14)$$

3.3.3 Experimental set-up

The burning unit

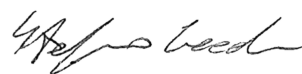
The main unit of the metabolic calibrator, used in this study, is the burning chamber: the jar into which the combustion reaction takes place.

It is constituted by a glass bell jar and a metal container, which presents an air inlet and an air outlet. The container has been designed in such a way to guarantee a good air mixing and avoid that an excessive airflow extinguishes the burning flame. The bell jar is equipped with a rubber O-ring to minimize the air leaks during the test. A ceramic vessel, which is filled of ethanol, is placed into the described closed volume (Fig. 1). A 5 mL graduated pipette (Brand GmbH & Co. KG, Germany) is used to measure the ethanol volume before and after the tests.

After the combustion reaction is started, the flow of fresh gases feeds continuously the flame and avoids the extinguishing. The whole system has an internal volume of 1200 mL.

The flame should be stable and small enough to match the relevant physiological range [16], and should have a blue color indicating a complete reaction.

The pneumatic circuit



Two different ventilators, Servo 900 C and Servo 300 A (Maquet GmbH & Co. KG, Germany), have been alternatively used to generate standard ventilatory patterns. The Servo 300 A has a ϕ equal to 2 L/min.

The turbine flowmeter (Fig. 1-3) of the Quark RMR (Fig. 1-5) is placed at the ventilator (Fig. 1-6) outlet and the gas sampling port (Fig. 1-4) is inserted in line with the patient circuit downstream to the 'Y': in this way it is possible to sample both "inspiratory" and "expiratory" gases. The burning unit (Fig. 1-1) and a test lung (Fig. 1-2), which simulates the compliance and the resistance of the respiratory system, are placed in series downstream the sampling port. The connections are made with same tubing to the one used in the clinical setup.

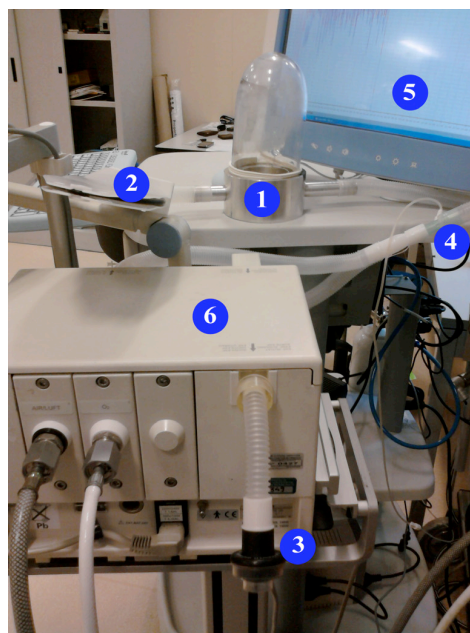


Figure 1 Experimental setup: burning unit (1), test lung (2), turbine flowmeter (3), gas sampling port (4), Quark RMR (5), mechanical ventilator (6).

Trials, in absence of a bias flow, are carried out with the Servo 900 C, whereas trials with bias flow are carried out with the Servo 300 A.

A volume controlled ventilation is chosen with a respiratory frequency of 20 bpm, minute volume of 7.5 L min^{-1} , and I:E ratio equal to 33%. Trials at different levels of PEEP and $F_{I\text{O}_2}$ are carried out. PEEP levels of 0 cmH₂O, 10 cmH₂O and 20 cmH₂O, and $F_{I\text{O}_2}$ values of 21 %, 40 % and 50 % are used.

During the inspiratory phase, the ventilator generates an airflow, which reaches the test lung passing through the burning unit, where the combustion reaction takes place and the gas fractions change according to the theoretical behaviour. In the expiration phase the gas flows into the expiratory circuit and it is discharged through the ventilator outlet.

Each test has duration of 5 minutes starting when the flame becomes stable and the RQ value varies less than 3 % between one breathing and the following (after the washing out of the circuit dead space).

3.3.4 Results

Quantitative tests

Quantitative trials are realized with the use of the described configuration at an $F_{I}O_2$ equal to 21% and PEEP 0 cmH₂O.

An amount of ethanol is burned until RQ, measured by the Quark RMR, reaches its steady value and maintains it for 5 minutes. The volume of ethanol, contained into the ceramic vessel before and after the test, is measured through the graduated pipette. The volume difference (V_C) gives the burnt amount of ethanol. As in STPD condition 1 mL of ethanol produces 764 mL of CO₂, the theoretical V_{CO_2} [mL] is calculated through the following equation:

$$V_{CO_2}^T = V_C \cdot 764 \quad (3.15)$$

A fixed value of RQ equal to 0.667 (Eq. 3.2) should be measured.

The discrepancy between the theoretical and measured values of V_{CO_2} and RQ are calculated according to Eq. (3.14) and reported in Table II.

The quantitative validation in ventilatory mode (ICU mode) confirms the reliability of the measurements on patients under mechanical ventilation: there is an average discrepancy rate of about 7% for the volume of CO₂ produced by the combustion, and about -8% for RQ.

Table II Measured data and discrepancies obtained with the ventilator configuration.

V_{CO_2} [mL]	$E_{V_{CO_2}}$ [%]	RQ_{mean}	E_{RQ} [%]
145.7	4.7	0.628	-5.8
306.4	-0.2	0.619	-7.2
137.9	9.8	0.586	-12.1
196.5	14.3	0.619	-7.2
210.0	8.4	0.611	-8.4

RQ estimation through the Monte Carlo method

With the aim to estimate RQ value and to perform the assessment of RQ uncertainty, the Monte Carlo method (MCM, Appendix A) is applied to the model described into the Eq. 3.12. Probability density functions (PDF) are assigned to the input quantities ($F_{I}O_2$, $F_{E}O_2$, $F_{I}CO_2$ and

F_ECO_2): Gaussian distributions with a mean value equal to the mean value of the measurements (μ) and a standard deviation (σ) equal to the normalized standard deviation of the measurements (S/\sqrt{N} , where S is the experimental standard deviation of the mean and N is the number of samples for each parameter) are chosen. The propagation of distributions is performed using the MCM in Matlab R2009a environment with a number of trials equal to 10^5 as recommended [17]. The data and the histograms concerning the input quantities in a particular ventilatory parameters setting (PEEP=0 cmH₂O, F_{IO_2} =21% and in absence of bias flow) are reported below (Table III and Fig. 2).

Table III Mean (μ), standard deviation (σ) and number of samples (N) of the input variables during the test at PEEP=0 cmH₂O, F_{IO_2} =21% and in absence of bias flow.

	μ [%]	σ [%]	N
F_{IO_2}	19.61	0.04	76
F_{EO_2}	15.25	0.04	76
F_{ICO_2}	0.82	0.03	76
F_{ECO_2}	4.02	0.03	76

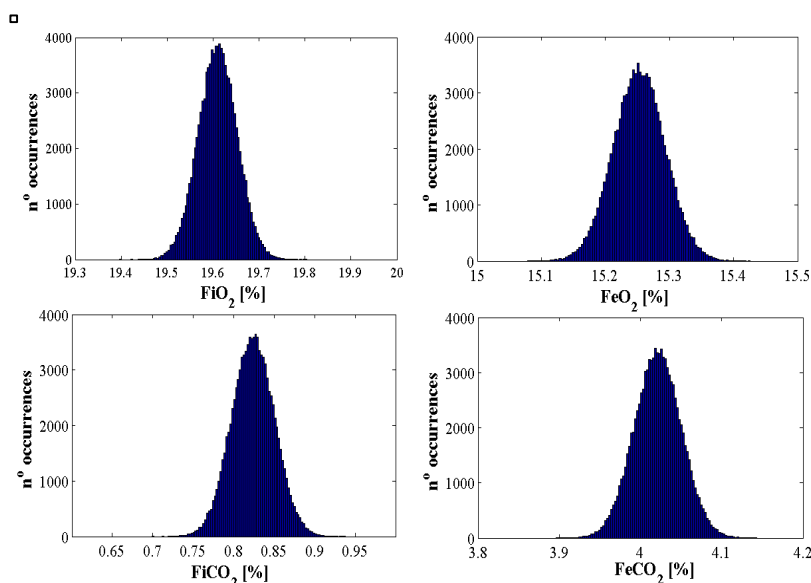


Figure 2 Histogram of each input (F_{IO_2} , F_{EO_2} , F_{ICO_2} and F_{ECO_2}) in the following setting: PEEP=0 cmH₂O, F_{IO_2} =21 % and in absence of bias flow.

The inaccuracy in the F_{IO_2} of delivered gas is also visible in Fig. 2: a bias is registered between average and desired F_{IO_2} values (19.6 % vs. 21 %).

Stefano Cecchini

The PDF of RQ obtained through the MCM (RQ_{MCM}) is compared with the PDF of RQ measured by the Quark RMR during the experimental trials. Three examples, at $F_{I}O_2$ equals to 21% and different PEEP levels, are reported below (Fig. 3).

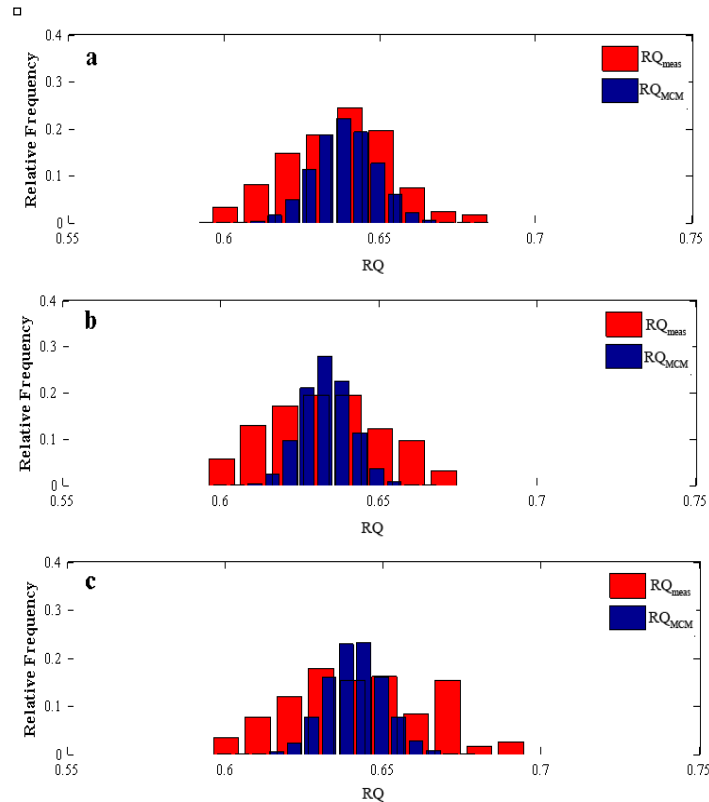


Figure 3 PDFs of RQ (blue) and measured data distributions (red) obtained from the trials in presence of bias flow, $F_{I}O_2=21\%$ and the following values for PEEP: 0 cmH₂O (a), 10 cmH₂O (b) and 20 cmH₂O (c).

As it can be seen in Fig. 3 the MCM histogram is less disperse than the measured one, showing, generally speaking, a lower standard uncertainty. RQ_{MCM} mean values differ from the mean values of RQ_{meas} less than 1.8%.

Considering the PDFs obtained through the MCM analysis for each configuration of the ventilatory parameters, the percentage discrepancy (E_{RQ} , Eq. 3.14) between the RQ calculated and the theoretical one (0.667, Eq. 3.2), and the standard uncertainty of the PDFs are reported in Tables IV and V. Values reported into these tables indicate that the Quark RMR has a good accuracy in estimating RQ and that the PDFs are not significantly scattered around the mean value.

The means of RQ_{meas} and RQ_{MCM} at the three PEEP levels, considering all the $F_{I}O_2$ settings, seem to grow with the decrease of PEEP. Both the “no bias flow” or the “bias flow” trials show this trend: the increase is about 5% going from PEEP 20 cmH₂O to 0 cmH₂O.

Stefano Cecchini

Table IV E_{RQ} [%] values at all the ventilatory settings.

No Bias Flow			
<i>PEEP/F_IO₂</i>	21 %	40 %	50 %
0 cmH ₂ O	-3.0	5.4	0.2
10 cmH ₂ O	4.2	0.4	-2.6
20 cmH ₂ O	3.0	-3.7	-3.4
Bias Flow			
<i>PEEP/F_IO₂</i>	21 %	40 %	50 %
0 cmH ₂ O	-3.9	-0.5	5.8
10 cmH ₂ O	-4.6	-5.7	5.5
20 cmH ₂ O	-3.3	-2.0	-9.3

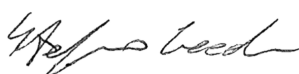
Table V Standard uncertainty of RQ_{MCM} at all the ventilatory settings.

No Bias Flow			
<i>PEEP / F_IO₂</i>	21 %	40 %	50 %
0 cmH ₂ O	0.01	0.06	0.04
10 cmH ₂ O	0.02	0.02	0.02
20 cmH ₂ O	0.02	0.01	0.03
Bias Flow			
<i>PEEP / F_IO₂</i>	21 %	40 %	50 %
0 cmH ₂ O	0.01	0.02	0.08
10 cmH ₂ O	0.01	0.02	0.08
20 cmH ₂ O	0.01	0.03	0.02

Resuming the main outcomes of this *in-vitro* study, a calibration method for a metabolic monitor, suitable for mechanically ventilated patients, is described and experimentally validated. Tests are performed with the Quark RMR, at different ventilation conditions (0 cmH₂O, 5 cmH₂O and 10 cmH₂O of PEEP; 21 %, 40 % and 50 % of F_IO₂; with and without bias flow).

The measurements show a good agreement with the theoretical values. An average error on the CO₂ production of about 7% is calculated through quantitative tests and an average percentage error equals to about 4% is calculated for RQ by using the Monte Carlo method.

These are objective evidences of the reliability of the Quark RMR measurements.



The results reported in this survey are in close agreement with those reported in other published studies [11,16,18].

The PDFs of RQ, evaluated through the MCM, have a mean value very close to the values measured by the metabolic monitor.

3.4 In-vivo validation of the Quark RMR [19]

3.4.1 Preamble

After the *in-vitro* study, a further survey has been performed *in-vivo* with the aim to verify the use of the Quark RMR equipment, with the ICU optional module and oxymeter, in intensive care wards for monitoring the ventilatory and metabolic parameters of patients undergoing mechanically assisted ventilation. As the Quark RMR is at the base of the CO estimation proposed in this study, it needs to be validated also on real patients.

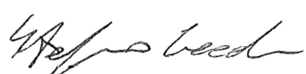
Some issues have been addressed in the metabolic monitoring of mechanically ventilated patients. Among them, one important issue is related to high values of PEEP that results critical for the correct functioning of the gas sensors [20]. Secondly, accurate measurements of $F_{I}O_2$ are essential in measuring V_{O_2} and RQ. This requires that a stable $F_{I}O_2$ is delivered to the patient throughout each breath and between breaths [21]. Stability thresholds of $F_{I}O_2$ become narrower with the decrease of inspired-expired oxygen difference [1]: this generally happens increasing the $F_{I}O_2$. Therefore, the higher the $F_{I}O_2$ the greater the potential error in measuring V_{O_2} [22,23].

Another issue is related to the bias flow (φ), even if the accuracy loss in metabolism assessment, caused by this flow, is still subject of debate [10,20,23]. Moreover, the interaction of φ with the breath identification algorithm needs further investigation.

The novelty of this work is investigating the effect of varying PEEP and $F_{I}O_2$ on the metabolic measurements (REE and RQ) in presence of φ . The accuracy of the metabolic monitor in measuring O_2 concentration is also analyzed through a comparison with the $F_{I}O_2$ delivered by the ventilator. Considerations about the potential effects of φ on the breathing act segmentation algorithm and the calculation of V_E are also reported.

The aims can be listed as follows:

- to verify that the measurements of ventilatory parameters (V_E , R_f , and $F_{I}O_2$) are consistent with the values indicated by the ventilator, and explain possible differences;
- to evaluate and characterize the potential effects of ventilatory settings on the parameters of interest;
- to evaluate how the system interfaces to the ventilator and identify potential interferences with the ventilator functioning;



- to verify that the RMR measured values are consistent with anthropometric values reported in literature (Harris-Benedict);
- to evaluate preventive measures for limiting the risk of cross-contamination during test execution.

3.4.2 Patients and protocol

The Quark RMR is utilized with the ICU module and oxymeter for the measurement of ventilatory and metabolic parameters, and oximetry.

12 patients, who underwent cardiac surgery under general anesthesia, are recruited in this study. During a deep sedation, the subjects are ventilated by Servo-i (Maquet GmbH & Co. KG, Germany) and Evita XL (Dräger AG & Co) ventilator, and their metabolic expenditure is monitored by the Quark RMR.

The study has been approved by the Ethical Committee of the University Campus Bio-Medico of Rome (Prot. N. 04/2010, March 31st 2010, ComEt CBM), and the recruited patients expressed their informed consent for the clinical protocol-based treatment and data collection.

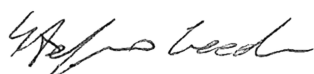
Patients are divided into two groups of 6. All patients are tested under two different ventilator modes (Pressure Control, PC, and Volume Control, VC): while in the Group 1, PEEP is maintained at a constant level of 5 cmH₂O with a variable F_IO₂, in the Group 2 the F_IO₂ is maintained constant at 50% with a variable PEEP. Six tests per patient are performed.

Variable limits are: 0 cmH₂O, 2 cmH₂O e 5 cmH₂O for the PEEP, and 21 %, 40 % and 50 % for the F_IO₂.

Patients are given a resting period of at least 60 minutes between the surgery and the test, and a pause of 5 minutes between each test, for the reaching of a steady ventilation after the setting modification.

The measurement set-up is displayed in Fig. 4 and consists of a sampling connector (A) between the Y circuit and the patient's mouth (in order to obtain inspiratory and expiratory air samples), a gas sampling line (B), and a turbine (E). This is connected at the ventilator outlet with the use of a wrinkled tube (G) and a dedicated adaptor (F).

A Nafion dryer tubing (C) has the property of removing moisture from the air sample, which is passing through the gas line, and an antisaliva filter (D) avoids water damages to the gas sensors of the Quark RMR.



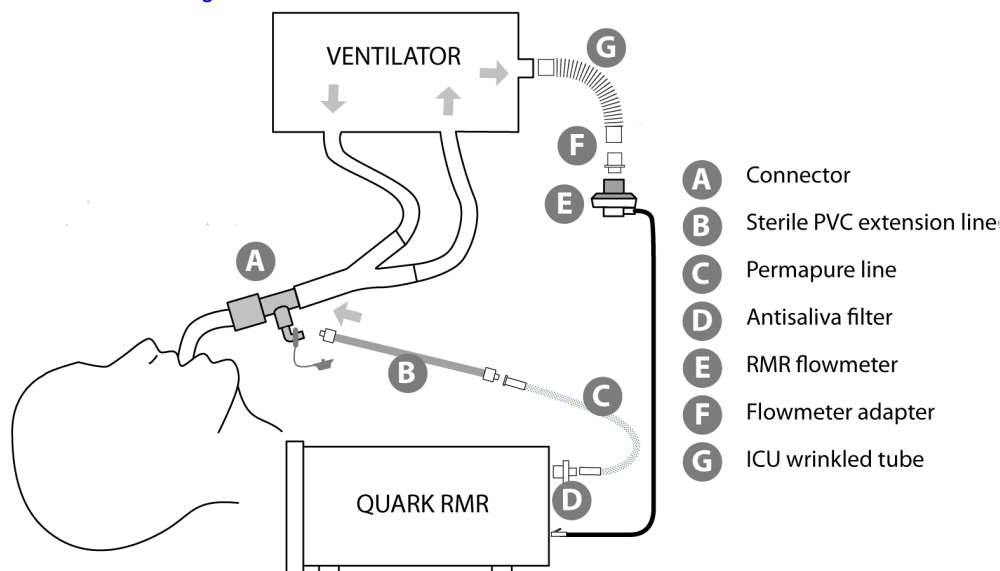


Figure 4 Schematic representation of the measurement set-up.

After connecting the breathing circuit to the patient (Fig. 4), it is essential to verify the ability of the Quark RMR to detect ϕ . Bias flow is automatically set at 2 L min^{-1} and is continuously delivered by the Servo-i in order to improve the ventilator's sensibility and reduce the response time to spontaneous triggering attempts by the patient. An auto-learning procedure enables the ICU software to compensate the parameter measurements in presence of this continuous flow. This is not necessary for the Evita XL, as it does not deliver a bias flow by default.

Each test has duration of about 20 minutes, during which the ventilatory settings remain unchanged and the breath-by-breath data are continuously collected by the Quark RMR. At the end of the test a report shows the averages and the ranges of variation of each parameter of interest (RQ , REE , V_{O_2} , V_{CO_2} , R_f , V_E , V_t , $F_{I O_2}$, SaO_2 , and $P_{et}CO_2$).

The software allows to delete those values that significantly differ from the mean, and the temperature at the flowmeter is manually set: this parameter, which is included into the algorithm of the ICU software, is considered 8°C below the temperature value set in the inspiratory branch using the humidifier MR 850-Fisher & Paykel (values between 28°C and 29°C). This consideration comes from an experimental observation conducted by placing a Type-K thermocouple sheathed with a flexible cuff (Y8102, Fluke Corp.) at the flowmeter and comparing the measured value with that one displayed by the humidifier: an average decrease of 8°C is registered.

The clinical trials have been individually stored on a breath by breath basis and the mean values, displayed on the final report, have been recorded in a summary table.

3.4.3 Results

Considering that this *in-vivo* survey is designed to test the performance and usability of the Quark RMR, when interfaced to the mechanical ventilator, also the results concerning the measurement procedure are of interest:

- the sensors' positioning (turbine and gas sampling line), as showed in Fig. 4, does not alter the correct functioning of the ventilators utilized in the present study; no alarms were activated nor any modifications of the gas delivery, with respect to the settings, were recorded. Regarding the ventilometry, during the inspiratory phase the turbine is excluded from the patient's circuit by the expiratory valve, which is closed, whereas during the expiratory phase the turbine is interested by the patient's expiratory flow. During this last phase, the introduction of the turbine flowmeter could only cause an increase of airway pressure related with a potential slowing of the expiration. In the worst case, this could be associated with the risk of air-trapping. However, this event does not occur as demonstrated by the perfect matching between the displayed flow curves before and after the introduction of the turbine at the ventilator outlet and by the inactivity of the "high airway pressure" alarm during all the tests performed.
- the measurement devices are applied to the ventilator with particular care to avoid contamination risks for the patient: the turbine (positioned at the ventilator outlet) is interested by the patient's expiratory flow, which is released into the ambient air without any risks of cross-contamination, whereas the disposable sampling line is connected by a dedicated extension, which is also disposable.

Other purpose of the present study is to identify and quantify possible influencing factors on Quark RMR performance such as: ventilatory mode, level of PEEP and $F_{I}O_2$.

Therefore, we separated the measured parameters in two categories:

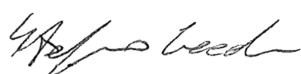
1. parameters that can be compared with the ones set on the ventilator (V_E , R_f , $F_{I}O_2$): category 1.
2. parameters, which cannot be compared with a reference value (RQ , REE , V_{O_2} , V_{CO_2} , SaO_2 , and $P_{et}CO_2$): category 2.

For the category 1, an error analysis has been performed by comparison with the parameter values measured by the ventilator.

For the category 2, an intra-patient analysis has been performed by varying the ventilatory mode and comparing the measured values of the same parameter.

Parameters of category 1

The discrepancy (EG), for the generic parameter (G), is calculated by the following equation:



$$EG = \frac{|GQ - GV|}{GV} 100 \quad (3.16)$$

Tables VI and VII display the mean deviations between values measured by the Quark (GQ) and those measured by the ventilator (GV). The mean deviation value of each group is shown in each cell, whereas the overall mean values are in the right-end column.

Analyzing the values for each row, it should be noticed that neither the $F_{I}O_2$ nor the PEEP causes a systematic discrepancy on the measurement by Quark RMR.

For the V_E , R_f , and $F_{I}O_2$ mean discrepancies lower than 7.05 %, 1.78 % and 5.53 % are recorded, respectively.

Table VI Mean discrepancies between measured values by the Quark RMR and by the ventilator, with regards to the Group 1.

$F_{I}O_2$ [%]	21	40	50	Mean
Pressure Controlled Mode				
Discrepancy V_E [%]	2.61	2.43	3.63	2.89
Discrepancy R_f [%]	0.17	0.72	1.25	0.71
Discrepancy $F_{I}O_2$ [%]	5.53	1.05	0.53	2.37
Volume Controlled Mode				
Discrepancy V_E [%]	2.76	2.15	1.92	2.28
Discrepancy R_f [%]	0.31	0.33	0.14	0.26
Discrepancy $F_{I}O_2$ [%]	4.79	1.16	0.57	2.17

Table VII Mean discrepancies between measured values by the Quark RMR and by the ventilator, with regards to the Group 2.

PEEP [cmH ₂ O]	0	2	5	Mean
Pressure Controlled Mode				
Discrepancy V_E [%]	6.30	4.05	3.68	4.68
Discrepancy R_f [%]	1.78	1.26	0.30	1.11
Discrepancy $F_{I}O_2$ [%]	0.58	0.52	0.56	0.55
Volume Controlled Mode				
Discrepancy V_E [%]	7.05	4.76	4.02	5.28
Discrepancy R_f [%]	1.67	0.56	0.59	0.94
Discrepancy $F_{I}O_2$ [%]	1.17	1.25	0.57	1.00

Bland-Altman plots (Fig.s 5 and 6) are used to evaluate the agreement between the Quark RMR and the ventilators about the measurement of V_E and $F_{I}O_2$. In Fig. 5 we report data coming from

Stefano Cecchini

all the tests (6 for each patient, corresponding to a total of 72 tests): on the x axis the averages of V_E values, measured by the Quark RMR and the ventilator, are reported, whereas their differences are represented on the y axis. The two dashed lines represent the limits of accuracy (LoA) of the Servo-i for the expiratory volume measurement ($\pm 8\%$ - Servo-i User's Manual), whereas the two solid lines are the LoA guaranteed by the Evita XL ventilator ($\pm 10\%$ - Evita XL User's Manual).

The same representation is utilized for the $F_{I}O_2$. As the effects of $F_{I}O_2$ variations are evaluated only in the Group 1, in Fig. 6 the tests belonging from this group are considered. The Servo-i assures limits of accuracy, in the O_2 fractions delivery, of $\pm 3\%$ (Servo-i - User's Manual), whereas the Evita XL assures the greater value between $\pm 5\%$ of the displayed $F_{I}O_2$ and $\pm 2\%$ (Evita XL - User's Manual) (Fig. 6).

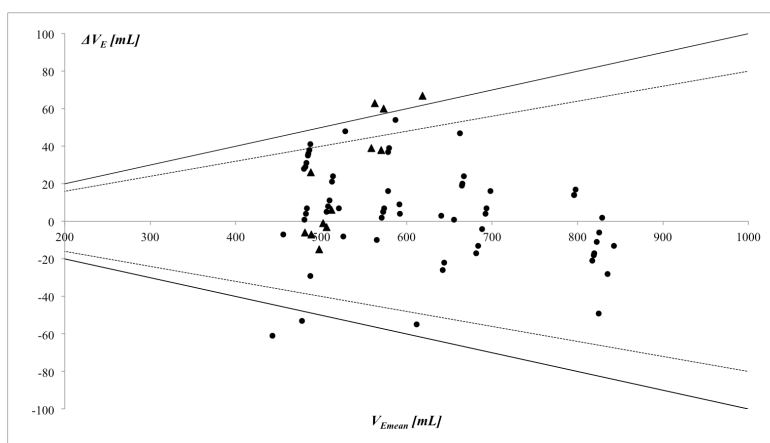


Figure 5 Agreement between the Quark RMR and ventilators about the measurement of V_E : (•) Servo-i measurements, (▲) Evita XL measurements, (--) limits of accuracy Servo-i, (-) limits of accuracy Evita XL.

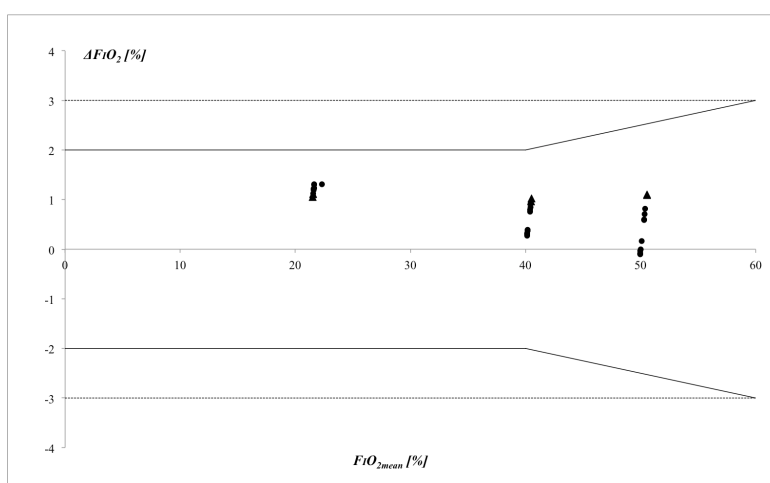


Figure 6 Comparison between the $F_{I}O_2$ levels measured by the Quark RMR and generated by the ventilators: (•) Servo-i, (▲) Evita XL, (--) limits of accuracy Servo-i, (-) limits of accuracy Evita XL.

Stefano Cecchini

It is noticeable that in Fig. 5 almost all the tests are inside the limits of ventilator accuracy. The mean deviation's rate for the V_E measurement between the Quark RMR and ventilators is about 3.5 %. The trials belonging to the Group 1 (fixed PEEP) seem to show a better agreement between the Quark RMR and the ventilator (mean difference of about 2.6 %) than the trials belonging to the Group 2, at a fixed $F_{I}O_2$, (mean difference of about 5 %).

In Fig. 6 it should be noticed that the limits of accuracy of the $F_{I}O_2$ delivered from the ventilator exceed the measurement discrepancy of the Quark RMR. According to the data reported in Tables VI and VII, the average error in $F_{I}O_2$ measurement is about 1.5 %.

The breath identification algorithm seems to be effective, even in presence of the bias flow: the mean discrepancy in the R_f measurement, considering all the 72 trials, is lower than 1 %. Considering that the patients are deeply sedated, i.e. no spontaneous breathings are detected, this endpoint demonstrates that the algorithm for the segmentation of respiratory trend is able to reject the influence of φ : in particular the procedure of φ detection allows the system to shift the threshold, for the breathing act recognition, of the right quantity to make a reliable breathing segmentation.

The described approach, in which some measurements obtained from the metabolic monitor are compared to the respective obtained from the pulmonary ventilator, could give a method to assess the correct functioning of the monitor, when used in mechanically ventilated patients, in presence of φ , as also reported *in-vitro* [10].

The good agreement reported above is a satisfying starting point for the CO assessment on mechanically-ventilated patients with the use of the Quark RMR.

Parameters of category 2

Histograms are reported below. They are related, for each patient, to each of the following parameter: V_{O_2} , V_{CO_2} , RQ and REE. Patients undergoing mechanical ventilation by the Evita XL are marked by the sign "XL".

Uncertainty bars are also reported: these are obtained using the law of propagation of uncertainty [24], which considers the measurement model of the Quark RMR (Section 3.3.2) and the accuracy values of the system's sensors (Table I).

Group 1

Pressure Control Mode (PC)

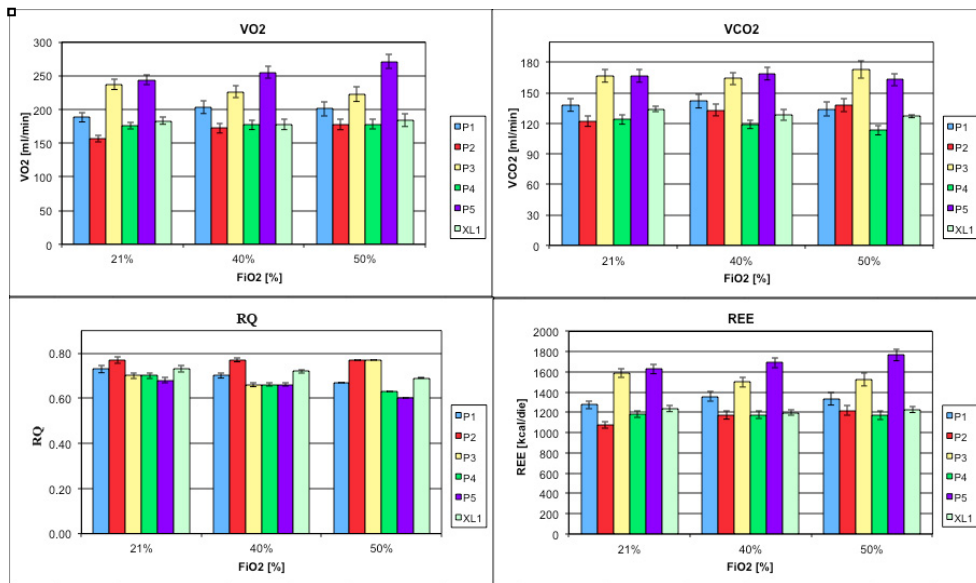


Figure 7 Results from the Group 1 in Pressure Control Mode (PC).

Volume Control Mode (VC)

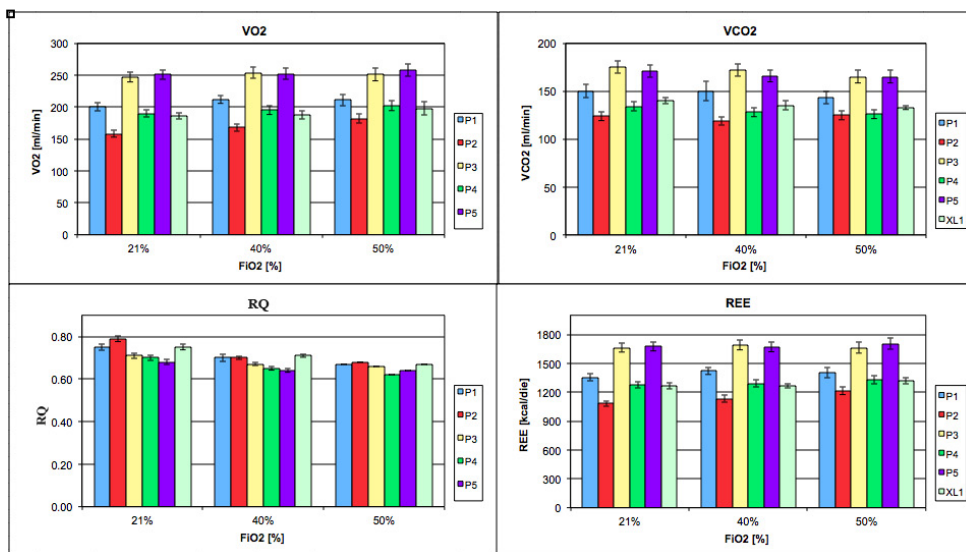


Figure 8 Results from the Group 1 in Volume Control Mode (VC).

As documented in previous studies [21,25,26], an increase in V_{O₂} related to the F_IO₂ increment has been observed, with a consequent decrease and increase of the RQ and REE values, respectively.

Table VIII reports RQ and REE mean values and standard deviations (SD) for both ventilation modes at different F_IO₂ values: the averages of REE and RQ do not show significant variations

Stefano Cecchini

as a function of $F_{I}O_2$. However, a slight variation as a function of $F_{I}O_2$ is deducible if an intra-patient analysis is conducted: i.e. changing $F_{I}O_2$ from 21 % to 40 %, the value of RQ decreases in 10 trials out of 11, whilst the only one left shows a constant RQ, and changing $F_{I}O_2$ from 40 % to 50 % the value of RQ decreases in 9 trials out of 11. These trends could be explained by the experimentally estimated increase of V_{O_2} with $F_{I}O_2$ (+3.3 % from $F_{I}O_2=21$ % to $F_{I}O_2=40$ %, and +5.9 % from $F_{I}O_2=21$ % to $F_{I}O_2=50$ %).

Table VIII Mean (SD) values of REE and RQ for the Group 1.

VC	REE _{mean} (SD) [kcal die ⁻¹]	RQ _{mean} (SD)
FiO ₂ =21 %	1411 (260)	0.726 (0.044)
FiO ₂ =40 %	1442 (242)	0.674 (0.025)
FiO ₂ =50 %	1462 (212)	0.654 (0.024)
PC	REE _{mean} (SD) [kcal die ⁻¹]	RQ _{mean} (SD)
FiO ₂ =21 %	1360 (262)	0.716 (0.035)
FiO ₂ =40 %	1381 (221)	0.690 (0.048)
FiO ₂ =50 %	1404 (246)	0.688 (0.079)

Group 2

Pressure Controlled Mode (PC)

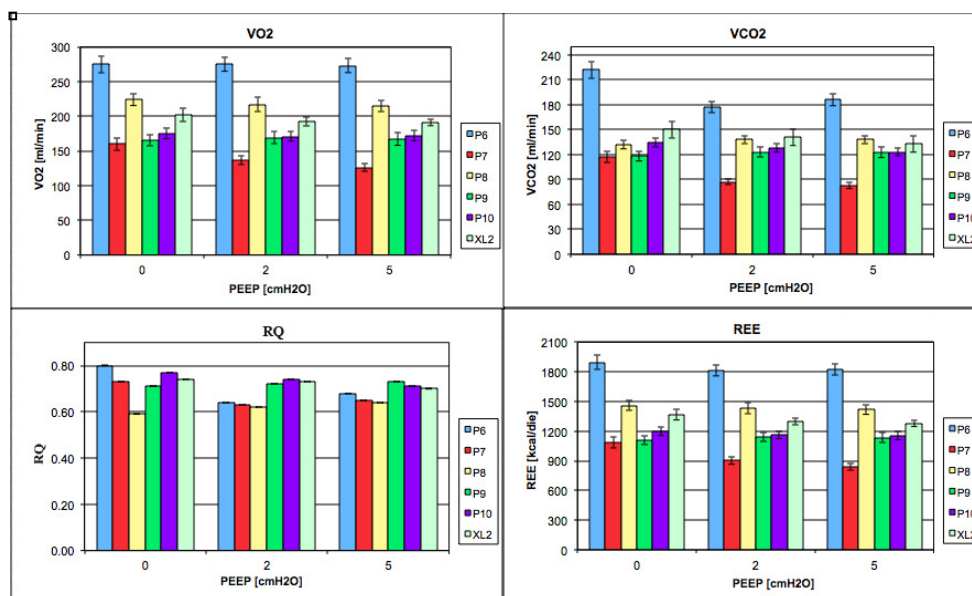


Figure 9 Results from the Group 2 in Pressure Control Mode (PC).

Volume Control Mode (VC)

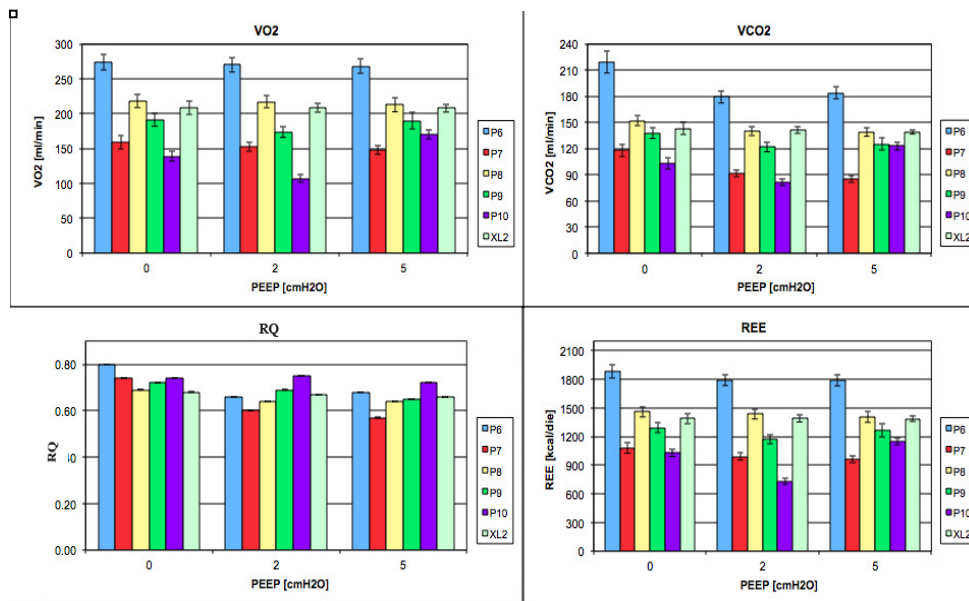


Figure 10 Results from the Group 2 in Volume Control Mode (VC).

From an intra-patient analysis, PEEP does not seem to have a net influence on the values of RQ and REE.

Defining F as the generic parameter, \bar{F} is the average obtained from 3 tests: i.e., considering each patient in each ventilatory mode. S_F represents the dispersion of measurements respect on \bar{F} .

If we indicate as F_1 , F_2 and F_3 the three values, which F assumes in each of the 3 tests by varying $F_{I}O_2$ (Group1) and PEEP (Group 2), S_F can be expressed by the following formula:

$$S_F[\%] = \frac{|\bar{F}-F_1|+|\bar{F}-F_2|+|\bar{F}-F_3|}{3\bar{F}} 100 \quad (3.17)$$

By calculating the mean (M_F) of the S_F of patients belonging to one group, we obtain a global index that quantifies the influence of $F_{I}O_2$ and PEEP on the measurement of single parameters.

In Table IX the M_F values of the six parameters of interest are also displayed: V_{O_2} , V_{CO_2} , RQ, REE, SaO_2 , and $P_{et}CO_2$.

The introduced index (M_F) is smaller for $F_{I}O_2$ variations (max: 4.3 %, for the $P_{et}CO_2$) than PEEP variations (max: 7.6 %, for the V_{CO_2}). In this respect, we can assume that an increase in the analyzers pressure may alter the measurement of the O_2 and CO_2 concentrations.

Looking at Table IX, and particularly at the mean values, it can be noticed that the variation in the ventilatory mode does not significantly affect the mean values of each parameter of interest in both the groups.

Table IX \bar{F} and M_F for the parameters belonging from the Category 2 for each group.

Group	Group 1 (variable F ₁ O ₂)		Group 2 (variable PEEP)	
<i>Ventilatory Mode</i>	<i>PC</i>	<i>VC</i>	<i>PC</i>	<i>VC</i>
\bar{V}_{O_2} [mL · min ⁻¹]/M _{V_{O₂} [%]}	202/2.6	211/2.4	195/2.5	195/3.9
\bar{V}_{CO_2} [mL · min ⁻¹]/M _{V_{CO₂} [%]}	142/2.6	146/2.0	136/5.9	135/7.6
\bar{RQ} /M _{RQ} [%]	0.70/3.2	0.69/4.0	0.70/3.9	0.68/4.7
Group	Group 1 (variable F ₁ O ₂)		Group 2 (variable PEEP)	
<i>Ventilatory Mode</i>	<i>PC</i>	<i>VC</i>	<i>PC</i>	<i>PC</i>
\bar{REE} [kcal · die ⁻¹]/M _{REE} [%]	1352/2.3	1412/1.8	1307/3.0	1320/4.8
$\bar{SaO_2}$ [%]/M _{SaO₂} [%]	95/1.6	93/2.7	94/1.9	99/0.0
$\bar{PetCO_2}$ [mmHg]/M _{PetCO₂} [%]	22/4.3	24/2.3	23/3.3	23/4.9

Comparison with REE predicted values

In the clinical practice a lot of predictive equations have been used, since the beginning of the last century, to estimate REE from sex and anthropometric variables like age, height and weight [27]. As reported in the Section 3.2, the most used one is the Harris-Benedict equation [7]:

$$REEman[kcal \cdot die^{-1}] = 66.5 + 13.8 \cdot weight[kg] + 5.00 \cdot height[cm] - 6.78 \cdot age[years] \quad (3.18)$$

$$REEwoman[kcal \cdot die^{-1}] = 655 + 9.56 \cdot weight[kg] + 1.85 \cdot height[cm] - 4.68 \cdot age[years] \quad (3.19)$$

A comparison between REE measured by the Quark RMR (Eq. 3.13) and the predicted values of REE, estimated using the Harris-Benedict's equation, is reported below.

Group 1

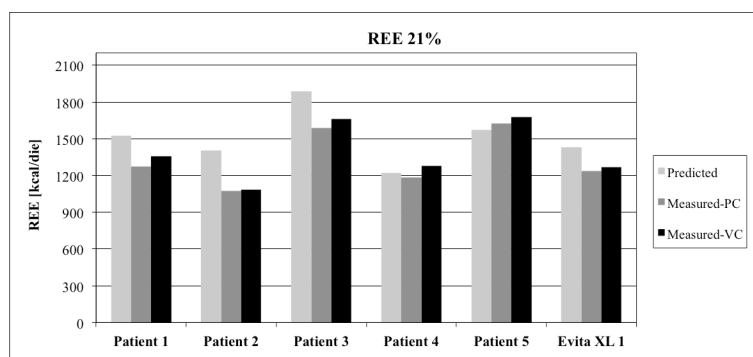


Figure 11 Comparison between predicted and measured values of REE, for both Pressure Control Mode (PC) and Volume Control Mode (VC), F₁O₂=21 % and PEEP=5 cmH₂O.

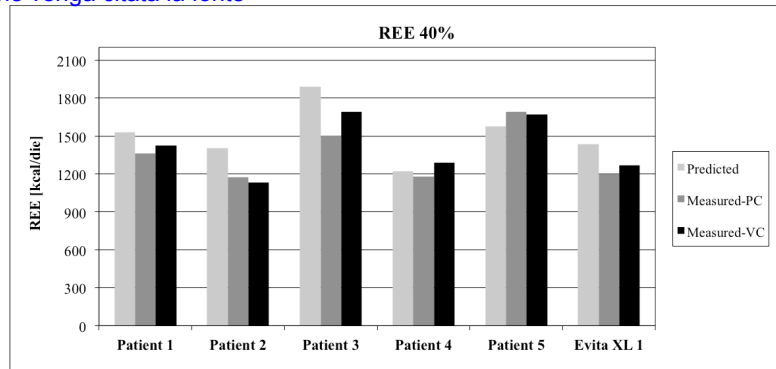


Figure 12 Comparison between predicted and measured values of REE, for both Pressure Control Mode (PC) and Volume Control Mode (VC), $F_{I}O_2=40\%$ and $PEEP=5\text{ cmH}_2\text{O}$.

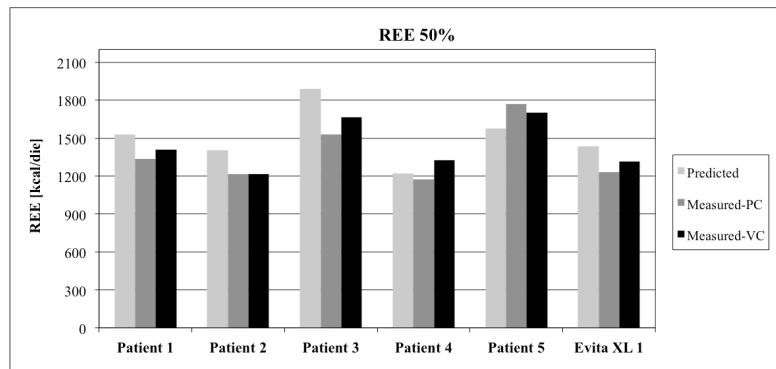


Figure 13 Comparison between predicted and measured values of REE, for both Pressure Control Mode (PC) and Volume Control Mode (VC), $F_{I}O_2=50\%$ and $PEEP=5\text{ cmH}_2\text{O}$.

Group 2

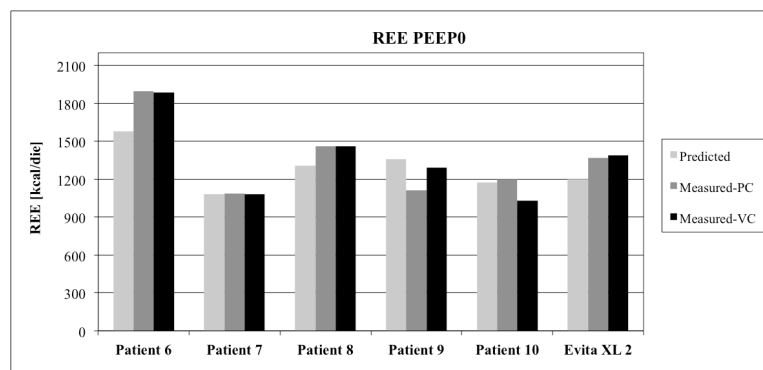


Figure 14 Comparison between predicted and measured values of REE, for both Pressure Control Mode (PC) and Volume Control Mode (VC), $F_{I}O_2=50\%$ and $PEEP=0\text{ cmH}_2\text{O}$.

Stefano Cecchini

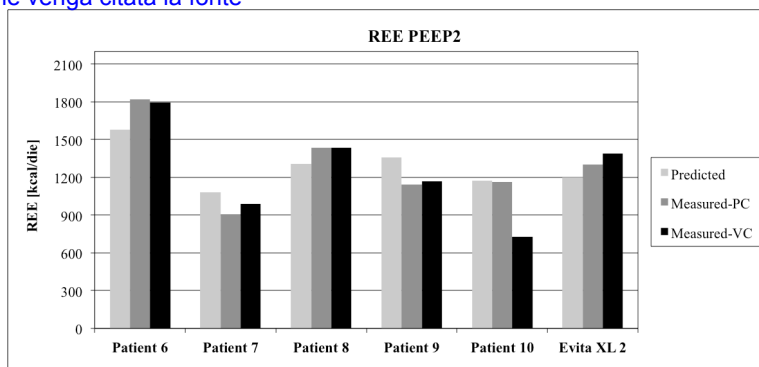


Figure 15 Comparison between predicted and measured values of REE, for both Pressure Control Mode (PC) and Volume Control Mode (VC), $F_{I}O_2=50\%$ and $PEEP=2\text{ cmH}_2\text{O}$.

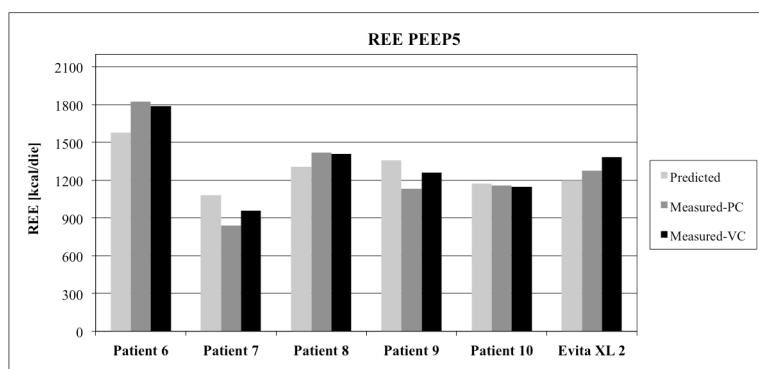


Figure 16 Comparison between predicted and measured values of REE, for both Pressure Control Mode (PC) and Volume Control Mode (VC), $F_{I}O_2=50\%$ and $PEEP=5\text{ cmH}_2\text{O}$.

In the histograms the predicted REE values (Eq.s 3.18 and 3.19) are compared with the values measured under different ventilatory conditions.

A detailed analysis of these data is performed by finding the correlation between measured and predicted values, and with the use of Bland-Altman analysis for both the ventilatory modes.

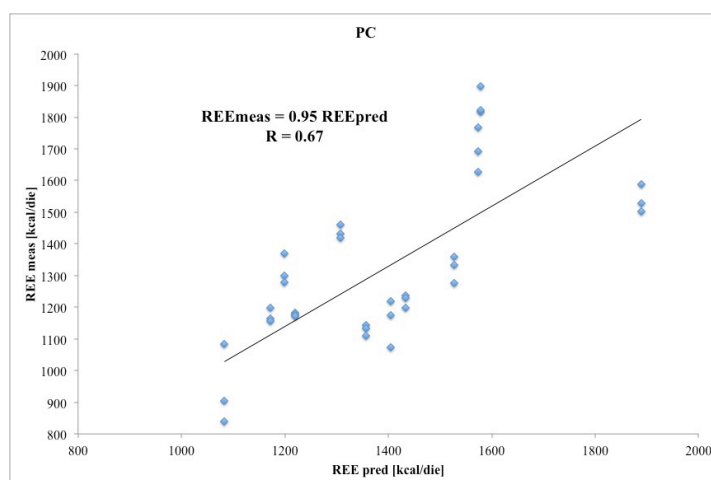


Figure 17 Comparison between predicted and measured values of REE for Pressure Control Mode.

Stefano Cecchini

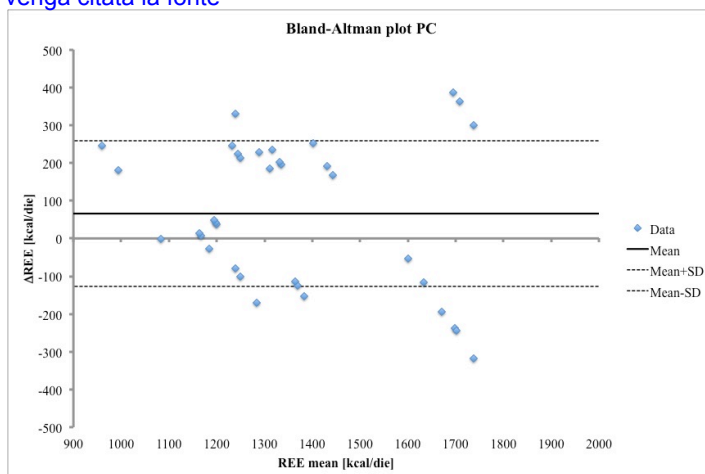


Figure 18 Bland-Altman representation between predicted and measured values for Pressure Control Mode.

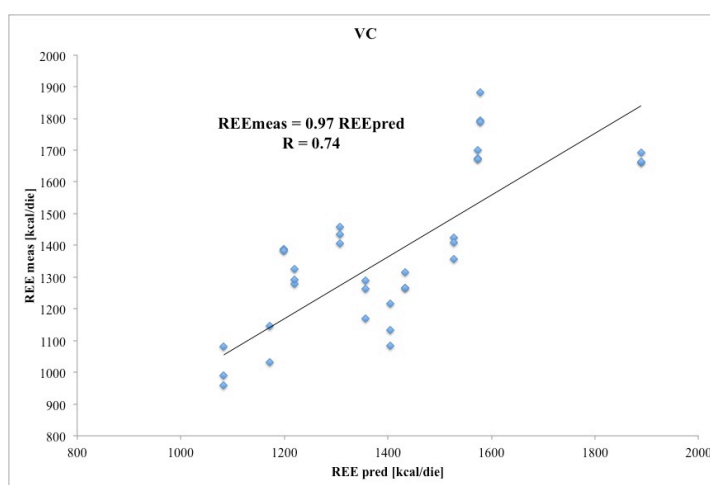


Figure 19 Comparison between predicted and measured values of REE for Volume Control Mode.

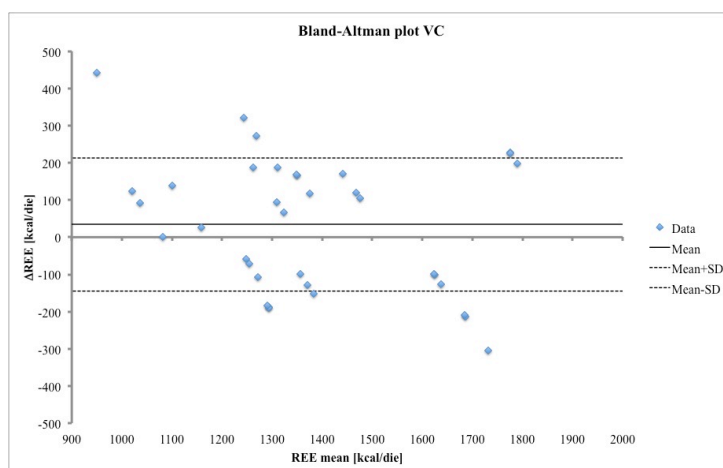


Figure 20 Bland-Altman representation between predicted and measured values for Volume Control Mode.

The coefficients of the linear regressions (Figs. 17 and 19) are both close but slightly lower than 1: this indicates that the predicted values obtained with the Harris-Benedict equation, on average,

Stefano Cecchini

overestimate the measurements of the Quark RMR. This is clearly shown in the Bland-Altman plots (Figs. 18 and 20) where the overestimation is on average 66 kcal die^{-1} , in PC mode, and 34 kcal die^{-1} , in VC mode.

In conclusion it should be underlined that:

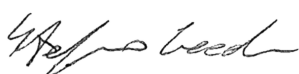
- the Harris-Benedict equation does neither consider the ventilatory settings, nor any spontaneous triggering attempt by the patient: on the other hand, the effective energy consumption could be influenced by these two factors. As a confirmation of this, in this survey a slight dependence of V_{O_2} from $F_{I}O_2$ has been found.
- as the breathing activity is under a “permissive” control in sedated patients, the presence of hyper- or hypo-ventilation may modify the energy consumption; therefore, direct measurements are more reliable.

These studies (*in-vitro* and *in-vivo*) results helpful in the evaluation of the Quark RMR in terms of measuring performance of ventilatory and metabolic parameters, when the monitor is interfaced to a mechanical ventilator. The overall satisfactory results obtained, in terms of accuracy, allow further research on the application of the Quark RMR to the non-invasive assessment of CO on mechanically ventilated patients. Stable behaviour and low discrepancies are fundamental, as the proposed method is based, almost exclusively, on the outputs of the metabolic monitor.

In the next chapter the method will be thoroughly described, starting from physiological notions, the measurement setup will be introduced and the main results will be presented.

References

- ¹ Browning, J. A., S. E. Linberg, S. Z. Turney, and P. Chodoff. The effects of a fluctuating $F_{I}O_2$ on metabolic measurements in mechanically ventilated patients. *Crit. Care Med.* 10:82-85, 1982.
- ² Brandi, L. S., R. Bertolini, and M. Calafà. Indirect calorimetry in critically ill patients: clinical application and practical advice. *Nutrition* 13:349–358, 1997.
- ³ Singer, P. and J. Cohen. Indirect calorimetry and metabolic monitoring. In *Textbook of Critical Care*, M. Fink, E. Abraham, J. L. Vincent, and P. M. Kochanek editors. Philadelphia: Elsevier Saunders, pp. 1895–1898, 2005.
- ⁴ Singer, P. The tight calorie control study (TICACOS): a prospective, randomized, controlled pilot study of nutritional support in critically ill patients. *Intensive Care Medicine* 37:601-609, 2011.
- ⁵ Strack van Schijndel, R. J. M., P. J. M. Weijs, R. H. Koopmans, H. P. Sauerwein, A. Beishuizen, and A. R. J. Girbes. Optimal nutrition during the period of mechanical ventilation decreases mortality in critically ill, long-term acute female patients: a prospective observational cohort study. *Critical Care* 13:R132, 2009.
- ⁶ Weir, J. B. New methods for calculating metabolic rate with special reference to protein metabolism. *J Physiol* 109:1-9, 1949.
- ⁷ Harris, J. A. and F. G. Benedict. A biometric study of human basal metabolism. *Proc. Natl. Acad. Sci.* 4(12):370-373, 1918.
- ⁸ Roza, A. M. and Shizgal H. M. The Harris-Benedict equation reevaluation: resting energy requirements and the body cell mass. *Am. J. Clin. Nutr.* 40:168-182, 1984
- ⁹ Bursztein, S., Elwyn D., Askanazi J., and Kinney J. Energy metabolism, indirect calorimetry, and nutrition. *Williams and Wilkins*, pp.17-20, 1989.
- ¹⁰ Cecchini, S., E. Schena, M. N. Di Sabatino, and S. Silvestri. Uncertainty evaluation of a calibration method for metabolic analyzer in mechanical ventilation. In *Medical Measurements and Applications Proceedings (MeMeA)*, 2011 IEEE International Conference, Bari, Italy, 30-31 May 2011, pp. 143-147.
- ¹¹ Damask, M. C., C. Weissman, J. Askanazi, A. I. Hyman, S. H. Rosenbaum, and J. M. Kinney. A systematic method for validation of gas exchange measurements. *Anesthesiology* 57:213-218, 1982.
- ¹² Takala, J., O. Keinänen, P. Väisänen, and A. Kari. Measurement of gas exchange in intensive care: laboratory and clinical validation of a new device. *Crit. Care Med.* 17:1041-1047, 1989.
- ¹³ Miodownik, S., J. Melendez, V. Arslan Carlon, and B. Burda. Quantitative methanol-burning lung model for validating gas-exchange measurements over wide ranges of $F_{I}O_2$. *J. Appl. Physiol.* 84:2177-2182, 1998.



- ¹⁴ Rosenbaum, A., C. Kirby, and P. H. Breen. New metabolic lung simulator: development, description and validation. *J. Clin. Monit. Comput.* 21:71-82, 2007.
- ¹⁵ Branson, R. D., and J. A. Johannigman. The measurement of energy expenditure. *Nutrition in Clinical Practice* 19:622-636, 2004.
- ¹⁶ Takala, J., and P. Meriläinen. *Handbook of gas exchange and indirect calorimetry.* Helsinki:Datex Inc, 1991.
- ¹⁷ Evaluation of measurement data-Supplement 1 to the “Guide to the Expression of uncertainty in Measurement”-Propagation of Distribution using Monte Carlo Method. *JCGM101:2008.*
- ¹⁸ Makita, K., J. F. Nunn, and B. Royston. Evaluation of metabolic measuring instruments for use in critically ill patients. *Crit. Care Med.* 6:638-644, 1990.
- ¹⁹ Cecchini, S., E. Schena, R. Cuttone, M. Carassiti, and S. Silvestri. Influence of ventilatory settings on indirect calorimetry in mechanically ventilated patients. In *Proc. of 33rd Annual International Conference of the IEEE Engineering in Medicine and Biology Society, Boston, Massachusetts, U.S., 30 Aug-3 Sept 2011*, pp. 1245-1248.
- ²⁰ Walsh, T. S. Recent advances in gas exchange measurement in intensive care patients. *Br. J. Anaesth.* 91:120-131, 2003.
- ²¹ AARC, Metabolic measurement using indirect calorimetry during mechanical ventilation. *Respiratory Care* 49:1073-1079, 2004.
- ²² Ultman, J. S., and S. Bursztein. Analysis of error in the determination of respiratory gas exchange at varying F_iO_2 . *J. Appl. Physiol.* 50:210-216, 1981.
- ²³ Joosten, K. F., F. I. Jacobs, E. van Klaarwater, B. G. Baartmans, W. C. Hop, P. T. Meriläinen, and J. A. Hazelzet. Accuracy of an indirect calorimeter for mechanically ventilated infants and children: the influence of low rates of gas exchange and varying F_iO_2 . *Crit. Care Med.* 28:3014-3018, 2000.
- ²⁴ Joint Committee for Guides in Metrology (JCGM/WG1). Evaluation of measurement data—guide to the expression of uncertainty in measurement. *JCGM 2008;100.*
- ²⁵ Kaufman, B. S., E. C. Rackow, and J. L. Falk. The relationship between oxygen delivery and consumption during fluid resuscitation of hypovolemic and septic shock. *Chest* 85:336-340, 1984.
- ²⁶ Danek, S. J., J. P. Lynch, J. G. Weg, and D. R. Dantzker. The dependence of oxygen uptake on oxygen delivery in the adult respiratory distress syndrome. *Am Rev Respir Dis.* 122:387-395, 1980.
- ²⁷ Noè, D., P. Lanzi, R. Spiti, M. Poli. Attendibilità delle equazioni predittive del dispendio energetico a riposo nella grande obesità. *G. It. Diabetol. Metab.* 26:54-62, 2006.

Chapter 4

4.1 The Kim method

As mentioned in Chapter 1, some existing techniques are already based on an indirect application of the Fick method (Section 1.7). Even if this could make the estimation less accurate, these methods allow avoiding any invasive measurement, such as S_vO_2 assessment, and reduce the risk for patients.

One of these methods results particularly suitable for mechanically-ventilated patients and, at the same time, would allow frequent measurements, as it is based on a prolonged expiration during a single respiratory act: it has never been used on mechanically ventilated subjects and some questions about the data processing are still open.

It was introduced by Kim *et al.* [1] and uses the Fick equation applied to CO_2 :

$$PBF = \frac{\dot{V}_{CO_2}}{C_vCO_2 - C_aCO_2} \quad (4.1)$$

$$PBF = \frac{\dot{V}_{CO_2}}{S(P_vCO_2 - P_aCO_2)} \quad (4.2)$$

The method estimates the value of $PaCO_2$ and $PvCO_2$, in the denominator of Eq. (4.2), using a prolonged expiration (P-E). The numerator (\dot{V}_{CO_2}) is calculated during the normal breathing. The approach obviously requires the analysis of the expired gas content during both the normal breathing and the prolonged expiration.

4.1.1 Physiological background

Before analyzing what happens during prolonged expiration, the instantaneous exchange ratio must be introduced:

$$R(t) = \frac{\dot{V}_{CO_2}^{inst}(t)}{\dot{V}_{O_2}^{inst}(t)} \quad (4.3)$$

$R(t)$ is an intra-breath parameter that represents the ratio between the CO_2 instantaneously delivered, $\dot{V}_{CO_2}^{inst}(t)$, and the O_2 instantaneously absorbed, $\dot{V}_{O_2}^{inst}(t)$.

As reported for the first time by Kim *et al.*, prolonging expiration takes to a rise of $PaCO_2$ and P_ACO_2 (alveolar partial pressure of CO_2), and this is the primary desired effect of the manoeuvre. If it is assumed that during this process $PvCO_2$, as well as PaO_2 , remain unchanged, then $PaCO_2$ will increase gradually and eventually become equal to $PvCO_2$. When the difference between the arterial and mixed venous blood will be only in the O_2 content, $PaCO_2$ will be higher than $PvCO_2$ by virtue of the Haldane effect³. At the limit this process makes CO_2 exchange cease and R approaches 0.

³ *Haldane effect*: deoxygenated Hb has a greater affinity for CO_2 than oxygenated Hb. Thus, O_2 release at the tissues facilitates CO_2 pickup, while O_2 pickup in the lungs facilitates CO_2 release. In this last situation it happens that, for every unit volume of

As at the beginning of the prolonged expiration P_aCO_2 is lower than P_vCO_2 and at the equilibrium point it is higher, there is a time when P_vCO_2 equals P_aCO_2 . This occurs at a precise value of R: since for every unit volume of oxygen taken up by hemoglobin, 0.32 volumes of CO_2 are displaced (Haldane effect) into the blood, when R is equal to 0.32, the amount of CO_2 displaced by the hemoglobin is expired and P_aCO_2 results equal to P_vCO_2 .

Thanks to the high diffusivity of CO_2 through the alveolar membrane and considering perfect mixing, alveolar partial pressures of CO_2 instantaneously equals the arterial blood partial pressure of CO_2 during the prolonged expiratory plateau: $P_ACO_2 = P_aCO_2$. It derives that P_vCO_2 is equal to P_ACO_2 when R is equal to 0.32 (Fig. 1).

To estimate the steady value of P_aCO_2 , it must be considered another index of the whole gas exchange and metabolic activity: RQ. It is the whole respiratory quotient and, differently from R, which is based on the instantaneous gas exchange, it is obtained by dividing the whole-act CO_2 production by the whole-act O_2 consumption, as introduced in the previous chapter.

Considering that $P_{et}CO_2$ equals the steady P_aCO_2 (according to the hypothesis reported at the end of the Section 1.6.2), the value of P_aCO_2 is obtainable from the R vs. P_ACO_2 curve when R equals RQ (Fig. 1).

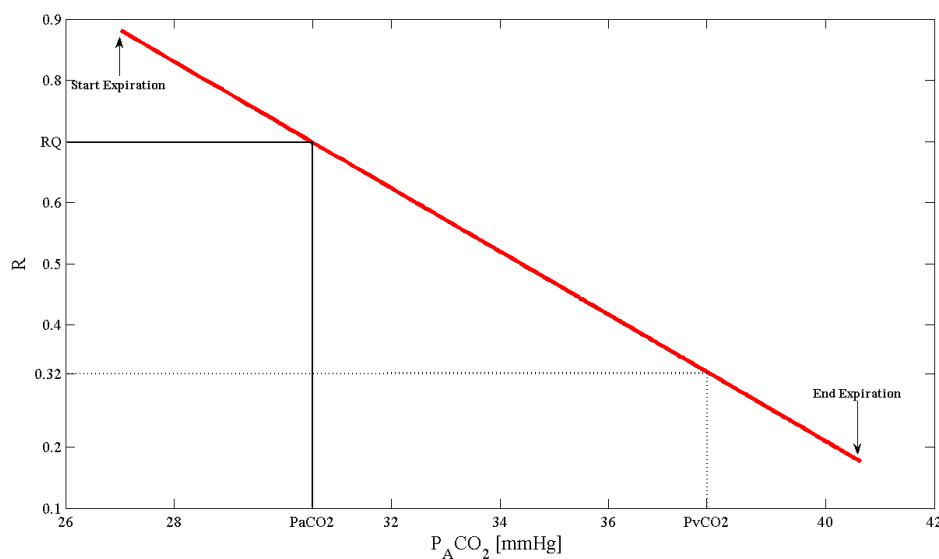


Figure 1 Linear relationship between P_ACO_2 and R during a prolonged expiration.

oxygen taken up by haemoglobin of the arterial blood, 0.32 volumes of CO_2 are displaced. The release of CO_2 causes a consequent increase in the CO_2 partial pressure into the blood.

4.1.2 The algorithm

Starting from the physiological background related to the prolonged expiration, an algorithm has been developed to obtain the value of CO from the analysis of O₂ and CO₂ contents into the respiratory gas flow.

During a slow exhalation, P_AO₂ and P_ACO₂ (as continuously measured at the patient's mouth) are plotted against each other (Fig. 2) and the instantaneous R value is calculated using the following formula [1] derived from the alveolar equation:

$$R = \frac{s - F_{I}O_2 \cdot s - F_{I}CO_2}{1 - F_{I}O_2 \cdot s - F_{I}CO_2} \quad (4.4)$$

where s is the slope of the parabolic curve obtained by plotting P_ACO₂ vs. P_AO₂.

In Fig. 2 an example of P_ACO₂ vs. P_AO₂ graph is shown. It has been obtained during a prolonged expiration performed by a patient ventilated with F_IO₂=40 %: both measured data and parabolic curve fitting are reported.

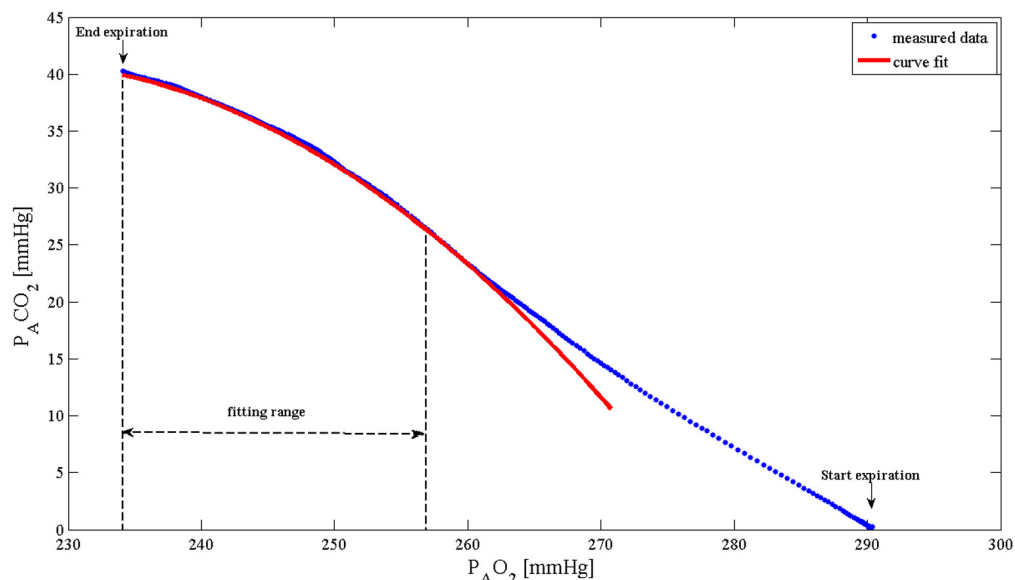


Figure 2 P_ACO₂ as a function of P_AO₂ during a prolonged expiration obtained from a patient ventilated with F_IO₂=40 %. Measured data (·) in blue and parabolic curve fit (-) in red.

The adopted data-reduction procedure rejects all the points with P_ACO₂ values lower than two thirds of the peak value, since these measurements are performed on gas coming predominantly from dead space. This criterion, based on experimental observations, allows the best agreement between the prolonged expiration method and the chosen reference method for almost every patient.

The data reduction procedure consists of two steps: 1) a preliminary parabolic regression, 2) the points having a P_ACO₂ value within the range 0 mmHg-0.7 mmHg from the related points on the

Stefano Cecchini

first fitted curve are considered for the calculation of a further parabolic regression [2]: this last regression is successively used to calculate s , and therefore R using Eq. (4.4). The least square method is applied to calculate all the fitting curves.

During a prolonged expiration, $P_{A}O_2$ diminishes at a fairly constant rate, whilst $P_{A}CO_2$ rises at a decreasing rate. According to Kim *et al.* R linearly diminishes with the increase of $P_{A}CO_2$ (Fig. 3), as discussed in the previous section.

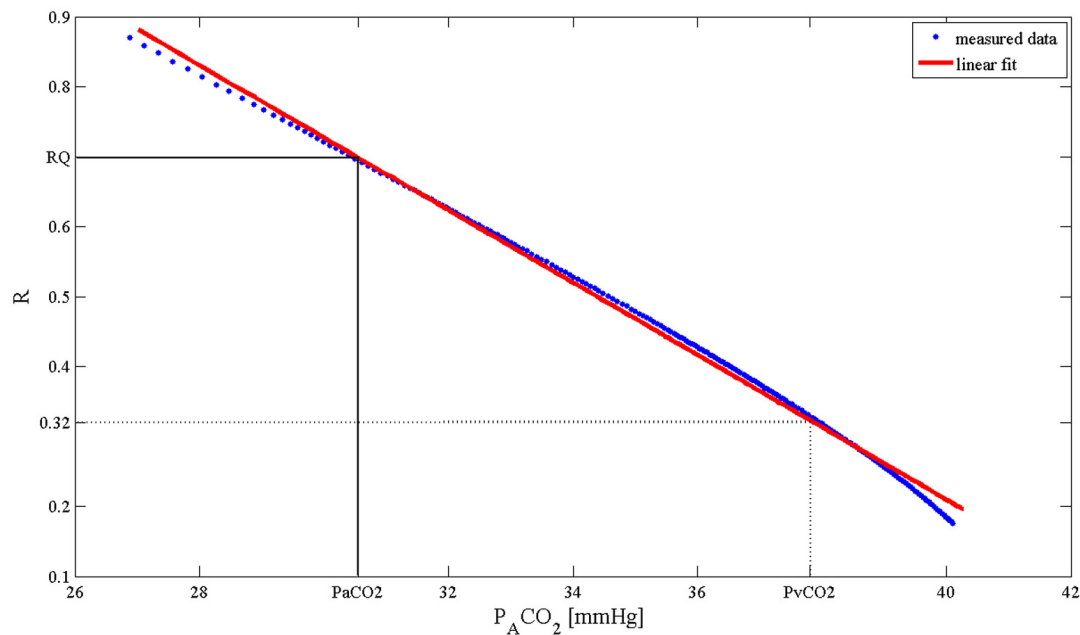


Figure 3 R as a function of $P_{A}CO_2$ during a prolonged expiration obtained from a patient ventilated with $F_{I}O_2=40\%$. Measured data (\cdot) in blue and linear fit ($-$) in red. $PaCO_2$ and $PvCO_2$ are obtained in correspondence of $R=0.32$ and $R=RQ$ respectively.

From the linear regression between R and $P_{A}CO_2$ data, and considering $P_{A}CO_2$ and $P_{A}O_2$ instantaneously equal to $PaCO_2$ and PaO_2 respectively, the two parameters of interest can be obtained in the following two steps: 1) $PaCO_2$ is obtained as the level of $P_{A}CO_2$ corresponding to a value of R equal to the mean of exchange ratio ($RQ = \dot{V}_{CO_2}/\dot{V}_{O_2}$) within the minute preceding the prolonged expiration; 2) $PvCO_2$ corresponds to the $P_{A}CO_2$ value, at which R equals 0.32, that is assumed to be the magnitude of the Haldane effect [1]. Moreover, if S is assumed constant and equal to $4.7 \text{ mL L}^{-1} \text{ mmHg}^{-1}$, the denominator of Eq. (4.2) is determined. By measurement of \dot{V}_{CO_2} during normal breathing, and by knowing the values of $PaCO_2$ and $PvCO_2$ determined as above described, Eq. (4.2) allows an estimation of PBF.

4.2 Calculation of the slope of the CO₂ dissociation curve: the Godfrey method

A second algorithm can be investigated to avoid the simplifying hypothesis of CO₂ dissociation curve linearity. Therefore, with reference to Eq. (4.1), the findings by McHardy [3] and Godfrey [4] about the CO₂ solubility in blood are considered. McHardy rearranged Visser's equation for the calculation of CO₂ concentration in blood (CbCO₂):

$$CbCO_2 = CpCO_2[1 - (k_1 + k_2 + k_3)] \quad (4.5)$$

where k_1 , k_2 , and k_3 are expressed by the following empirical relationships:

$$k_1 = 0.0288Hb \quad (4.6)$$

$$k_2 = \frac{1}{2.244 - 0.422SaO_2} \quad (4.7)$$

$$k_3 = \frac{1}{8.74 - pH} \quad (4.8)$$

CpCO₂ can be calculated using the Henderson-Hasselbach (H-H) equation:

$$CpCO_2 = 2.226 \cdot 0.0307PaCO_2[1 + 10(pH - pK)] \quad (4.9)$$

where, using the H-H equation once again, but for plasma bicarbonate [4]:

$$pK = pH - \log \frac{[HCO_3]}{0.0307PaCO_2} \quad (4.10)$$

with 2.226 being the conversion factor from mEq L⁻¹ to mLCO₂ (100 mL)⁻¹ and 0.0307 the solubility coefficient of CO₂ in plasma [mEq (L mmHg)⁻¹].

By posing CbCO₂ = CaCO₂ the arterial concentration of CO₂ is obtained using Eq.s (4.5)-(4.10). Considering the values of PaCO₂ and PvCO₂, determined as previously described, CvCO₂ has the following expression [4]:

$$CvCO_2 = CaCO_2 \left(10^{S^* \log \frac{PvCO_2}{PaCO_2}} - 1 \right) \quad (4.11)$$

where S^* is defined by the following equation:

$$S^* = \frac{1}{2.5 + (BE \cdot 0.0469)} - 0.0141 \cdot (15 - Hb) \quad (4.12)$$

PBF can, therefore, be expressed by introducing Eq. (4.11) in Eq. (4.1):

$$PBF = \frac{\dot{V}_{CO_2}}{CaCO_2 \left(10^{S^* \log \frac{PvCO_2}{PaCO_2} - 2} \right)} \quad (4.13)$$

The values of the parameters SaO₂, pH, Hb, [HCO₃] and BE are measured by arterial blood-gas analysis.

The two above described methods *per se* estimate the non-shunted portion of the PBF, i.e., the fraction of blood taking part to gas exchange. The shunting fraction, F, is here calculated using F_IO₂ and PaO₂, obtained from arterial blood-gas analysis, as reported at the end of the Section 1.7.1. Iso-shunt diagrams are used to obtain F: these diagrams are a series of continuous curve showing the relationship between PaO₂ and F_IO₂ for different shunting fractions [5].

$$F = \frac{Q_S}{Q_T} \quad (4.14)$$

Finally, CO is calculated using the following equation:

$$CO = \frac{PBF}{1-F} \quad (4.15)$$

All data are elaborated by a custom made application implemented in LabVIEW® environment (National Instruments Corporation), also able to detect the respiratory act and recognize the inspiration and the expiration phases on the basis of flow measurements and gas concentration trends. It also calculates the mean values of \dot{V}_{CO_2} and RQ within a time interval of about 1 minute preceding the prolonged expiration to assess the steady state conditions of the patient's gas exchange (Appendix B).

4.3 Measurement setup

Here we introduce a measurement set-up, which allows the use of the presented methods on mechanically ventilated patients. This setup and other forms of application of the described technique on mechanically ventilated patients have been covered by an Italian Patent [6].

In steady state conditions, measurements of \dot{V}_{CO_2} , V_E , RQ, F_{EO_2} , and F_{ECO_2} are continuously recorded using the metabolic monitor Quark RMR, which operates by sampling gas from the Y-piece of the mechanical ventilator's breathing circuit (Fig. 4).

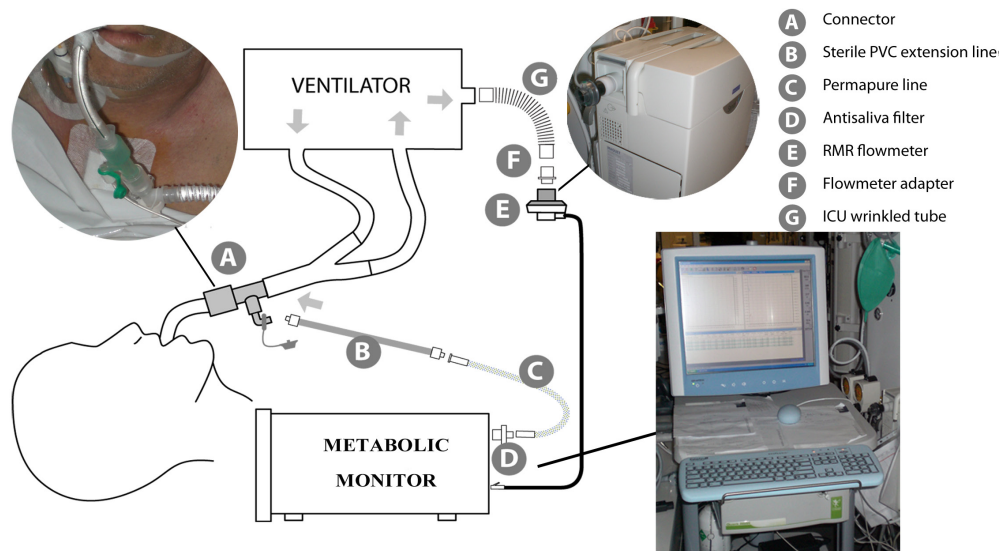


Figure 4 Schematic representation of the measurement setup.

The inspired and expired O_2 and CO_2 fractions are measured by the Quark RMR's sensors. A continuous gas flow is withdrawn from the breathing circuit in correspondence of the Y-piece

(Fig. 4-A) by means of a suction pump. In order to equalize the humidity of sample gas to the level of ambient air, a special Nafion tubing (Fig. 4-C) is used for the gas sampling line. All gas values are corrected to standard temperature and pressure dry conditions (STPD). The air-flow is measured by the 18 mm-turbine flowmeter, available for the Quark RMR, placed at the ventilator outlet (Fig. 4-E). The oxygen and carbon dioxide sensors of the Quark RMR, and the turbine flowmeter measure the gas fractions and the expiratory flow with a frequency of 25 samples per second.

As reported in the previous chapter, the metabolic monitor has been previously validated and tested *in-vitro* and *in-vivo* (on mechanically ventilated patients) to assess accuracy and reproducibility [7,8]. Under a variety of simulated ventilatory conditions, the average uncertainties of \dot{V}_{CO_2} and RQ were about 7 % and 4 % respectively [7], and clinical trials showed also a good accuracy in the measurement of the expiratory volume and $F_{I}O_2$ [8].

Both Kim and Godfrey algorithms for the estimation of CO require the assessment of P_vCO_2 and $PaCO_2$ through the induction of a prolonged expiration.

In order to obtain a prolonged expiration, the set-up showed in Fig. 4 was slightly changed by adding a custom developed element (Fig. 5) in the expiratory branch.

P-E circuit

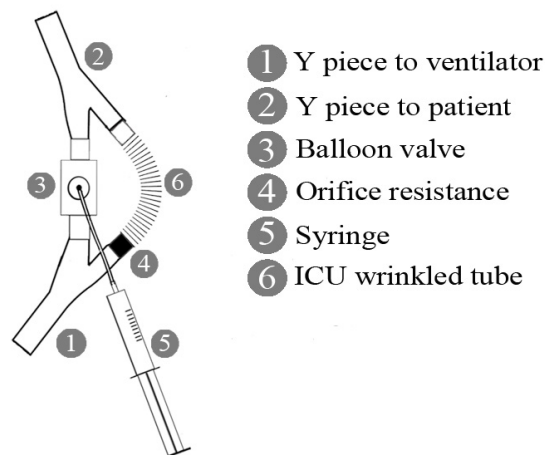


Figure 5 Scheme of the by-pass device for realizing prolonged-expiration [6].

The device shown in Fig. 5 has 2 branches with a pipe diameter of about 12 mm and connected one another with two Y pieces (1-2). In one of these, an orifice pneumatic resistance with a diameter of 1.2 mm (4) is inserted to increase the expiratory time: this branch presents also an ICU wrinkled tube (6). The other branch is equipped with a balloon valve (3) (9300 inflatable

balloon-type valve, Hans Rudolph, Inc.): when it is open, the majority of the expired flow goes through it, whilst, when it is closed, the whole expiratory flow goes through the orifice resistance (4). This makes the patient expire with a longer time constant. The valve is inflated and deflated using a syringe (5).

The positioning and a detail of the P-E circuit are reported in Fig. 6.A and Fig. 6.B, respectively.

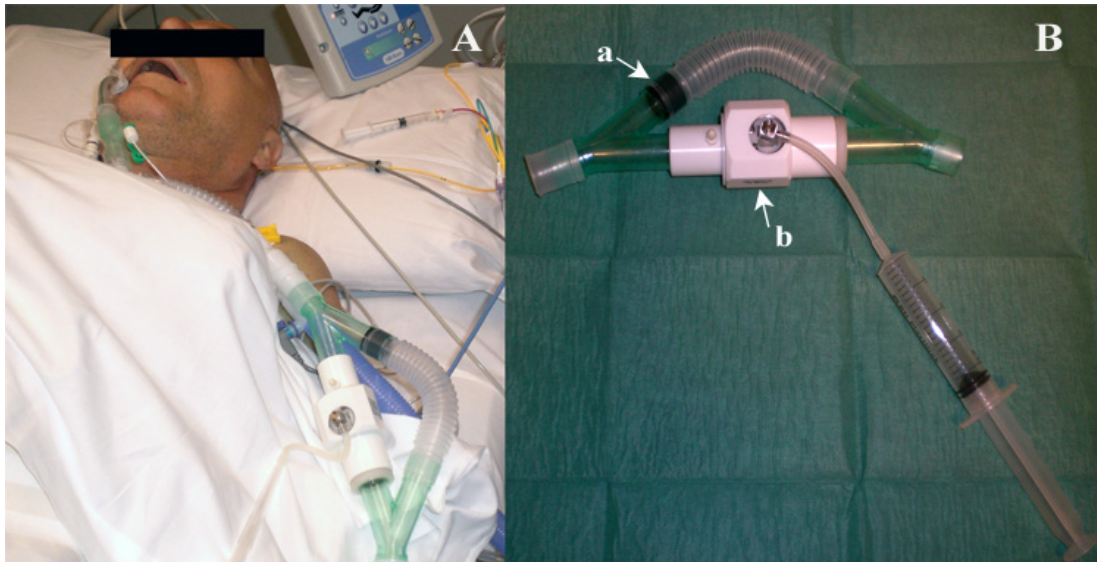


Figure 6 Custom made 2-branch device for realization of prolonged expiration: *in-vivo* application (A), detail (B).
 In B the orifice pneumatic resistance (a) and the balloon-type valve (b) are indicated.

In the new setup (Fig. 7) the P-E element (H) is added at the expiratory branch of the patient's circuit.

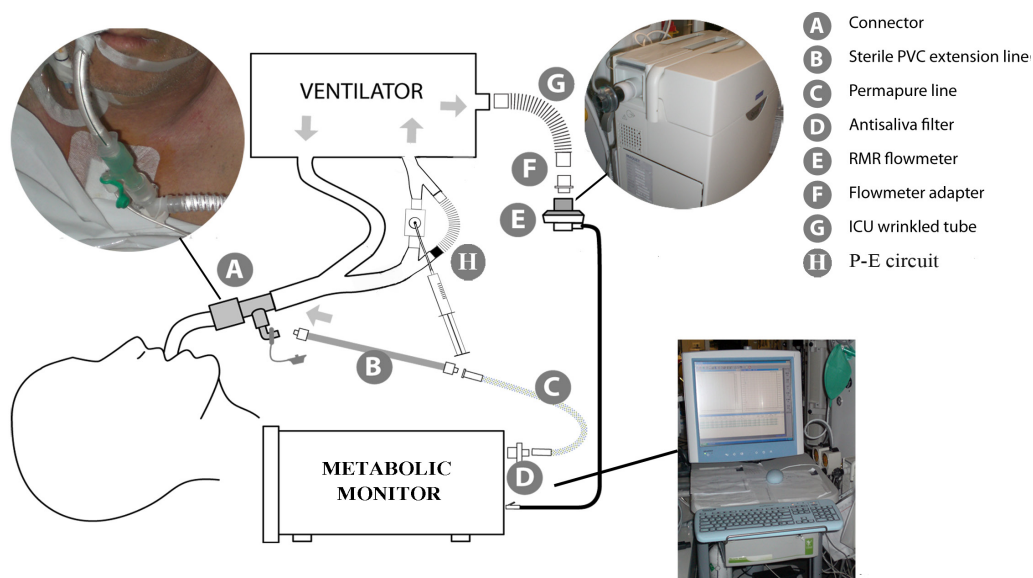


Figure 7 Measurement setup, which allows the induction of prolonged expirations [6].

Stefano Cecchini

The addition of the element (H) does not alter the correct functioning of the mechanical ventilator as it continues to deliver the same gas-flow and pressure profiles, without any alarm signals.

During the prolonged expiration, the 'expiratory pause hold' key of the ventilator is pushed to avoid the delivery of an inspiratory act and the risk of *volutrauma*⁴ and *barotrauma*⁵ for the patient. In particular:

- *barotrauma*: during the prolonged expiration alveolar pressure cannot, in any case, exceed end-inspiratory pressure, which is much lower of peak pressure. This is guaranteed by the passive nature of the manoeuvre, in which the patient exhales naturally, but through a higher load.
- *volutrauma*: no additional gas volume is delivered during the manoeuvre. By pushing the expiratory hold button, the ventilator is paused and the delivery of a breath during the expiration is avoided.

At the end of the manoeuvre the valve's balloon is deflated and the ventilator unlocked: then an inspiratory act is delivered.

Experimental data of CO₂ and O₂ concentrations are recorded and processed after the measurement session thanks to an *ad hoc* developed LabVIEW® application (Appendix B), which implements the above described procedures for the estimation of the CO (Sections 4.1 and 4.2). In particular: 1) it converts the gas fractions into partial pressures (P_ACO₂ and P_AO₂); 2) it compensates for STPD conditions (T= 0 °C, P= 760 mmHg, and no water vapor); 3) it segments the trends; 4) it executes the data-reduction; and 5) after obtaining the values of P_vCO₂ and P_aCO₂ as described, it calculates the CO using the above mentioned algorithms. Other parameters are manually set, through the user interface, before the execution of the software application: PaO₂, F_IO₂, SaO₂, pH, Hb, [HCO₃] and BE.

4.3.1 Orifice resistance characterization

The orifice pneumatic resistance, used in the developed adaptor for prolonged expiration, has been *in-vitro* characterized by delivering various volumetric flow rate values and recording the pressure drop. A flow rate controller (Bronkhorst El- Flow, range 0.05 L min⁻¹ to 10.00 L min⁻¹, accuracy 0.2 % of the set-point value) was utilized, and a pressure sensor (163PC01D48, Honeywell, range -1.96 kPa to +11.8 kPa, accuracy ±0.15 % full scale) measured the pressure drop across the orifice. Data acquisition has been performed through a DAQ card (E-series,

⁴ Lung damage caused by overdistension by a mechanical ventilator delivering an excessively high volume of gas.

⁵ Lung damage caused by overpressure by a mechanical ventilator rising too much the pulmonary pressure.

National Instruments, Inc.) with a LabVIEW®-based application, setting a sampling frequency of 10 kS/s.

Pressure drop measurements were performed delivering airflow ranging from 0 L/min to 9 L/min: steps of 1 L/min were used between 4 L/min and 9 L/min, whilst reduced step sizes were chosen in the range from 0 L/min to 4 L/min: e.g., flow rate values in step of 0.2 L/min were set in the range 0 L/min - 0.6 L/min to obtain additional information at low flow rates.

The Matlab® Toolbox, CFT, was used to fit the experimental data with a theoretical quadratic model [9]:

$$\Delta P = a \cdot Q^2 = 0.215Q^2 \quad (4.16)$$

An $R^2 > 0.989$ and $MSE < 0.2 \text{ kPa}^2$ were calculated.

The pressure-flow rate relation is reported in Fig. 8.

As the mean measured expiratory flow, during the clinical trials, was about 1.6 L min^{-1} , we could consider that the orifice introduces a mean pneumatic resistance of about $5 \text{ cmH}_2\text{O L}^{-1} \text{ min}$.

This value appears to improve the repeatability of the CO measurements accordingly to the findings of Hlastala [10], who obtained a higher repeatability than unconstrained prolonged expiration by placing a resistance of $0.33 \text{ cmH}_2\text{O L}^{-1} \text{ min}$ at the subject's mouth. A higher value of resistance could improve this effect.

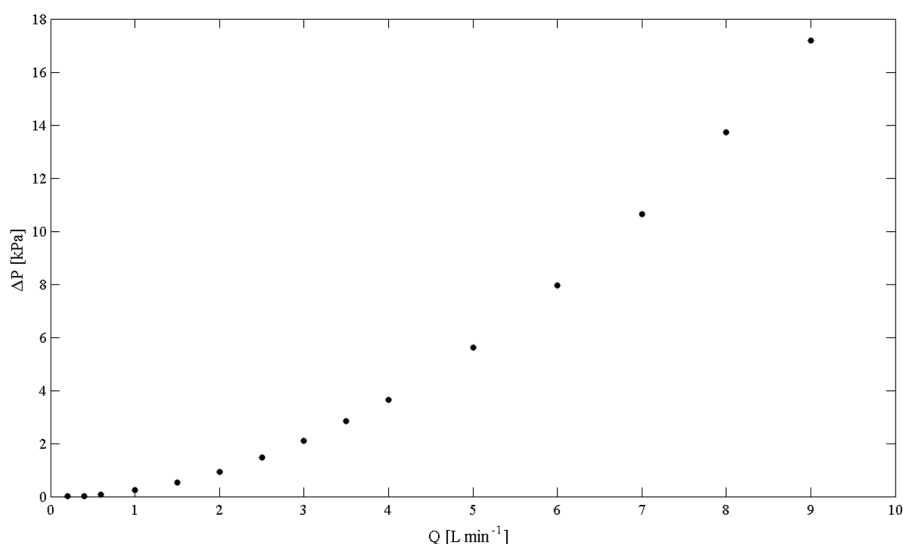


Figure 8 Pressure (ΔP) vs. flow rate (Q) for the orifice resistance used to realize the prolonged expiration.

4.3.2 Another solution for P-E realization

On the base of the method's description reported above, it is clear that the main function of the P-E circuit is inducing a prolonged expiration avoiding any malfunctioning of the ventilator and

Stefano Cecchini

any risk for the patient. Another system to induce the P-E manoeuvre has been conceptualized and designed.

The P-E ring is represented in Fig. 9.

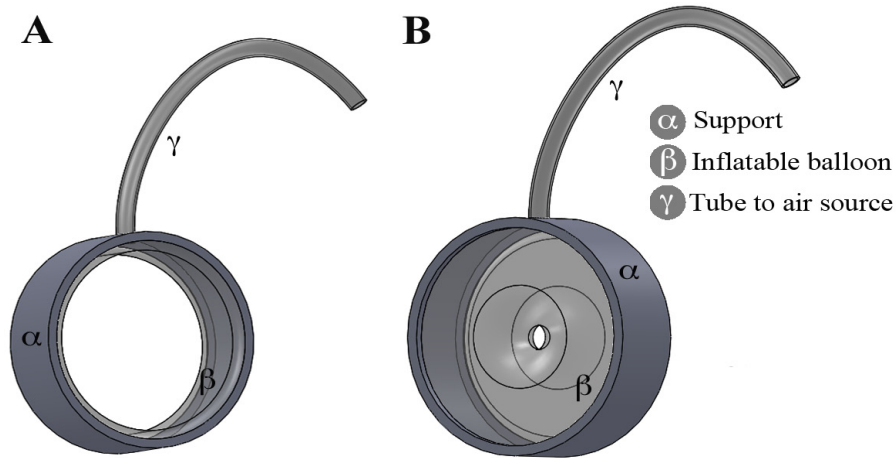


Figure 9 Design of the P-E ring [6].

The ring presents a support (α), an inflatable balloon (β), a tube (γ) to an air source, and a 3-way valve.

When the valve connects β to the air source, the balloon is inflated and expands leaving an orifice in the middle of the ring: i.e., a 1.2 mm orifice (Fig. 9.B). When the valve connects β to the external environment, the balloon deflates by leaving the ring section free (Fig. 9.A).

The setup in Fig. 7 can be changed as shown in Fig. 10.

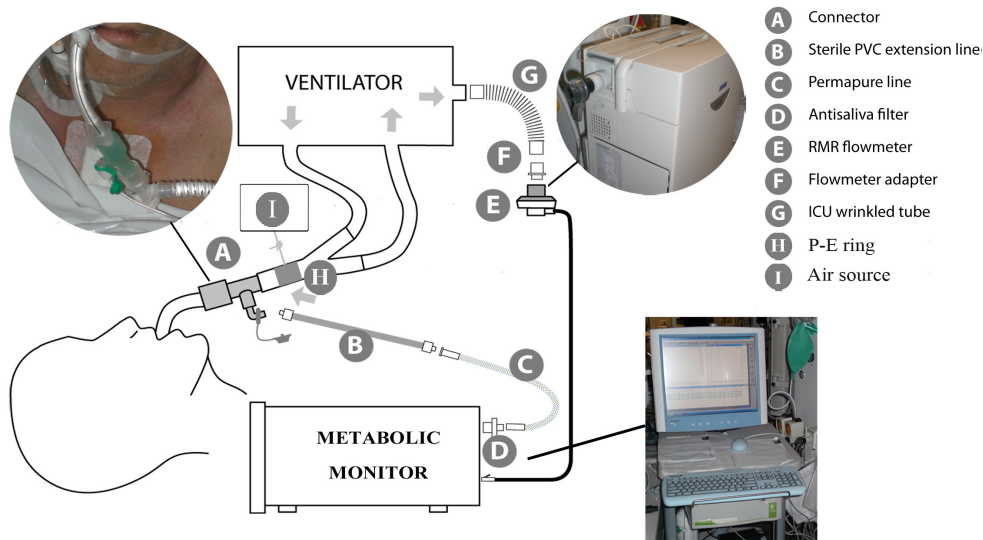


Figure 10 Measurement setup when the P-E ring (H) and the air source (I) are used [6].

With reference to the Fig. 10, the functioning of the system is exactly the same as reported above: the only difference stays in the use of the described P-E ring (H) for inducing the prolonged expiration manoeuvre. When H is in the state reported in Fig. 9.A, the patient expires normally, whilst, when H is in the state reported in Fig. 9.B, the expiration is slowed as seen in the previous configuration.

Although this system has not been realized yet, it would result less cumbersome and would minimize the addition of dead space.

In the next chapter we will describe the *in-vivo* application of the setup reported in Fig. 7. Moreover, the suitability of the proposed method for CO assessment will be verified by comparing it with one of the two “gold standards”.

References

- ¹ Kim, T. S., H. Rahn, and L. E. Fahri. Estimation of true venous and arterial PCO₂ by gas analysis of a single breath. *J. Appl. Physiol.* 21(4):1338-1344, 1966.
- ² Chen, H., N. P. Silverton, and R. Hainsworth. Evaluation of a method for estimating cardiac output from a single breath in humans. *J. Appl. Physiol.* 53(4):1034-1038, 1982.
- ³ McHardy, G. J. The relationship between the differences in pressure and content of carbon dioxide in arterial and venous blood. *Clin. Sci.* 32:299-309, 1967.
- ⁴ Godfrey, S. Manipulation of the indirect Fick principle by a digital computer program for the calculation of exercise physiology results. *Respiration* 27(6):513-532, 1970.
- ⁵ Jaffe, M. B. Partial CO₂ rebreathing cardiac output—operating principles of the NICO™ system. *J. Clin. Monit. Comput.* 15(6):387-401, 1999.
- ⁶ Cecchini, S., E. Schena, M. Carassiti, and S. Silvestri. Apparato per la stima della gittata cardiaca. Patent N° RM2011A000650, filed on the 9th of December 2011.
- ⁷ Cecchini, S., E. Schena, M. N. Di Sabatino, and S. Silvestri. Uncertainty evaluation of a calibration method for metabolic analyzer in mechanical ventilation. In *Medical Measurements and Applications Proceedings (MeMeA)*, 2011 IEEE International Conference, Bari, Italy, 30-31 May 2011, pp. 143-147.
- ⁸ Cecchini, S., E. Schena, R. Cuttone, M. Carassiti, and S. Silvestri. Influence of ventilatory settings on indirect calorimetry in mechanically ventilated patients. In *Proc. of 33rd Annual International Conference of the IEEE Engineering in Medicine and Biology Society*, Boston, Massachusetts, U.S., 30 Aug-3 Sept 2011, pp. 1245-1248.
- ⁹ R.W. Miller, *Differential Producers: Engineering Equations*, Chapter 9, in: R. W. Miller, *Flow Measurement Engineering Handbook*, third ed., McGraw-Hill, United States of America, chapter 9, 1996.
- ¹⁰ Hlastala, M. P. Model of fluctuating of alveolar gas exchange during the respiratory cycle. *Respiration Physiol.* 15(2):214-232, 1972.

Chapter 5

5.1 Clinical experimentation

Finally, we have *in-vivo* validated the method described in the Chapter 4 by comparing it to one of the two “gold standards” in the CO assessment: the thermodilution method.

Previous studies, which have investigated the prolonged expiration method on collaborative subjects, have not used the thermodilution as reference, since the invasiveness of this method makes it unsuitable to be used when healthy subjects are enrolled. Only one survey, performed on animals, compared the prolonged expiration method against a method similar to thermodilution, the dye-dilution method, and no significant difference was found [1].

In the following, we will describe the clinical protocol and the main results of this clinical experimentation. This chapter is widely taken from a paper accepted for publication [2].

5.2 Patient population and therapy

Twenty patients were recruited in this prospective study, underwent cardiac surgery under general anesthesia, and had to be mechanically ventilated after surgery. We excluded patients who were hemodynamically unstable requiring high doses of vasoactive medications ($>5 \mu\text{g kg}^{-1} \text{min}^{-1}$ of dopamine or dobutamine), fluids or colloidal solutions to maintain their pressure, or inspired oxygen concentration higher than 60 %.

Positioning of a Swan-Ganz catheter was considered necessary to monitor the clinical and therapeutic courses of the recruited patients. A continuous infusion of morphine at 1 mg h^{-1} , Propofol at $1\text{-}3 \text{ mg kg}^{-1} \text{ h}^{-1}$ and vecuronium bromide at 10 mg in bolus sedated and paralyzed all the patients who took part in the study. They all were in reasonably stable conditions; neither spontaneous respiratory efforts nor spontaneous muscular activity were registered. Patients were all ventilated by Servo-i ventilators (Maquet GmbH & Co. KG) in Synchronized Intermittent Mandatory Volume (SIMV) mode with tidal volume equal to $6 \text{ mL kg}^{-1} - 8 \text{ mL kg}^{-1}$. F_iO_2 ($\geq 40\%$) and PEEP remained unchanged during the trial.

5.3 Protocol and measurements

The study was approved by the local Ethical Committee of the University Campus Bio-Medico of Rome, and the recruited patients or the closest relatives expressed their informed consent for the clinical protocol-based treatment and data collection (Prot. N. 19/2011, ComEt CBM).

Patients were lying supine during the whole period of study. The beginning of the trials was at least 90 minutes after any intervention or perturbation that would change the circulatory or ventilatory state of the patient. Furthermore, any intervention or perturbation of the system (patient-ventilator) was avoided during the study, and none of the patients had any alterations in

their therapy. A Swan-Ganz catheter (131 HVF, Edwards Lifesciences, Inc.) and a radial artery catheter, previously inserted for intra-operative management, were used to monitor all the patients. The Swan-Ganz catheter was interfaced to the CO module of the patient's monitor (MP70 IntelliVue, Philips Healthcare, Inc.). Before the study, an inspection of the pulmonary artery pressure waveform checked the correct positioning of the Swan-Ganz catheter and the code for the injection bolus temperature and the patient's anthropometric characteristics were manually set in the patient's monitor. All the patients received infusion of saline solution during the study.

Before each individual study period, the oxygen and carbon dioxide analyzers of the metabolic monitor were calibrated with a precise mixture containing 5 % of CO₂ and 15 % of O₂, according to the manufacturer's instruction. The turbine flowmeter was calibrated once a day using a calibration syringe of 3 L.

The determination of cardiac output by thermodilution (CO_T) was performed ten times: 4 times at steady condition, 3 times after a sequence of 10 prolonged expirations (CO_K-CO_G), and 3 times at the end of the session.

Injections of 10 mL of a room-temperature (21 °C – 24 °C) solution of 0.9 % NaCl were given. Injection time was always shorter than 4 s to reduce any effect of varying injection rates on calculations. The same operator executed all the injections. The morphology of thermodilution curves was always monitored to detect artifacts.

At the end of the session, arterial and mixed venous blood samples were taken using syringes (BD Preset Case Becton, Dickinson and Company) for blood-gas analysis (ABL 700, Radiometer Medical ApS).

The prolonged expiration manoeuvre was executed 20 times for each patient: a pause of about 2 minutes between consecutive maneuvers allowed the recovering of steady conditions by the subject and the assessment of the subject's gas exchange.

In summary, the sequence of trials, as scheduled by the clinical protocol, was the following (Fig. 1): 4 measurements by thermodilution, 10 by prolonged expiration, 3 by thermodilution, 10 by prolonged expiration, and 3 measurements by thermodilution at the end of the session.

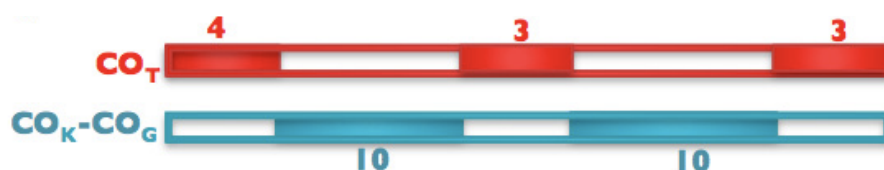


Figure 1 Sequence of trials as established by the clinical protocol.

5.4 Statistical analysis

CO measurements were repeated ten times using thermodilution method and twenty times with the two non-invasive approaches (Kim and Godfrey algorithms) for each patient. In the following, all experimental data are reported as mean \pm the expanded uncertainty, which is calculated by multiplying the standard uncertainty by a coverage factor (CF) of 2.26 for thermodilution and of 2.09 for non-invasive approaches. The two CFs are obtained by considering a Student's reference distribution with 9 and 19 degrees of freedom for thermodilution and non-invasive approaches respectively, and a level of confidence of 95 % [3]. In order to assess the agreement between the two non-invasive methods and thermodilution, each non-invasive measurement is paired to the set of thermodilution closer in time (Fig. 2): then, the single CO value obtained by the prolonged expiration is compared to the mean value calculated from the set of thermodilution, to which it is paired.

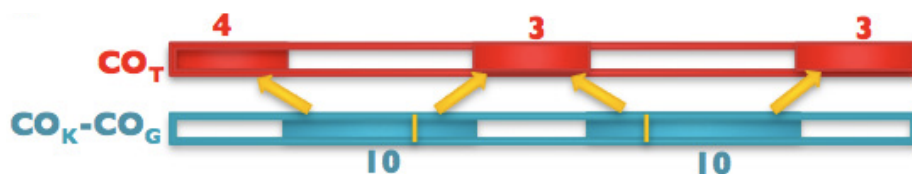


Figure 2 Pairing of the measures for the statistical analysis.

Both the comparison between the Kim and Godfrey algorithms and the thermodilution, and the analysis of their agreement are performed using several methods: 1) the analysis of the correlation between paired measurements, evaluated using the mean square error algorithm; 2) the Bland-Altman analysis [4]; 3) the percentage differences (ΔCO) for each patient. These differences were calculated as the relative percentage error between the CO mean values assessed by the non-invasive methods and those assessed by thermodilution:

$$\Delta CO = \frac{CO_{NI} - CO_T}{CO_T} 100 \quad (5.1)$$

where: CO_{NI} is the CO value estimated with a non-invasive approach (Kim or Godfrey method) and CO_T is the CO value obtained by thermodilution; and 4) Student's t-test used to compare the average of the 10 values of CO_T and the average of the 20 values of CO_{NI} for every patient. Values of $p < 0.05$ were considered statistically significant.

The bias of the non-invasive method is expressed as the mean difference between paired measurements. In the same way, the precision of the non-invasive methods is expressed as one standard deviation (1 SD) of the differences between paired measurements.

Limits of agreement (LoA) introduced into the Bland-Altman plot are the extremes of the interval, which contains 95 % of the differences between paired measurements: lower and upper

limit of agreement are calculated by dividing 2 SD of the CO measurement bias by the overall average CO [5]. Critchley and Critchley proposed that the limits of agreement should be $\pm 30\%$ to represent proper agreement between two techniques [5], while Peyton and Chong accept a cut-off value of 45% [6].

Percentage error (E) is calculated from the SD of agreement and the mean CO value assessed by thermodilution (\overline{CO}_T):

$$E[\%] = \frac{2SD}{\overline{CO}_T} \quad (5.2)$$

All the statistics have been developed in MATLAB® (MathWorks, Inc.) environment.

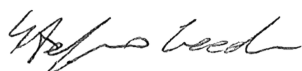
5.5 Results

The CO values, obtained using the three different methods, are reported in Table I: for each patient, throughout a period of about 45 min, thermodilution (CO_T) was executed 10 times, and prolonged expiration 20 times. Elaborations according to the Kim algorithm (CO_K) and the Godfrey algorithm (CO_G) were executed after the measurement session.

Table I CO measurements for every patient (mean \pm expanded uncertainty).

Patient	CO_T [L·min ⁻¹]	CO_K [L·min ⁻¹]	CO_G [L·min ⁻¹]
P1	3.8 \pm 0.1	3.7 \pm 0.2	5.4 \pm 0.3
P2	2.2 \pm 0.2	1.7 \pm 0.3	2.3 \pm 0.3
P3	4.6 \pm 1.0	4.5 \pm 0.5	6.0 \pm 0.6
P4	4.3 \pm 1.0	4.0 \pm 0.3	5.1 \pm 0.3
P5	2.6 \pm 0.1	2.4 \pm 0.2	3.3 \pm 0.3
P6	2.7 \pm 0.1	2.8 \pm 0.6	3.8 \pm 0.8
P7	4.8 \pm 1.0	4.2 \pm 0.4	6.0 \pm 0.6
P8	2.4 \pm 0.4	2.5 \pm 0.3	3.3 \pm 0.4
P9	4.0 \pm 0.3	3.5 \pm 0.9	4.9 \pm 1.0
P10	6.8 \pm 3.0	6.6 \pm 2.0	8.7 \pm 2.0
P11	4.6 \pm 0.3	4.3 \pm 0.3	6.6 \pm 0.5
P12	4.6 \pm 1.0	4.6 \pm 1.0	6.6 \pm 1.0
P13	3.3 \pm 1.0	3.1 \pm 0.6	4.2 \pm 0.6
P14	3.4 \pm 0.2	2.8 \pm 0.4	3.8 \pm 0.4
P15	3.6 \pm 0.2	3.6 \pm 0.7	5.1 \pm 0.9
P16	4.1 \pm 0.3	3.5 \pm 0.6	5.3 \pm 0.8
P17	4.0 \pm 0.2	3.8 \pm 0.3	4.3 \pm 0.4
P18	2.6 \pm 0.1	2.6 \pm 0.7	3.6 \pm 0.8
P19	3.6 \pm 0.2	3.8 \pm 0.3	4.3 \pm 0.4
P20	2.6 \pm 0.2	2.6 \pm 0.3	4.4 \pm 0.4

Experimental data show that CO values, estimated using the Godfrey algorithm, are, on average, greater than the values obtained using the Kim algorithm ($CO_G > CO_K$ for all patients). The Kim



algorithm appears to slightly underestimate CO_T : a difference of about -6 % occurs and an underestimation lower than -15 % is reported in 90 % of the cases. On the other hand the Godfrey algorithm overestimates CO_T : CO_G is greater than CO_T of about +30%, the percentage difference is greater than +30 % in 11 patients (55 % of the cases), and +67 % in the worst case. The percentage differences between the CO average values, obtained using Kim and Godfrey algorithms, with the thermodilution for each patient are reported in Fig. 3.

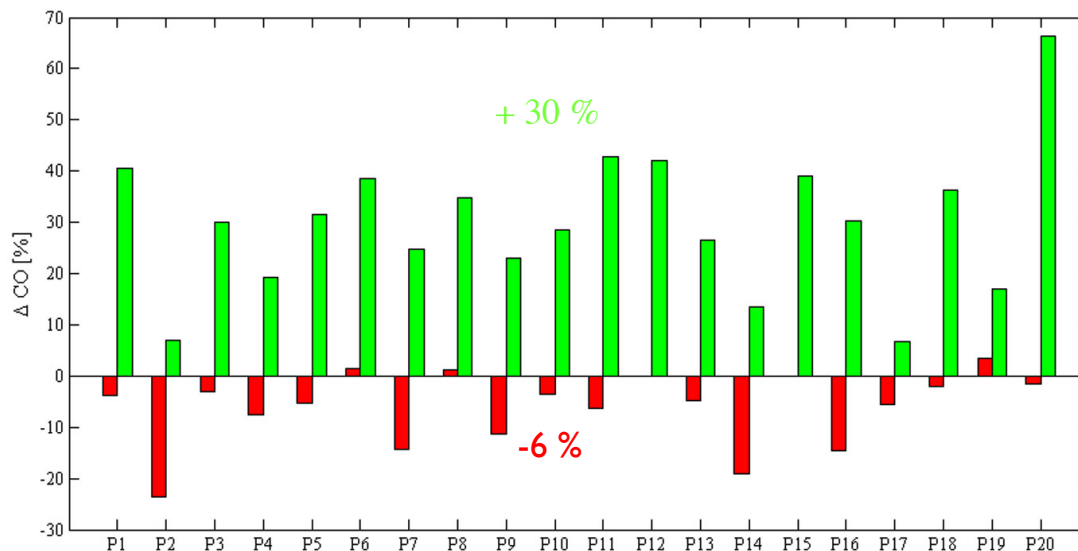


Figure 3 Percentage difference between CO values obtained with different methods, for each patient: CO_K and CO_T (red bars), CO_G and CO_T (green bars).

A further analysis to compare the CO values measured using the abovementioned two algorithms has been carried out by implementing the Student's t-test: the values are significantly different ($p < 0.05$) for only one patient.

All the values of CO_K and CO_G vs. CO_T are shown in Fig. 4. As reported in the Statistical Analysis section, each non-invasive estimation is paired with the mean CO value belonging to the set of thermodilution assessments closer in time.

The trends confirm the slight underestimation obtained by the Kim algorithm and the more marked overestimation by the Godfrey algorithm. The linear regression implemented between CO_K or CO_G (dependent variable) and CO_T (independent variable) shows: in the first case (CO_K vs. CO_T), a slope of the best fitting line equal to 0.95 ($R=0.82$), and in the second one (CO_G vs. CO_T) a slope equal to 1.30 ($R=0.81$) (Fig. 4).

Stefano Cecchini

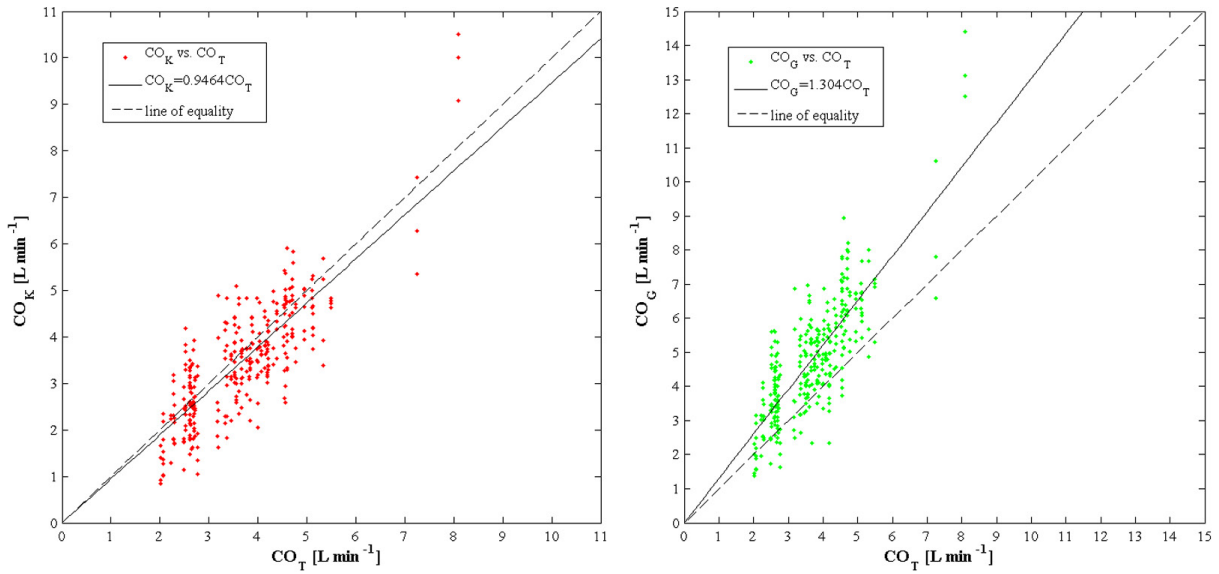


Figure 4 Data correlation: CO_K vs. CO_T (left) and CO_G vs. CO_T (right).

Bland-Altman plots are reported to show the rate of agreement between the methods (Fig. 5).

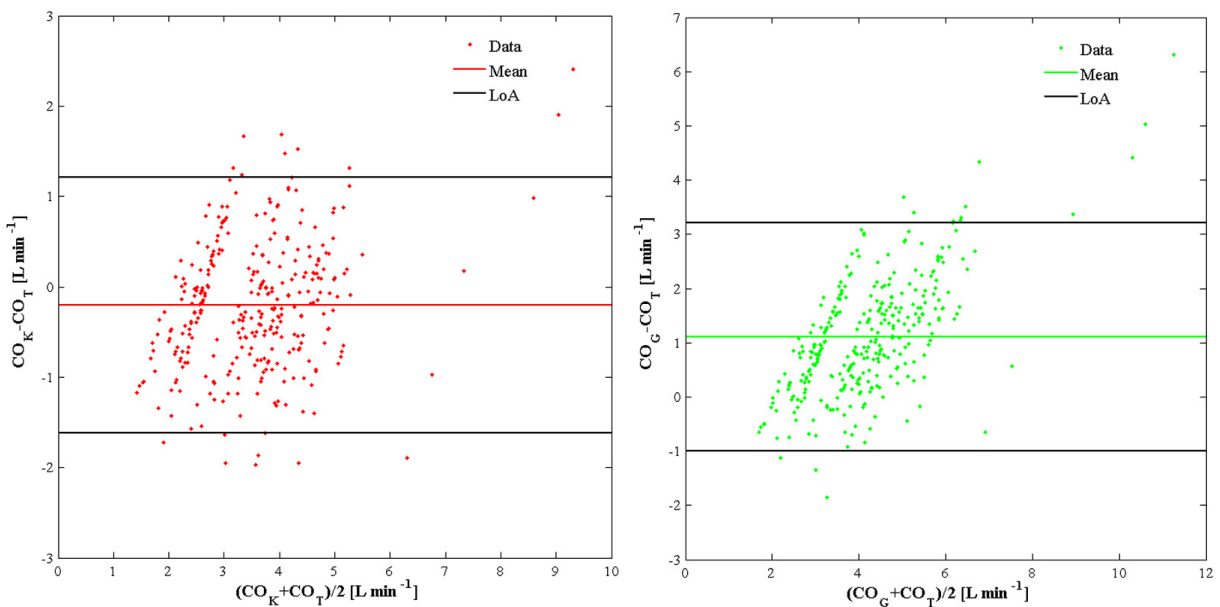


Figure 5 Bland-Altman plots: CO_K vs. CO_T (left) and CO_G vs. CO_T (right).

The following table shows the main endpoints of the comparison between the two non-invasive techniques and the thermodilution.

Stefano Cecchini

Table II Agreement between both methods and thermodilution.

Method	n	Bias [L·min ⁻¹]	Precision [L·min ⁻¹]	LoA [L·min ⁻¹]	Percentage error [%]
Kim	400	-0.21	0.72	Lower: -1.63 Upper: +1.21	39 %
Godfrey	400	+1.11	1.07	Lower: -1.00 Upper: +3.22	58 %

5.6 Discussion

Before giving an interpretation of the results obtained, here is a brief overview about the comparative evaluations found in literature of minimally invasive techniques with respect to the thermodilution method. Peyton *et al.* [6] analyzed the results from 47 studies about the comparison between pulse contour technique, partial CO₂ rebreathing, esophageal Doppler and transthoracic electrical bioimpedance respectively, and thermodilution. They reported that none of the four methods showed a percentage difference lower than 30 % as compared with thermodilution values (a suggested criterion of acceptability [5]).

The prolonged expiration method has also been compared with other methods, although never before with thermodilution: for example, Chen *et al.* [7] and Inman *et al.* [8] stated that the Kim algorithm is not statistically different from the Fick method and the partial CO₂ rebreathing, respectively.

In the present study, the Kim algorithm shows a good agreement with the thermodilution (-0.21 L min⁻¹, -6%), which is in line with the outcomes reported by Peyton *et al.* [6] and lower than the threshold considered acceptable by Bartels *et al.* (0.7 L min⁻¹) [9].

Differently from the Kim algorithm, the Godfrey one shows a systematic and substantial overestimation of the thermodilution (+30 %).

The Kim method seems to have a precision and a percentage error (0.72 L min⁻¹, 39%) slightly lower than other minimally invasive techniques (about 1.1 L min⁻¹, 42%) (see Table III), whilst the precision and percentage error estimated for the Godfrey method are comparable to those reported by Peyton *et al.*

Table III Agreement between the minimally invasive methods considered by Peyton *et al.* [6] and the thermodilution.

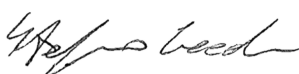
Method (N Studies)	n	Bias L/min Mean [±95% CI]	Precision L/min	Percentage Error Mean [±95% CI]
Pulse contour (N = 24)	714	-0.00 [±0.09]	1.22	41.3 [±2.7]%
Esophageal Doppler (N = 2)	57	-0.77 [±0.29]	1.07	42.1 [±9.9]%
Pco ₂ RB (N = 8)	167	-0.05 [±0.17]	1.12	44.5 [±6.0]%
TEB (N = 13)	435	-0.10 [±0.11]	1.14	42.9 [±3.6]%

In considering the methods' precision, it must be reported that successive repetition of the thermodilution method under stable hemodynamic conditions result in alterations of CO by >1.0 L min⁻¹ [10]: this indicates that CO can vary substantially during a short period of time. This is confirmed by a previous study, in which the precision and the percentage error calculated by comparing thermodilution to aortic transit-time ultrasound, i.e. a true gold standard, were 1.01 L min⁻¹ and 41.7 %, respectively [11]. Also Bajorat *et al.* reported a percentage error between the two methods of about 48 % [12].

In a previous study, Hlastala *et al.* [13] applied the prolonged expiration method to collaborative subjects, and they reported a mean SD, over 13 patients, of about 1.7 L min⁻¹. This higher variability, compared to the one obtained from our study, might be related to the data-reduction procedure, as discussed by Christensen *et al.* [14], to an expiratory phase variability, which is higher in collaborative subjects than in sedated ones, and to the use of a lower pneumatic resistance with respect to the one used in the present research (0.33 cmH₂O L⁻¹ min vs. 5 cmH₂O L⁻¹ min). The influence of pneumatic resistance has already been underlined by Hlastala *et al.* themselves.

Moreover, it must be reported that cardiac surgery patients generally show marked hemodynamic and respiratory changes, which might increase the variability of the CO measurements. This can add to the limitations intrinsic to the method to cause a reduced repeatability.

The CO underestimation obtained by the Kim method could be explained by two classes of factors. Firstly, those directly related to the method: 1) systematic overestimation of the slope value of the P_ACO₂-R linear relationship; 2) underestimation of CO₂ values measured at the mouth, probably caused by contamination of gas during expiration by dead space, and storage of some expired CO₂ in the lungs; 3) decrease in venous return to the heart that accompanies the prolonged expiration, similarly to the Valsalva manoeuvre; and 4) underestimation of the shunt fraction. Secondly, factors related to the overestimation of CO by thermodilution: i.e., Botero *et al.* found an overestimation of about 0.18 L min⁻¹ [11] with respect to a method using an aortic flow probe.



Moreover, thermodilution can be affected by injection time and bolus temperature, and its agreement with the Fick method remains a debate [15,16].

The method introduced by Godfrey, as shown, leads to an overestimation of the CO value. Considering that the model introduced by Godfrey took into account exclusively healthy subjects, some parameter values measured in this study may exceed the normal ranges and specifically: all the post-surgery ventilated patients enrolled in the trials have high value of SaO₂ (near to 100 %) and low value of Hb, under 10 g (100 mL)⁻¹. This might account for an underestimation of the artero-venous difference of CO₂ concentration.

5.7 Limitations and assumptions

It is important to highlight some limitations and assumptions regarding the utilized method. An underlying assumption, shared with the Fick method, and with all those methods not allowing beat-to-beat estimates, including thermodilution, is that the obtained value constitutes the mean value of CO during the whole measurement period. Moreover, it is assumed that CO is not altered by the prolonged expiration. Generally speaking, the underlying theory considers that gas exchange in pulmonary capillaries is equal to the one taking place in the alveolar gas. This implies that all CO₂ participating to the alveolar exchange is released, without any retention in the lungs, while expiration proceeds and CO₂ partial pressure raises. Another hypothesis is that the alveolar gas equilibrates with the gas in the mixed arterial blood and that all the dead space is soon exhaled, corresponding to the linear increase in the partial pressure curves of CO₂.

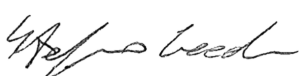
The method also assumes that the concentrations and fractions of the expired gas in the curve plateaus are equal to those of the alveolar gas, considering the hypothesis of perfect mixing.

A further potential limitation of the Kim algorithm is the difficulty in the assessment of PvCO₂ changes during the prolonged expiration: these can be caused by a CO₂ accumulation in the blood, related to re-circulation.

Moreover, another potential source of error can be associated to pulsations in gas flow due to pulsatile blood flow: fast changes in the alveolar gas concentration induce further oscillations in O₂ and CO₂ flow [13]. Such oscillations cause slight irregularities in alveolar gas pressures as a function of time [17].

It should also be noted that the prolonged expiration method is probably not suitable for subjects with obstructive pulmonary disease, since a representative mixed alveolar sample cannot be obtained with any degree of certainty in these subjects, and in subjects with uneven ventilation-perfusion.

The present study is based on a limited set of observations and, therefore, caution should be used when considering the general clinical applicability of the described method. The results obtained



motivate further clinical studies and also analytical work to better determine the potential of this application in ICU for the monitoring of critically-ill patients.

5.8 Risk assessment and precautions

The described method, as executed in this study, results safe thanks to three precautionary measures: 1) the 'expiratory pause hold' key of the ventilator was pushed during the manoeuvre, which resulted completely passive: this avoided any risk of *volutrauma* and *barotrauma*; 2) patients were continuously monitored by both ventilator and cardiac monitor; 3) the physician never left the patients and was ready to interrupt the manoeuvre in case of potential hazard.

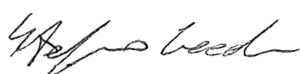
Potential risks of hypoxia and hypercapnia could be related to interposing an obstruction in the expiratory branch of the breathing circuit: a slight hypoxia can be caused by a longer time, in which the patient does not receive "fresh gases", and a slight hypercapnia by a progressive reduction of CO₂ expulsion rate during the prolonged expiration. In view of this, no potentially negative effects have been registered in any patient enrolled in the study: 1) infrequent transitory desaturations or end-tidal CO₂ increases went back to normal, on average, within a few breathing acts [18] without increasing F_IO₂ or breathing rate, 2) the worst SaO₂ values, after the prolonged expiration, were comprised between 95% and 100%, which is an acceptable range (at F_IO₂≥40%), and 3) PaO₂ and PaCO₂ values, measured at the end of the session through blood-gas analysis, were always within physiological ranges. This confirms that no cumulative effects were induced and that the transitory ones fully recovered within the pause period of 2 minutes.

5.9 Strengths

The encouraging results reported in this study should be evaluated also considering the advantages that the technique could bring, together with the absence of cannulation and blood sampling: it is simple to perform, cumbersome equipment is not needed, the measurements can be repeated at short time intervals, and the time required to perform the manoeuvre is relatively brief. This allows a serial execution of the manoeuvre on a subject, without requiring an excessive recovery time: this makes the method suitable for relatively unsteady states, as it happens in patients undergoing intensive care [19].

Furthermore, the recent developments in the field of mechanical ventilation could allow for the integration and automatization of the proposed approach into modern artificial ventilators, making non-invasive CO measurements a routine part of post-surgery monitoring for ventilated patients.

As stated by De Waal *et al.*, the ideal CO monitor should be reliable, continuous, noninvasive, operator-independent, cost-effective, and should have a fast response time (beat-to-beat) [20].



The proposed method, at the moment, seems to meet 4 out of these 6 aspects: reliability, non-invasiveness, operator-independency, and cost-effectiveness. Moreover, we can argue that the system allows a semi-continuous assessment of CO, one measurement every 2 minutes: considering that thermodilution requires about 30 s and rebreathing about 3-4 minutes, this is a satisfying result.

5.10 Conclusions

In conclusion, a single breath method for the non-invasive assessment of CO on mechanically ventilated patients has been described, and a system for the realization of passive prolonged expirations, to be connected to the patient circuit, has been designed, realized, and characterized. An *in-vivo* validation of the method has been performed on post-surgery mechanically ventilated patients receiving an $F_{I}O_2$ ($\geq 40\%$) higher than air. The method showed good agreement with the thermodilution and a precision comparable to those of other minimally invasive methods. Main issues related to the connection to mechanical ventilator, the preservation of patient's clinical conditions, and the potential causes of error have been addressed. In this work it has also been showed that, in the application of the prolonged expiration on mechanically ventilated patients, the standardization and automation of the single breath procedure is feasible.

Even if this approach needs a further validation, it could foster the development of a new monitoring device for the non-invasive estimation of CO, which would reduce the risks derived from the use of catheters.

References

- ¹ Mohammed, M. M. J. and R. Hainsworth. Evaluation using dogs of a method for estimating cardiac output from a single breath. *J. Appl. Physiol.* 50(1):200-202, 1981.
- ² Cecchini, S., E. Schena, M. Notato, M. Carassiti, and S. Silvestri. Non-invasive estimation of cardiac output in mechanically ventilated patients: a prolonged expiration method. *Annals of Biomedical Engineering*, published online (2012): DOI 10.1007/s10439-012-0534-3.
- ³ Joint Committee for Guides in Metrology (JCGM/WG1). Evaluation of measurement data—guide to the expression of uncertainty in measurement. *JCGM* 2008; 100.
- ⁴ Bland, J. M. and D. G. Altman. Statistical methods for assessing agreement between two methods of clinical measurement. *Lancet* 1(8476):307-310, 1986.
- ⁵ Critchley, L. A. and J. A. Critchley. A meta-analysis of studies using bias and precision statistics to compare cardiac output measurement techniques. *J Clin. Monit. Comput.* 15:85-91, 1999.
- ⁶ Peyton, P. J. and S. W. Chong. Minimally invasive measurement of cardiac output during surgery and critical care: a meta-analysis of accuracy and precision. *Anesthesiology* 113(5):1220-1235, 2010.
- ⁷ Chen, H., N. P. Silverton, and R. Hainsworth. Evaluation of a method for estimating cardiac output from a single breath in humans. *J. Appl. Physiol.* 53(4):1034-1038, 1982.
- ⁸ Inman, M. D., R. L. Hughson, and N. L. Jones. Comparison of cardiac output during exercise by single-breath and CO₂-rebreathing methods. *J. Appl. Physiol.* 58(4):1372-1377, 1985.
- ⁹ Bartels, S. A., W. J. Stok, R. Bezemer, R. J. Bocksem, J. van Goudoever, T. G. V. Cherpanath, J. J. van Lieshout, B. E. Westerhof, J. M. Karemaker, and C. Ince. Noninvasive cardiac output monitoring during exercise testing: Nexfin pulse contour analysis compared to an inert gas rebreathing method and respired gas analysis. *J. Clin. Monit. Comput.* 25:315-321, 2011.
- ¹⁰ Jansen, J. R., J. J. Schreuder, J. P. Mulier, N. T. Smith, J. J. Settels, K. H. Wesseling. A comparison of cardiac output derived from the arterial pressure wave against thermodilution in cardiac surgery patients. *Br. J. Anaesth.* 87(2):212–222, 2001.
- ¹¹ Botero, M., D. Kirby, E. B. Lobato, E. D. Staples, and N. Gravenstein. Measurement of cardiac output before and after cardio-pulmonary bypass: comparison among aortic transit-time ultrasound, thermodilution, and non-invasive partial CO₂ rebreathing. *J. Cardiothorac. Vasc. Anesth.* 18:563–572, 2004.
- ¹² Bajorat, J., R. Hofmockel, D. A. Vagts, M. Janda, B. Pohl, C. Beck, and G. Noeldge-Schomburg. Comparison of invasive and less-invasive techniques of cardiac output measurement under different haemodynamic conditions in a pig model. *Eur. J. Anaesthesiol.* 23:23–30, 2006.

- ¹³ Hlastala, M. P., B. Wranne, and C. J. Lenfant. Single breath method of measuring cardiac output- a reevaluation. *J. Appl. Physiol.* 33(6):846-848, 1972.
- ¹⁴ Christensen, P. and J. Grønlund. Repeatability of the single-breath method for estimation of pulmonary blood-flow: comparison among four data-reduction procedures. *Clinical Physiology* 6:221-234, 1986.
- ¹⁵ Dhingra VK, Fenwick JC, Walley KR, Chittock DR, Ronco JJ. Lack of agreement between thermodilution and Fick cardiac output in critically ill patients. *Chest* 2002; 122(3): 990–997.
- ¹⁶ Espersen, K., E. W. Jensen, D. Rosenborg, J. K. Thomsen, K. Eliassen, N. V. Olsen, and I. L. Kanstrup. Comparison of cardiac output measurement techniques: thermodilution, Doppler, CO₂-rebreathing and the direct Fick method. *Acta Anaesthesiol. Scand.* 39(2): 245–251, 1995.
- ¹⁷ Hlastala, M. P. Model of fluctuating of alveolar gas exchange during the respiratory cycle. *Respiration Physiol.* 15(2):214-232, 1972.
- ¹⁸ Gedeon, A., P. Krill and B. Österlund. Pulmonary blood flow (cardiac output) and the effective lung volume determined from a short breath hold using the differential Fick method. *J. Clin. Monit. Comput.* 17(5):313-321, 2002.
- ¹⁹ Peyton, P. J., D. Thompson, and P. Junor. Non-invasive automated measurement of cardiac output during stable cardiac surgery using a fully integrated differential CO₂ Fick method. *J. Clin. Monit. Comput.* 22(4):285-292, 2008.
- ²⁰ de Waal, E. E., F. Wappler, W. F. Buhre. Cardiac output monitoring. *Curr. Opin. Anaesthesiol.* 22(1):71–77, 2009.

Appendix A

When the desired quantity to be measured, the measurand q , is not directly measurable, the MCM could be implemented to provide the PDF of q , $p(q)$, schematically reported in Fig. 1. The MCM formulation phase requires the following steps: 1) defining the measurand (q); 2) determining the input quantities (x_1, x_2, \dots, x_n); 3) defining the PDF shape and properties (i.e., mean and standard deviation for a gaussian PDF) of the input quantities, $p(x_1), p(x_2), \dots, p(x_n)$, and the number of samples (N); 4) developing the model that relates q to the input quantities, $q=f(x_1, x_2, \dots, x_n)$.

After the formulation phase, the PDFs of the input quantities can be propagated through the model to obtain the $p(q)$. The knowledge of $p(q)$ allows for the calculation of the mean value of q (\bar{q}), the normalized standard deviation of the distribution (S_q), the expanded uncertainty associated to a general level of confidence (δq), and the relative error associated to a general level of confidence ($\frac{\delta q}{q}$).

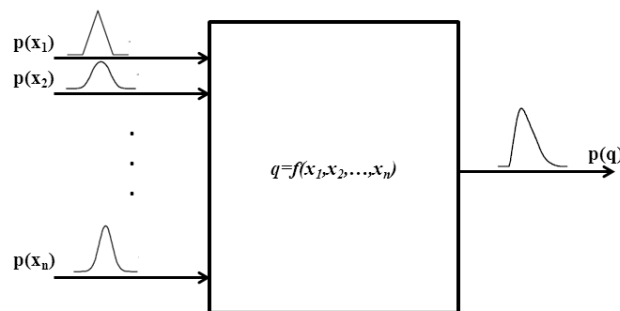


Figure 1 Schematic illustration of the PDFs propagation for a general number, n , of input quantities.

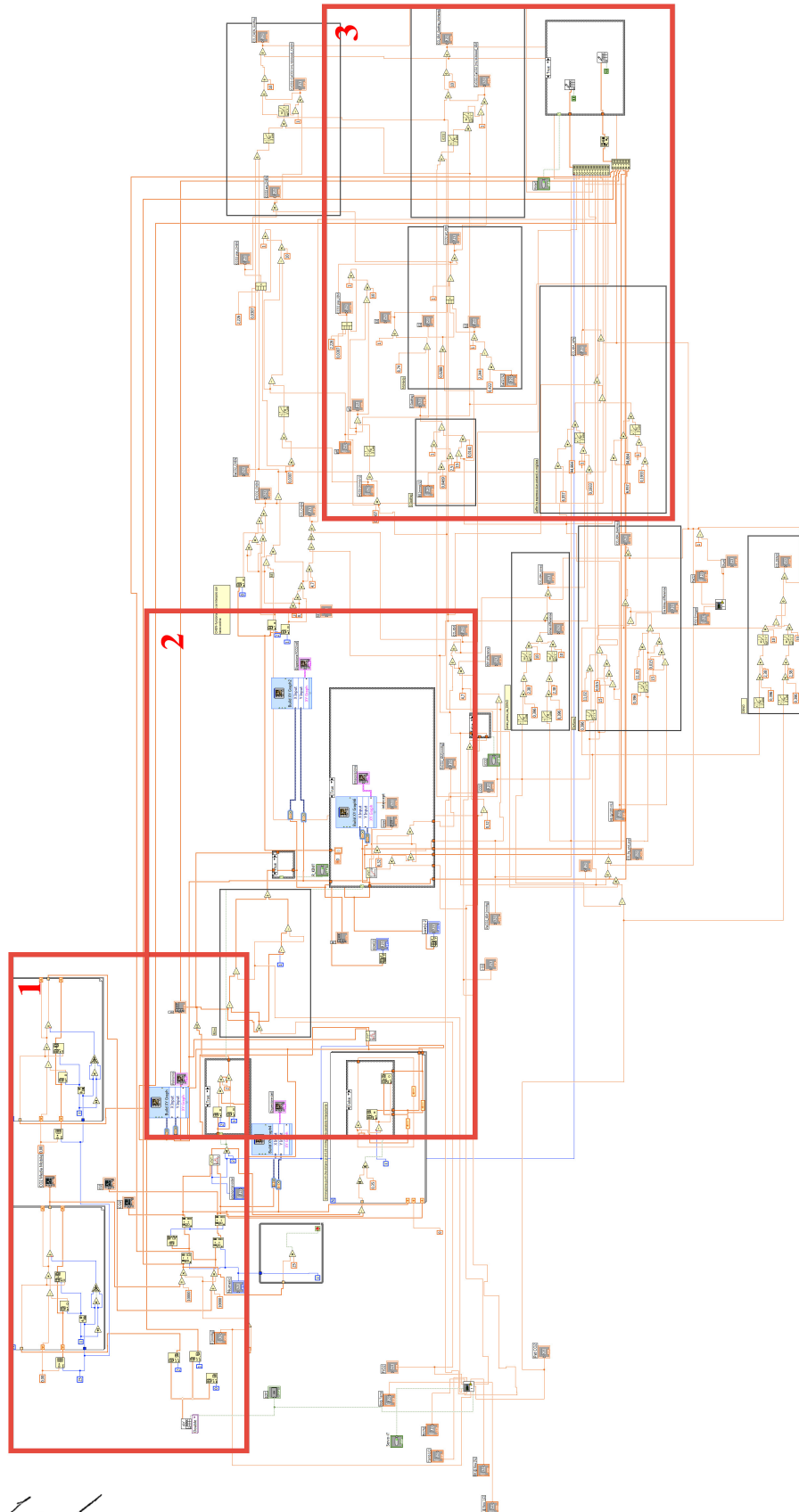
The following script of Matlab® R2009a (Mathworks Inc.) has been used to implement MCM for the two parameter configurations (A and B):

```
% defining PDFs
N=10000;
VO2=200;
Svo2=5;
hb=15;
Shb=0.15;
SaO2_A=1;
SsaO2_A=0.01;
SaO2_B=0.9;
SsaO2_B=0.009;
SvO2_A=0.6;
SsvO2_A=0.006;
SvO2_B=0.8;
SsvO2_B=0.008;
```

```
pdfVO2=randn(1,N)*Svo2+VO2;
pdfhb=randn(1,N)*Shb+hb;
pdfSaO2_A=randn(1,N)*SsaO2_A+SaO2_A;
pdfSaO2_B=randn(1,N)*SsaO2_B+SaO2_B;
pdfSvO2_A=randn(1,N)*SsvO2_A+SvO2_A;
pdfSvO2_B=randn(1,N)*SsvO2_B+SvO2_B;
% developing the model of PBF
PBF_A=(pdfVO2./(13.8.*pdfhb.*(pdfSaO2_A-pdfSvO2_A)));
PBF_B=(pdfVO2./(13.8.*pdfhb.*(pdfSaO2_B-pdfSvO2_B)));
mPBF_A=mean(PBF_A);
sPBF_A=std(PBF_A);
mPBF_B=mean(PBF_B);
sPBF_B=std(PBF_B);
% representing the results
m=[1.95:0.04:2.95];
n=[6:0.32:14];
subplot (1,2,1);
hPBF_A=histc (PBF_A,m);
bar (m, hPBF_A/N,'b');
axis([1.9 3 0 0.18]);
xlabel ('PBF [L/min]', 'FontName', 'times new roman', 'FontSize', 18);
ylabel ('Relative Frequency', 'FontName', 'times new roman', 'FontSize', 18);
subplot (1,2,2);
hPBF_B=histc (PBF_B,n);
bar (n, hPBF_B/N,'r');
axis([5.5 14.5 0 0.18]);
xlabel ('PBF [L/min]', 'FontName', 'times new roman', 'FontSize', 18);
ylabel ('Relative Frequency', 'FontName', 'times new roman', 'FontSize', 18);
```

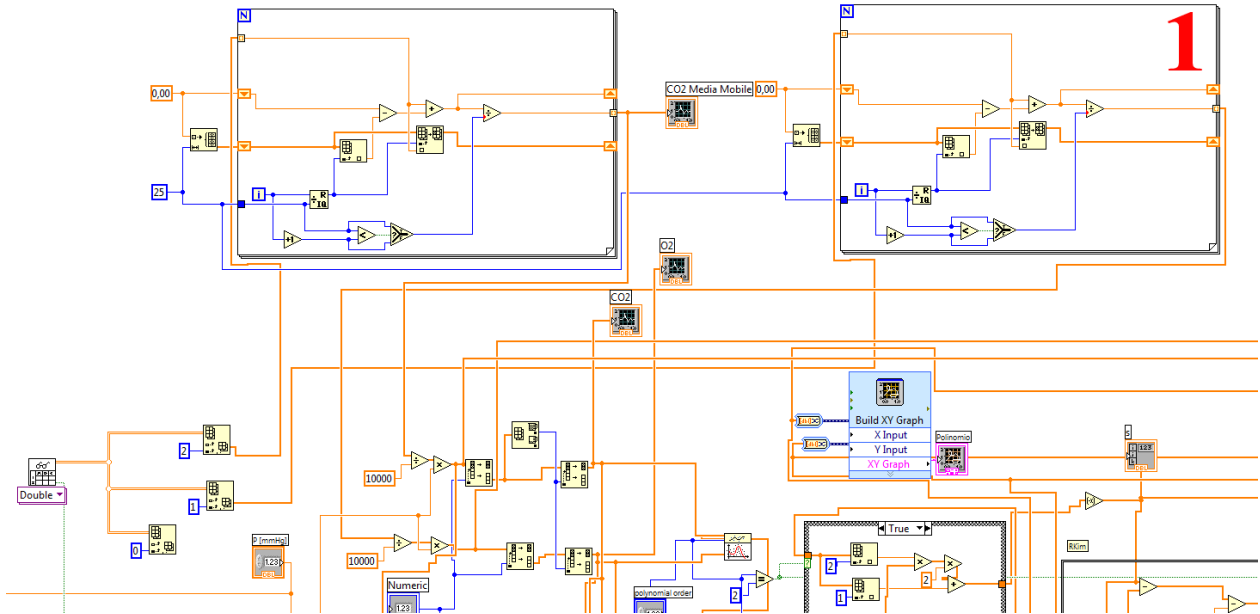
Appendix B

The following screenshots reports the main functions of the application developed in LabVIEW® 2010 environment.

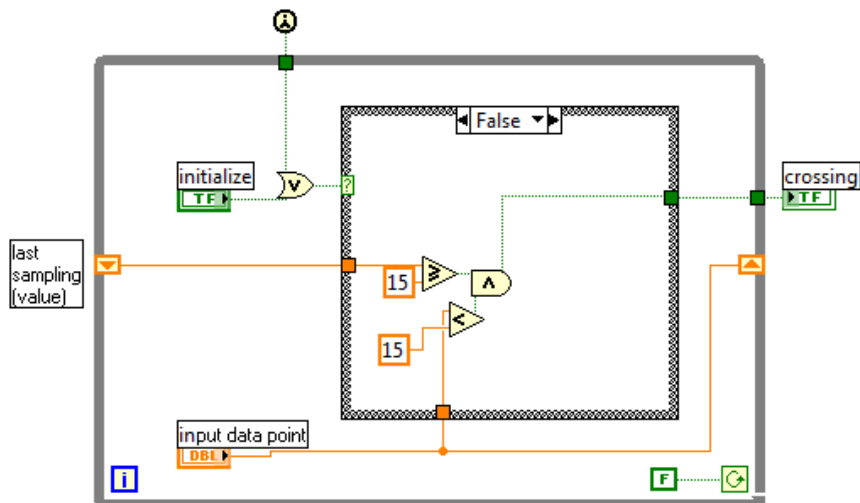


Stefano Cecchini

Data acquisition and conversion into partial pressures and STPD conditions

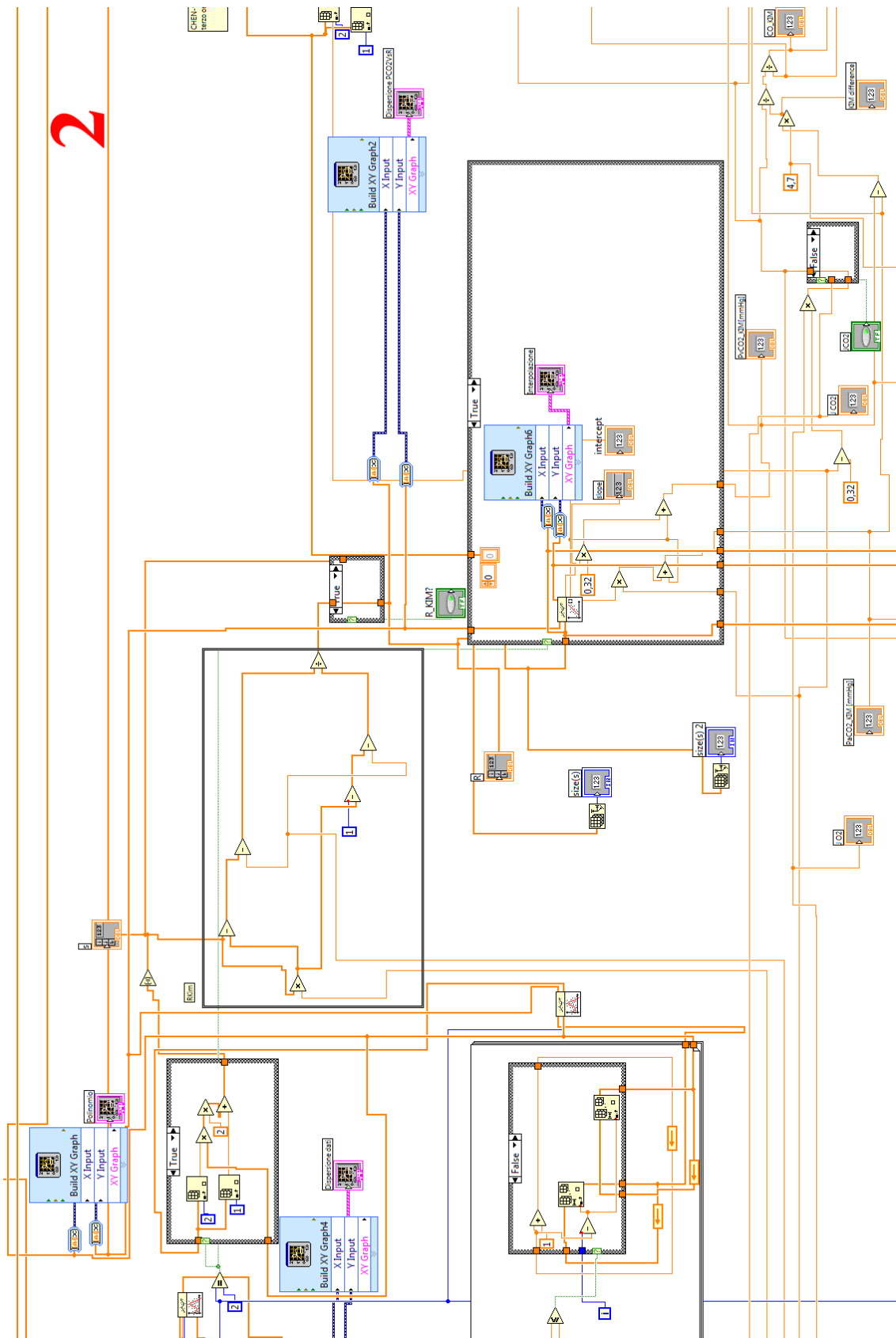


Breath detection



Stefano Cecchini

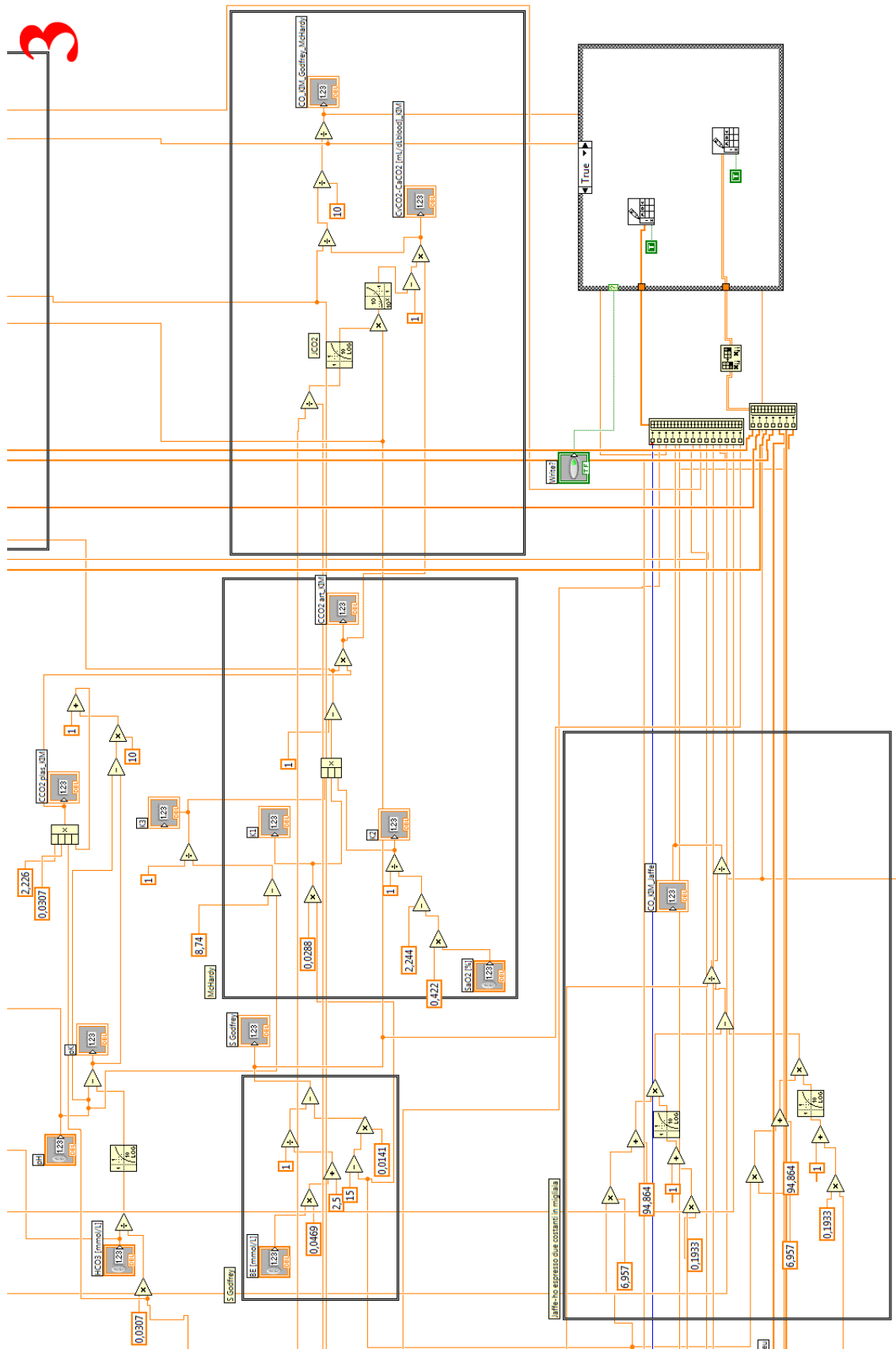
Kim algorithm



2

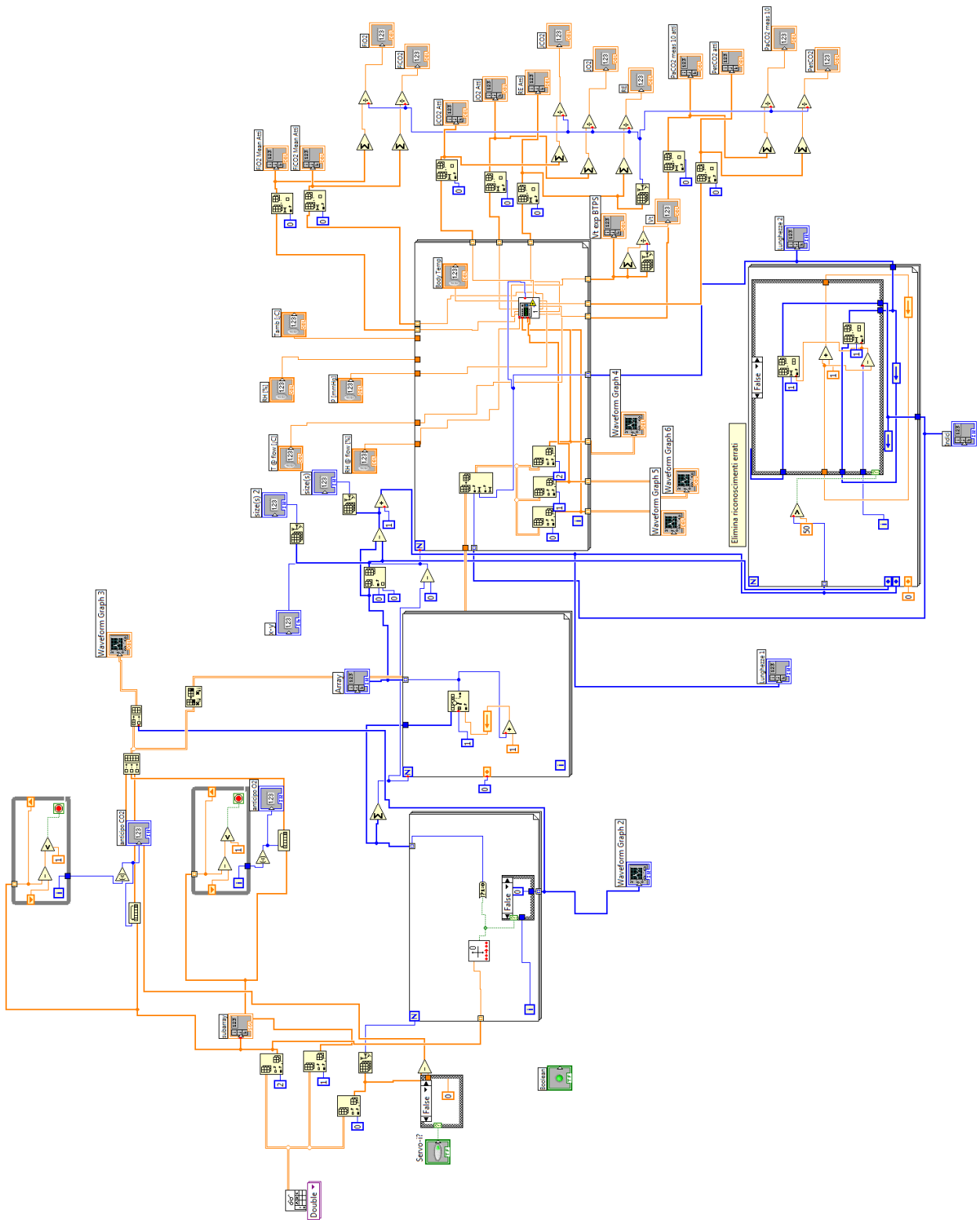
Stefano Cecchini

Godfrey algorithm



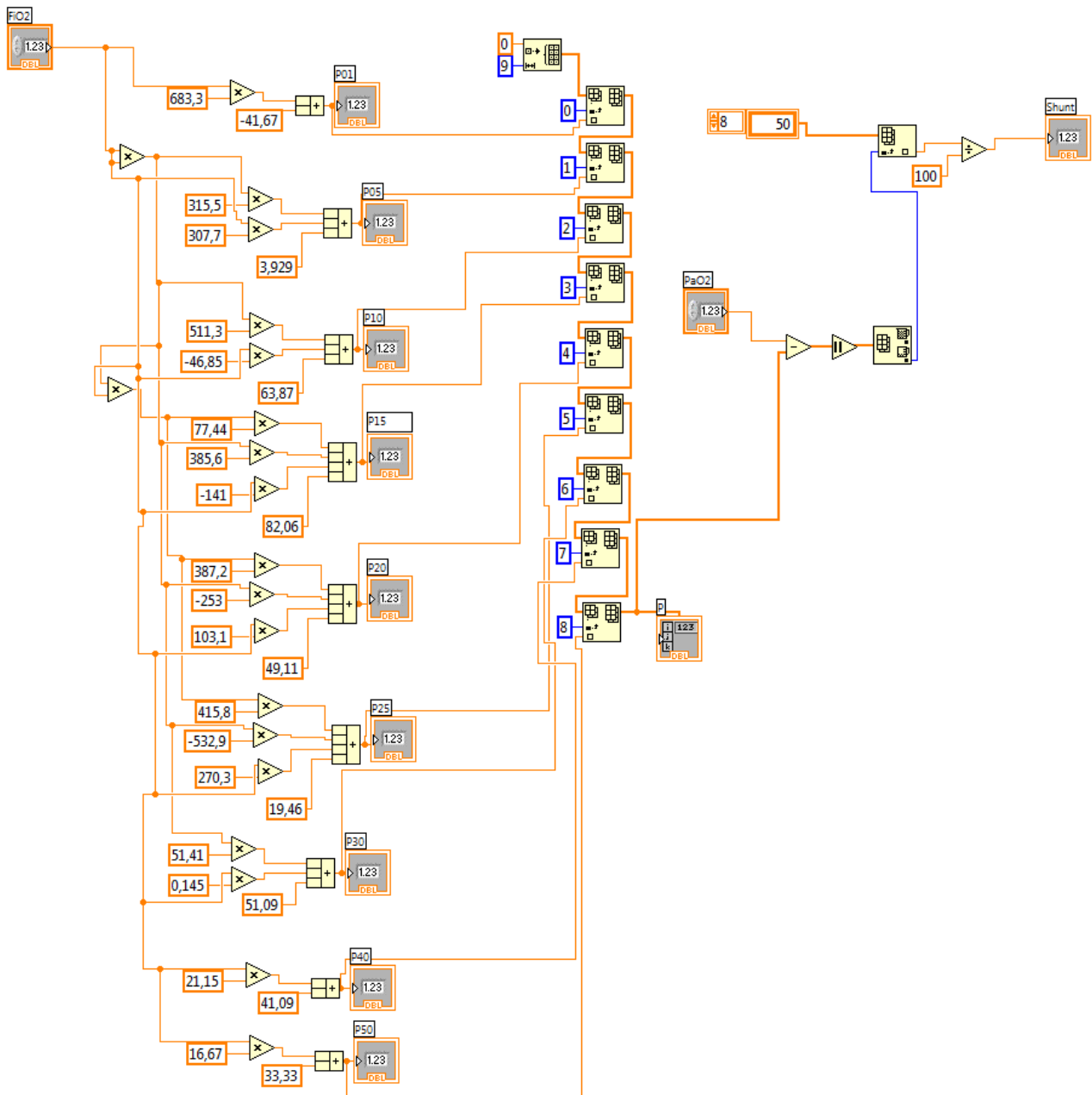
Stefano Cecchini

Breathing pattern segmentation



Stefano Cecchini

Shunt estimation algorithm



Stefano Cecchini

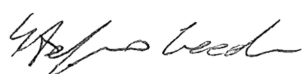
List of publications

Journal papers

1. **S. Cecchini**, E. Schena, and S. Silvestri, "AN OPEN-LOOP CONTROLLED ACTIVE LUNG SIMULATOR FOR PRETERM INFANTS", *Medical Engineering & Physics* 2010, vol. 33 (1), pp. 47-55.
2. **S. Cecchini**, I. Sardellitti, and S. Silvestri, "A NEW METHODOLOGY FOR INTRA-BREATH CONTROL OF MECHANICAL VENTILATION", *Medical Engineering & Physics* 2012, vol. 34, pp. 256-260.
3. M. Carassiti, R. Zanzonico, **S. Cecchini**, S. Silvestri, R. Cataldo, and F.E. Agrò, "QUANTIFICATION OF FORCE AND PRESSURE DISTRIBUTION APPLIED WITH MACINTOSH AND GLIDESCOPE LARYNGOSCOPES IN NORMAL AND DIFFICULT AIRWAY BY TRAINED AND UNTRAINED MEDICAL PERSONNEL: A MANIKIN STUDY", *British Journal of Anaesthesia* 2012, vol. 108 (1), pp.146-151.
4. E. Schena, G. Lupi, **S. Cecchini**, and S. Silvestri, "LOW DEAD SPACE FLEISCH PNEUMOTACHOGRAPH FOR NEONATAL VENTILATION: CALIBRATION AND COMPENSATION FOR GAS TEMPERATURE AND COMPOSITION CHANGES", *Measurement*, submitted for consideration.
5. **S. Cecchini**, E. Schena, M. Notato, M. Carassiti, S. Silvestri, "NON-INVASIVE ESTIMATION OF CARDIAC OUTPUT IN MECHANICALLY VENTILATED PATIENTS: A PROLONGED EXPIRATION METHOD", *Annals of Biomedical Engineering*, published online (2012): DOI 10.1007/s10439-012-0534-3.
6. E. Schena, **S. Cecchini**, G. Sabatino, S. Silvestri, "A BIDIRECTIONAL ORIFICE FLOWMETER: DESIGN, REALIZATION AND METROLOGICAL CHARACTERIZATION", to be submitted.
7. M. Carassiti, V. Biselli, **S. Cecchini**, R. Zanzonico, S. Silvestri, and R. Cataldo, "FORCE AND PRESSURE DISTRIBUTION USING MACINTOSH AND GLIDESCOPE LARYNGOSCOPES IN A NORMAL AIRWAY: AN IN-VIVO STUDY", *British Journal of Anaesthesia*, submitted for consideration.

Peer-reviewed international conferences


1. **S. Cecchini**, S. Silvestri, M. Carassiti, and F.E. Agrò, "THEORETICAL ANALYSIS AND MEASURING OF THE FORCES AT WORK IN THE ORO-TRACHEAL INTUBATION LARYNGOSCOPY". *Proc. of 31st Annual International Conference of the IEEE*



- Engineering in Medicine and Biology Society, Minneapolis, Minnesota, U.S., 2–6 Sept 2009, pp. 865-868.
2. I. Sardellitti, **S. Cecchini**, S. Silvestri, and D.G. Caldwell, “PROPORTIONAL MECHANICAL VENTILATION THROUGH PWM DRIVEN ON/OFF SOLENOID VALVE”, Proc. of 32nd Annual International Conference of the IEEE Engineering in Medicine and Biology Society, Buenos Aires, Argentina, 31 Aug–4 Sept 2010, pp. 1222-1225.
 3. F. Bastianini, E. Schena, S. Silvestri, **S. Cecchini**, and S. Sterzi, “EVALUATION OF PULMONARY REHABILITATION AFTER LUNG RESECTION THROUGH OPTO-ELECTRONIC PLETHYSMOGRAPHY”, Proc. of 32nd Annual International Conference of the IEEE Engineering in Medicine and Biology Society, Buenos Aires, Argentina, 31 Aug–4 Sept 2010, pp. 2481-2484.
 4. **S. Cecchini**, E. Schena, M. N. Di Sabatino, and S. Silvestri, “UNCERTAINTY EVALUATION OF A CALIBRATION METHOD FOR METABOLIC ANALYZER IN MECHANICAL VENTILATION”, In Medical Measurements and Applications Proceedings (MeMeA), 2011 IEEE International Conference, Bari, Italy, 30-31 May 2011, pp. 143-147.
 5. **S. Cecchini**, E. Schena, R. Cuttone, M. Carassiti, and S. Silvestri, “INFLUENCE OF VENTILATORY SETTINGS ON INDIRECT CALORIMETRY IN MECHANICALLY VENTILATED PATIENTS”. In Proc. of 33rd Annual International Conference of the IEEE Engineering in Medicine and Biology Society, Boston, Massachusetts, U.S., 30 Aug-3 Sept 2011, pp. 1245-1248.
 6. G. Sabatino, E. Schena, **S. Cecchini**, and S. Silvestri. “DESIGN AND EXPERIMENTAL CHARACTERIZATION OF A GAS FLOW GENERATOR TO CALIBRATE FLOW METERS FOR NEONATAL VENTILATION”. BioRob 2012, submitted for consideration.
 7. **S. Cecchini**, E. Schena, P. Saccomandi, F. Polisca, I. Di Cecca, M. Notaro, M. Carassiti, and S. Silvestri. “CARDIAC OUTPUT ESTIMATION IN MECHANICALLY VENTILATED PATIENTS: A COMPARISON BETWEEN PROLONGED EXPIRATION METHOD AND THERMODILUTION”. 34th Annual International Conference of the IEEE Engineering in Medicine and Biology Society, to be submitted.

Other publications

1. **S. Cecchini**, E. Schena, and S. Silvestri, “DEVELOPING AN OPEN-LOOP CONTROL ACTIVE LUNG SIMULATOR FOR PRETERM INFANTS”, National Instruments Days 2011, Milano, February 23rd, 2011 (web: <http://sine.ni.com/cs/app/doc/p/id/cs-13450>). Italian version: <http://sine.ni.com/cs/app/doc/p/id/cs-13304>.



2. **S. Cecchini**, E. Schena, and S. Silvestri, “AN OPEN-LOOP CONTROLLED ACTIVE LUNG SIMULATOR FOR PRETERM INFANTS”, invited paper Scope, the IPER magazine, Dec. 2011.

Patents

1. **S. Cecchini**, E. Schena, M. Carassiti, and S. Silvestri, “APPARATO PER LA STIMA DELLA GITTATA CARDIACA”, Patent N° RM2011A000650, filed on the 9th of December 2011.
2. E. Covino, **S. Cecchini**, and S. Silvestri, “POSIZIONATORE DI SHUNT CORONARICO”, to be filed.

Technical reports

1. **S. Cecchini**, M. N. Di Sabatino, and S. Silvestri, “VALIDAZIONE IN-VITRO DEL MONITOR METABOLICO QUARK RMR”, provided to the R&D Department of Cosmed s.r.l. on the 16th of November 2010.
2. **S. Cecchini**, R. Cuttone, S. Silvestri, and M. Carassiti, “IN-VIVO VALIDATION OF THE METABOLIC CART QUARK RMR”, provided to the R&D Department of Cosmed s.r.l. on the 4th of July 2011.